

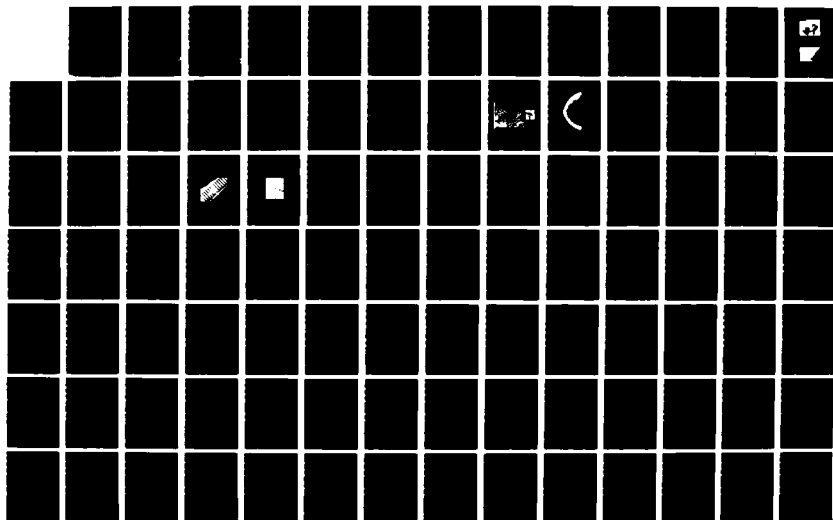
AD-A189 858

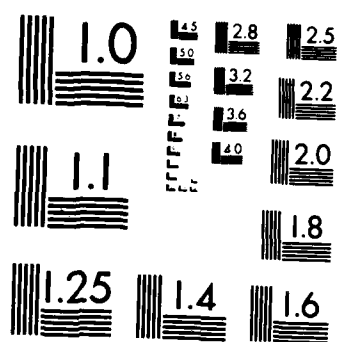
THEORETICAL ANALYSIS OF CANCER DETECTION IN THE HUMAN
BREAST BY TRANSLUMINATION(U) AIR FORCE INST OF TECH
WRIGHT-PATTERSON AFB OH SCHOOL OF ENGI D M SANDERS
DEC 87 AFIT/GEQ/EMP/87D-4 F/G 6/5

1/2

UNCLASSIFIED

NL

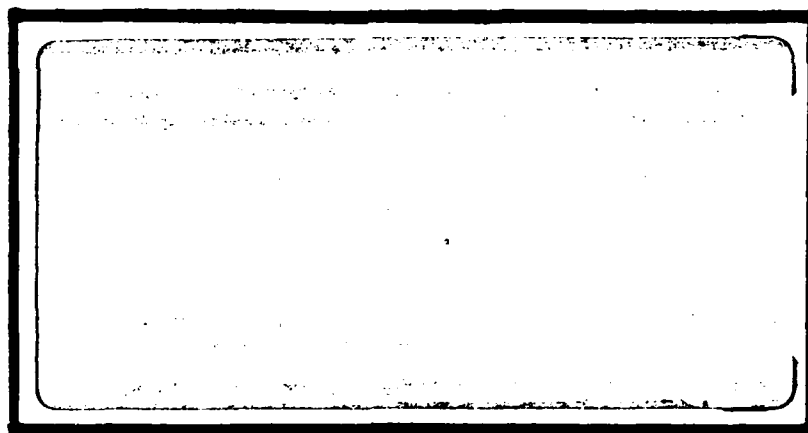




MICROCOPY RESOLUTION TEST CHART
NATIONAL BUREAU OF STANDARDS-1963-A

DTIC FILE COPY

AD-A189 850



DTIC
ELECTE
MAR 07 1988

DEPARTMENT OF THE AIR FORCE
AIR UNIVERSITY

AIR FORCE INSTITUTE OF TECHNOLOGY

Wright-Patterson Air Force Base, Ohio

DISTRIBUTION STATEMENT A

Approved for public release;
Distribution Unlimited

88 3 01 114

AFIT/GEO/ENP/87D-4

THEORETICAL ANALYSIS OF CANCER DETECTION
IN THE HUMAN BREAST BY TRANSILLUMINATION

THESIS

David W. Sanders
Captain, USAF

AFIT/GEO/ENP/87D-4

DTIC
ELECTE
MAR 07 1988
S H

Approved for public release; distribution unlimited

THEORETICAL ANALYSIS OF CANCER DETECTION
IN THE HUMAN BREAST BY TRANSILLUMINATION

THESIS

Presented to the Faculty of the School of Engineering
of the Air Force Institute of Technology
Air University
In Partial Fulfillment of the
Requirements for the Degree of
Master of Science in Electrical Engineering

David W. Sanders, B.S.

Captain, USAF

December 1987

Approved for public release; distribution unlimited

Preface

The primary purpose of this research was to investigate possible means of improving imaging of breast cancers by transillumination using near infrared radiation. The need for such a detection scheme was clear considering the possible carcinogenic properties of x-ray mammography which is the standard modality for breast cancer detection today.

Lack of experimental data related to optical parameters of breast tissue set limits on the degree of applicability of the methods presented. Nevertheless, the model of light propagation in the breast employed in the study yielded results for transmittance which are in agreement with actual breast transillumination to a remarkable degree considering the paucity of quantitative data available.

The encouraging results obtained with time gating and spatial filtering (described in Chapter III) of light propagating through a dilute blood medium should be followed up by applying the same method to breast transillumination.

In writing this thesis, I received invaluable help from a number of people. I am deeply grateful for the cogent questioning and guidance which my faculty advisor, Dr. Theodore Luke, provided me. I also wish to thank Maj James Lupo and Capt Steven Rogers for the helpful suggestions they made in the course of the research. Thanks go also to Mrs. Melony Marciniak for her excellent typing of the manuscript. Finally, I wish to thank my patient wife, Yonghwa, and my sons, William and Matthew, for the sacrifice they made while I was engrossed in work and unable to devote to them the time they so deserve.



on For	
RA&I	<input checked="" type="checkbox"/>
3	<input type="checkbox"/>
need	<input type="checkbox"/>
action	<input type="checkbox"/>
By	
Distrib	
Avail	
Dist	
Dist	
A-1	

Table of Contents

	Page
Preface	ii
List of Figures	v
List of Tables.	vii
Abstract.	viii
I. Transillumination	1
Introduction	1
Background	3
Breast Anatomy	7
The Normal Breast	7
An Optical Model for the Human Breast	13
Absorption Properties of the Breast	13
Light Scattering Properties of the Breast	17
Light Scattering in Whole Blood	26
II. Scattering Theory.	28
The Correlation Function from Analytic Theory.	30
The Connection Between the Analytic and Transport Theories	31
Limitation on Image Resolution Due to a Scattering Medium.	33
The Signal to Noise Ratio.	37
Interpretation of the Signal to Noise Ratio.	43
III. Some Methods of Improving Imaging in Transillumination	47
Time Gating and Spatial Filtering of the Transmitted Radiation.	47
Simulation of Laser Tomoscopy	47
Description of the Simulated Model.	48
Optical Parameters Used in the Model.	50
Transmittance and Reflectance Characteristics	50
Simulation of Imaging by Transillumination.	55
Discussion of Results Obtained by Simulated Transillumination.	60
Comparison of Transmittances Obtained by Monte Carlo Simulation and Theoretical Calculation.	61
Implementing Monte Carlo Simulation Using the Gaussian Approximation to the Phase Function.	67

IV. Conclusions and Recommendations.	75
Appendix A: Multiple Scattering Theory	78
Integral Formulation	82
Appendix B: The Correlation Function	86
Appendix C: The Transport Theory	93
Appendix D: The Connection Between the Analytic and Transport Theories	98
Appendix E: Plane Wave Illumination of a Plane-Parallel Medium	101
Appendix F: The Correlation Function in the Small Angle Approximation: Plane Wave Solution	106
Appendix G: Limitation on Image Resolution Due to a Scattering Medium.	109
Appendix H: Phase Retrieval.	120
Calculation of the Minimum Error in Image Reconstruction by Phase Retrieval as Applied to Transillumination.	121
Calculation of the MTF.	123
Appendix I: The Scattering Cross Section	133
Appendix J: Solution of the Transport Equation Using the Large Particle Approximation	134
Appendix K: Calculation of the Fourier Transform of the Gaussian Phase Function	141
Bibliography	143
Vita	146

List of Figures

Figure	Page
1. Carcinoma Imaged by Transillumination and X-ray Mammography . . .	2
2. The Normal Breast	8
3. Microscopic Structure of the Breast	11
4. Normal Craniocaudad View of the Breast.	12
5. Spectral Transmittance and Remittance of Human Dermis	15
6. Diffuse Scattering and Absorption of Human Dermis	16
7. Rat Tail Tendon Collagen Fibril	20
8. Human Collagen.	21
9. Scattering Angle Dependence on Wavelength	22
10. Flux Through a Surface.	32
11. A Monochromatic Plane Wave Propagating Through a Random Distribution of Scatterers.	33
12. Coherent and Incoherent Intensities in the Image Plane.	37
13. Schematic Representation of Tissue Model in Monte Carlo Simulation.	49
14. Variations of the Number of Transmitted Photons for Three Values of Medium Thickness	51
15. Variations of Transmittance and Reflectance with Time Gating and Spatial Filtering	53
16. Variations of Normalized Transmittance as a Function of Blood Vessel Position (Small Vessel).	56
17. Variations of Normalized Transmittance as a Function of Blood Vessel Position (Medium-sized Vessel)	58
18. Variations of Normalized Transmittance (Blood Vessel Shifted Towards Unilluminated Side of Medium)	59
19. Typical Transmission Curves Obtained via Monte Carlo Simulation .	70
20. Normalized Transmission Curves After Time Gating and Spatial Filtering	71

21. The Scattered Wave.	79
22. Scattering by a Single Particle	80
23. Multiple Scattering	80
24. Multiple Scattering Operator.	87
25. Scattering Process for the Correlation Function	88
26. The Scattering Process for Determining the Operator v_s^a	89
27. Flux Through a Surface.	93
28. Scattering of Specific Intensity.	94
29. Physical Quantities in the Integral Formulation of the Average Intensity	97
30. A Monochromatic Plane Wave Propagating Through a Random Distribution of Scatterers.	109

List of Tables

Table	Page
I. Breast Types	10
II. Optical Densities.	66
III. Exact Theory and Twersky's Theory.	81

Abstract

This investigation is a theoretical analysis of the propagation of near infrared light through human breast tissue with a view to improving imaging of breast cancers by transillumination. The analysis employed multiple scattering and radiation transport theory.

Calculation showed that breast tissue is optically thick and does not allow for imaging details of tumors which may be imbedded in the tissue. An example calculation carried out on the method of phase retrieval demonstrated that the error in the estimate of the Fourier modulus is, for normal breast tissue, nearly 100 percent and that, therefore, the phase of an object (tumor) cannot be retrieved by this method.

A Monte Carlo simulation employing time gating and spatial filtering (TGSF) was presented showing that, in some cases, an improvement in image contrast of 77 percent is theoretically possible when transilluminating a dilute blood medium containing a blood vessel. A calculation of total transmittance obtained by Monte Carlo simulation on one hand and by multiple scattering and radiation transport theory on the other, indicated an essential agreement of the results for tissue thicknesses less than 60mm.

A method of tying the results of Monte Carlo simulation to those of multiple scattering and radiation transport is presented. An effective optical thickness reduced by TGSF is defined and a method is described to determine if the reduced effective thickness allows for reasonable images to be obtained.

THEORETICAL ANALYSIS OF CANCER DETECTION IN THE HUMAN BREAST BY TRANSILLUMINATION

I. Transillumination

Introduction

Concern over the limitations and risks (6) associated with x-radiation in the imaging and diagnosis of human breast cancer is motivating researchers to seek other, safer methods of detecting breast lesions. One such method, transillumination, is a technique of imaging structures of human tissue by propagating light through them (See Figure 1). The technique has gone by different names depending on light sources and methods of light detection used. The term transillumination initially served to name a procedure which used white light as a source and where observation of the illuminated tissue was made by the unaided eye. In cases where white light sources are used, but detection is performed via infrared photography, the transillumination procedure has been called diaphanography (23:123). The term diaphanography will not, however, be used in this paper as the more advanced transillumination methods employ infrared illumination (by filtering white light) and infrared video camera detection, amplification, and video display schemes. In these cases, transillumination is referred to as light scanning or infrared light scanning (5:409). The reader will note that the term transillumination can be used at times, in its generic sense, to refer to any of the optical imaging techniques mentioned above.

Structures within the human breast have varying optical properties such that, when the structures are transilluminated, variations result in the distribution of light intensity and color in their images.



(a)



(b)

Figure 1. (a): Carcinoma imaged by transillumination (23:127).
(b): Same carcinoma imaged by x-ray mammography (23:127).

Researchers have found that breast cancers may be identified by the shadows they cast, and benign lesions by the areas of increased brightness they create in the image (39:14). However, the transillumination technique has, to date, demonstrated only sufficient effectiveness to perform as an augmentation to traditional mammography and has not reached a level of development whereby it could be considered as an alternative to mammography as the primary imaging tool in the diagnosis of breast cancer.

The following section of Chapter I is a review of the current literature relevant to transillumination as an aid in the diagnosis of diseased breast tissue. The references cited were collected by means of a computerized literature search using the medical library of DIALOG software. The reader will find that, save for the article by Watmough (which is the last presented here), the review is organized chronologically, showing the improvements made, and as a consequence, the problems which have confronted and continue to define the limits of the applicability of transillumination.

Background

The first diagnostic use of transillumination of the breast was made by Culter in 1929 (9). He employed visible wavelengths of white light and reported some success in identifying tissue variations. However, it was recognized early on that "it was not possible to differentiate shadows of benign from malignant lesions, and that light diffusion from the available probe often prevented smaller lesions from being seen" (23:123).

Lafreniere, et al. reported that, in spite of initial support for the new transillumination technique, the procedure fell into disrepute, probably due to inadequacy of the available equipment (23:123). Over

the years a number of improvements were made to both the equipment and technique. Among these improvements were (1) illumination with longer wavelength, narrower spectrum sources which increased tissue penetration and reduced scattering, (2) the introduction of infrared photography, and (3) the use of fiber optic bundles to create a cold light source to convey the light energy to the tissue (this overcame an early problem with heat generated by the light source). Despite these improvements, reports indicated the technique was cumbersome and did not add significantly to the conventional physical examination and mammogram (18).

Better results were obtained by Morton (25) who, in 1981, reported using a red and infrared light source to illuminate the tissue. In addition, he introduced an infrared video camera and displayed its images on a black and white video monitor. This allowed for amplification of the image and thereby reduced the intensity requirement of the source. As a result of Morton's improvements, internal structures which had previously been unrecognizable to the unaided eye could be viewed and identified on the video monitor (26).

Morton's technique had been based on Cartwright's (7) observation made in 1930 that greater transmission through human tissue was possible with infrared illumination. The work of Anderson and Parrish (2:17) supports Cartwright's findings showing that transmittance of light through human skin is decreased in the shorter wavelength spectrum and increases in the near infrared.

In 1983, Bartrum and Crow (5:409) reported that transillumination light scanning can yield clinical results comparable to mammography if the personnel who are interpreting light scan images are trained and have some knowledge of other clinical data related to the patient. When

the light scan interpreter is blind to other relevant clinical data, a diagnosis based on the light scan is generally poorer than that obtained from mammography. In their report, Bartrum and Crow cite conditions they feel must be met to obtain optimal results from light scanning. First, diffuse incident light is required since breast tissue is a highly scattering medium. When focused light is used the light scan becomes more difficult to interpret. Second, the optical absorption differences between cancerous and adjacent tissue can be blurred if the transilluminating light is too intense. Third, vigorous physical compression of the breast is necessary since the farther a lesion is located from the skin surface, the weaker is the shadow cast by the lesion. Bartrum and Crow found that the "shadow from a 1-cm-diameter lesion (in a breast phantom) begins to fade rapidly when the lesion is more than 15mm from the skin surface; at 25mm, the shadow is obscured" (5:413). For this reason a breast lesion may be invisible if "it is not compressed to within 2cm of a skin surface" (5:413). Fourth, because a lesion may become undetectable a short distance beneath the tissue surface, light scanning from multiple angles is required to ensure maximum possible coverage of the tissue. Fifth, and lastly, since carcinomas absorb light differentially in narrow spectra, a narrow spectrum of illuminating light should be used as a source (this could be accomplished by filtering a white light source). Bartrum and Crow go on to say ". . .we performed in vivo spectral analysis of 11 carcinomas. . . which showed preferential tumor absorption in two relatively narrow wavelength bands, one in the far visible red spectrum and another in the infrared spectrum" (5:413). In 1986, Lafreniere et al. (23) reported the results of a clinical evaluation of transillumination and infrared light scanning as compared with conventional physical examination and

mammography. The test involved 600 patients with 79 biopsies performed revealing 26 carcinomas (23:124). These researchers reported that

examination, conventional mammography; simple transillumination, I.L.S. (infrared light scanning), and simple transillumination combined with I.L.S. respectively showed a true positive interpretation in 21, 22, 19, 25, and 25 of 26 breast lesions histologically positive for malignancy (sensitivity 81%, 85%, 73%, 96%, 96%) (19:124).

These results indicate that infrared light scanning missed only one of 26 carcinomas verified histologically. In this case, the interpreters of the images of mammography, transillumination, or infrared light scanning techniques were trained in each technique but had no knowledge of other clinical data relating to the patients.

An explanation of the physical mechanism responsible for the appearance of the images produced by transillumination and infrared light scanning was given by Watmough in 1982 (39:14). Watmough had set out to measure the transmission coefficient of sections of tissue removed from the female breast during surgical operation. He had expected to find that "different lesions would transmit light to the extent dependent on the type of disease process" (39:11). Instead, he found that despite large variations (size and shape) in tissue samples taken, there was no clear distinction between transmission characteristics of malignant tumors and benign lesions. Watmough argued that since the variations in light transmission were not caused by the diseased tissues themselves, transillumination and light scanning were simply not imaging the diseased tissues. He reports, ". . .the spectro-photometric traces in every case demonstrated the absorption bands of oxyhaemoglobin [oxygenated hemoglobin] . . ." (39:11). From these findings, Watmough postulated that the transillumination procedure actually measured the number density of red cells in the illuminated tissue. To determine the accuracy of his hypothesis, Watmough

transilluminated (with a xenon flash tube) samples of whole blood at varying degrees of dilution and exposed infrared color film to the light scan images of the breast. A spectral analysis of samples of diluted blood was then carried out; the results showing that the samples ceased to transmit light at frequencies (colors) related to the color of whole blood in a sample. For samples with higher blood densities the frequency cut-offs occurred in the longer wavelength regions (red and orange). The more diluted samples showed frequency cut-offs toward the blue end of the spectrum. Watmough writes, ". . .These experiments provide excellent confirmation of how red cell densities in effect provide a range of colour filters. . . ." (39:13).

Breast Anatomy

The Normal Breast.

The description given here of the anatomy and histology of the human breast is taken from Egan (12:17-24). The structure of the normal breast will be presented first to be followed by the formulation of an optical model of the breast.

The breast is located between the superficial and deep layers of the superficial fascia (see Figure 2). The superficial layer of fascia, separated from the skin by 0.5 to 2.5 cm of subcutaneous fat and areolar tissue (the areola is the region of darker skin surrounding the nipple), forms an irregular boundary for the surface of the glandular tissue. Projections of collagenous fibrous tissue extend from the fascia and surround lobules of fat. These masses of collagen fibers (low in water content) form suspensory ligaments called Cooper's ligaments (12:17). Younger women tend to have breast tissue which is primarily fibrous with comparatively small amounts of fat (28). This fact is of particular importance since transillumination is targeted at younger persons below

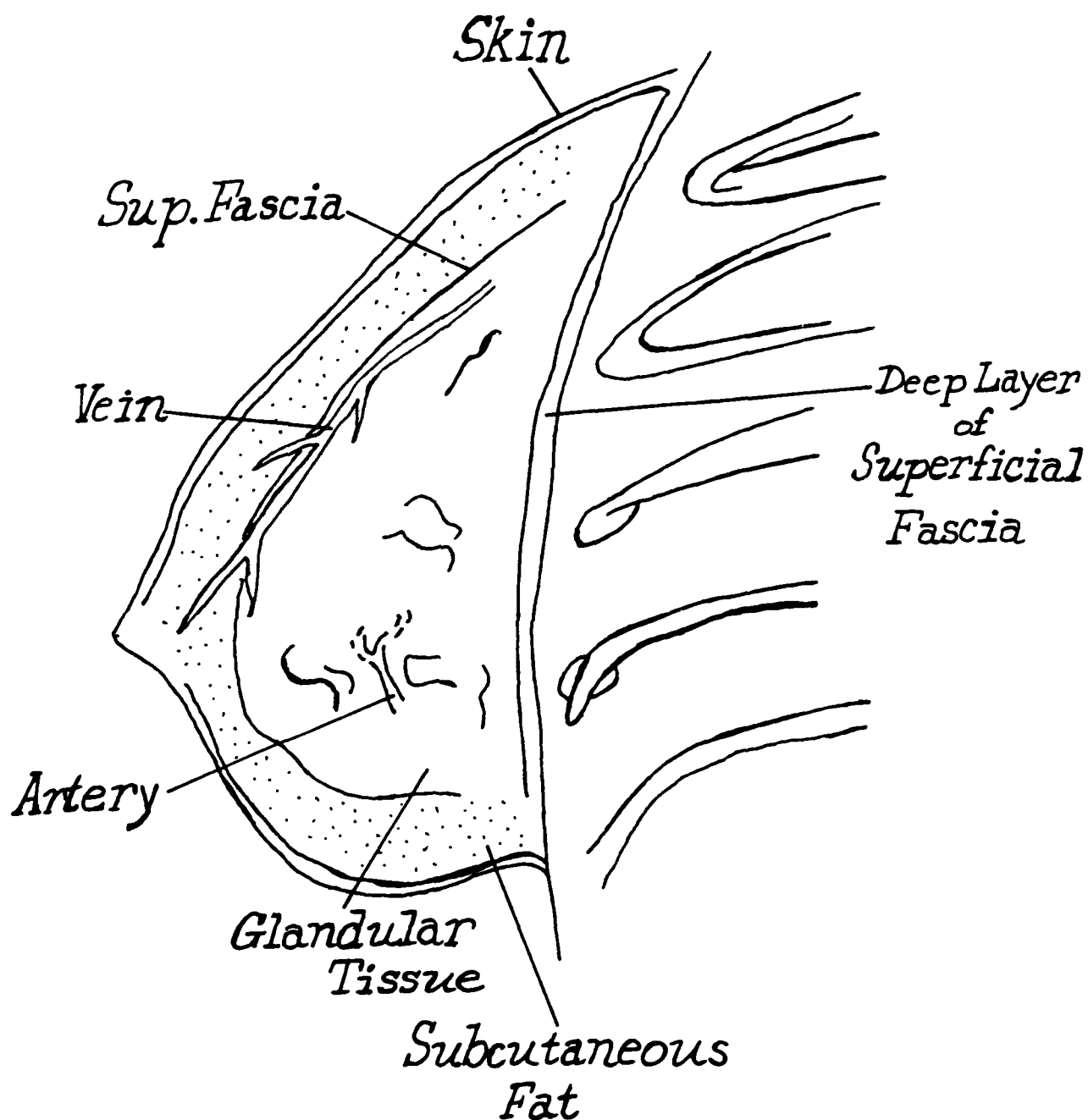


Figure 2. The Normal Breast (12:18). An artist's conception of the various anatomic structures of the breast.

the age of 50 (see Table I). This means that, for the purposes of transillumination, the breast may be considered primarily fibrous. When fat lobules occur they do so with dimensions on the order of centimeters (8:43-48).

Within the breast are fifteen to twenty irregular lobes, converging to the nipple. Each lobe is drained by its own lactiferous duct, and is provided with an excretory duct, 2 to 4.5 mm in diameter (12:17). These lobes are macroscopic in size and are, therefore, many times larger than the collagen fibers which have dimensions on the order of a hundred nanometers.

The anatomic structures of the breast are, for purposes of classification, divided between functional structures called the parenchyma, and supporting structures called the stroma (see Figure 3). Because the parenchyma (such as the lactiferous ducts and lobes) tend to be very large compared to wavelength of radiation in transillumination, they cannot be considered to contribute greatly to light scattering-also, in the non-lactating breast they are of low water content and, therefore, are not highly absorbing. For these reasons, the description given here of the macroscopic structure of the breast concentrates on the fibrous tissue of the stroma. The stroma consists of dense, collagenous, intralobular connective tissue (see Figure 3), containing the large blood vessels, nerves, lymphatics and varying amounts of adipose tissue. This connective tissue produces the poorly defined septa between the lobules and lobes of the mammary gland (12:19).

In the craniocaudal view (see Figure 4) the dense inner triangle of tissue produces the varying degrees of diffuse opacity to x-rays. Contrast (in x-ray mammography) in the image is dependent upon the relative density of fatty and fibrous tissues. A reticular appearance

TABLE I
BREAST TYPES

Classification of breast types showing percent fibrous and fatty tissues for various age groups.

<u>Age Group</u>	<u>FIBROUS</u>		<u>FATTY</u>		<u>Total</u>
	<u>Number</u>	<u>Percent</u>	<u>Number</u>	<u>Percent</u>	
21-25	13	100	-	-	13
26-30	11	91.6	1	8.4	12
31-35	39	88.7	5	11.3	44
36-40	27	81.8	6	11.2	33
41-45	34	75.5	11	24.5	45
46-50	38	65.5	20	34.5	58
51-55	54	55.1	44	44.9	98
56-60	35	37.2	59	62.8	94
61-65	55	39.8	83	60.2	138
66-70	41	35.9	73	64.1	114
71-75	51	52.2	46	47.4	97
76-80	24	64.8	13	35.2	37
81-85	8	66.6	4	33.4	12
86-90	4	80.0	1	20.0	5
-----	-----	-----	-----	-----	-----
21-90	434	54.3	366	45.8	800

(28)

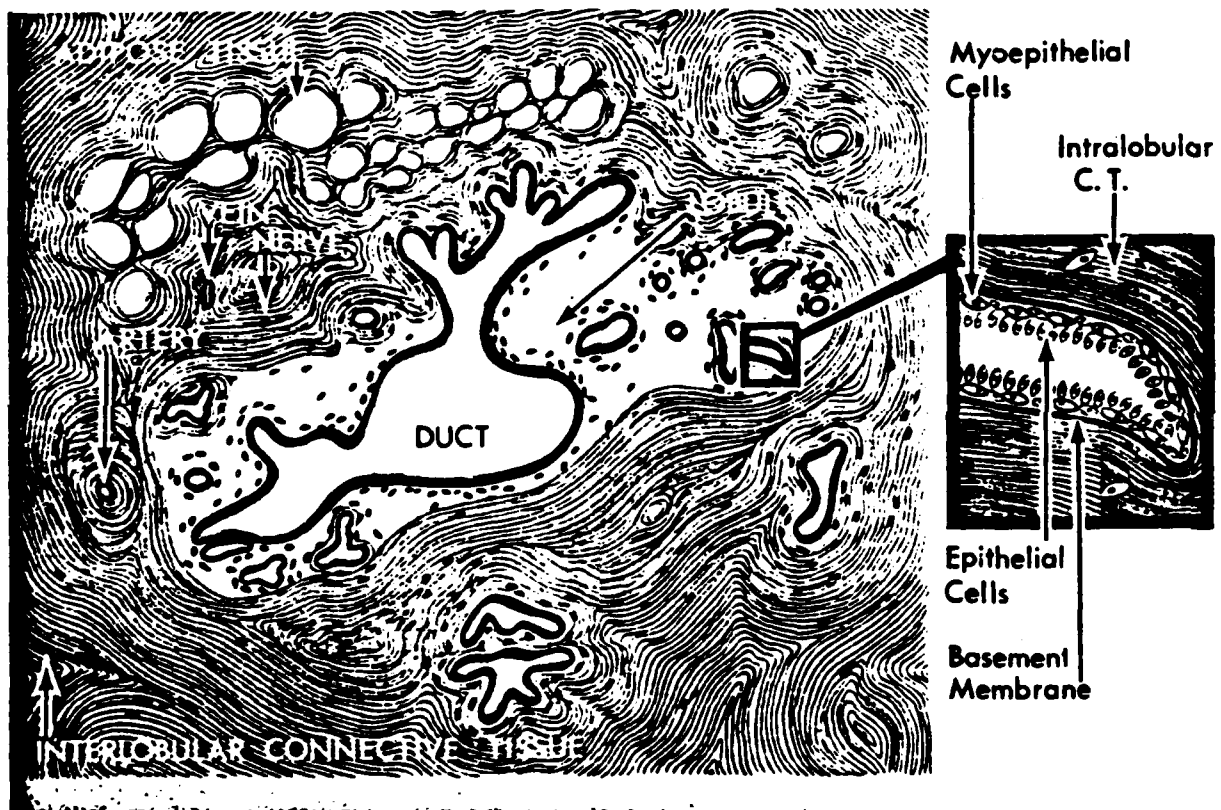


Figure 3. Microscopic (Histologic) Structure of the Breast (12:19). The microscopic appearance of the essential histologic elements of the mammary gland. For reference, the lactiferous duct in the center of the drawing is around 2 to 4.5 mm in cross sectional size.

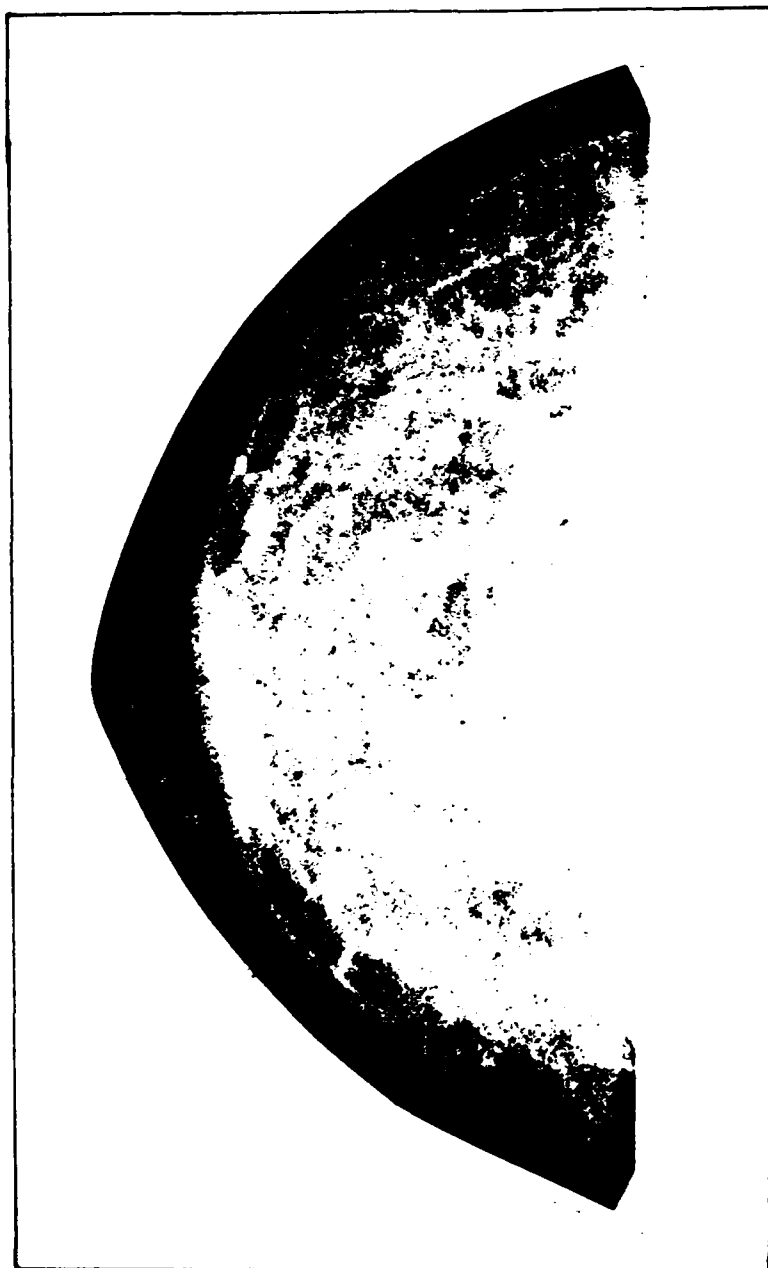


Figure 4. Normal Craniocaudal View of the Breast (12:24). A thirty-one year old white female with mammogram done for routine check-up.

caused by the stroma or connective tissue framework is evident in x-ray images; the connective tissue may be nearly homogeneous in the very dense breast (12:22). Again, in transillumination, the fatty lobules are not considered either highly scattering or absorbing (31).

To the extent that the breast is a light absorbing optical medium, the absorption experienced is due, on a comparative basis, almost entirely to the freely flowing plasma in veins and arteries. Accurate values for the volumetric content of blood in the breast were not available for this writing. The subject of the scattering and absorption characteristics of whole blood (blood cells and plasma) will be covered in greater detail in the theoretical model of breast to be described below.

An Optical Model for the Human Breast.

Theoretical models of the breast where scattering is of relative unimportance often consider the breast to be a medium made up of water and fat (27). This approximation seems suited to irradiation of the breast with x-rays where absorption plays the primary role in attenuation. However, in the red and near infrared region of the spectrum where transillumination occurs, both absorption and scattering play a role in determining transmission properties of the breast.

Absorption Properties of the Breast.

By far, the greatest amount of absorption in biological media is found to occur in blood-borne pigments and blood plasma (2:17). In tissues of low blood or water content relatively little absorption is noted (21:695). Specific optical data on the breast which would allow one to isolate transmission losses due to scattering from those due to absorption are lacking. The optical characteristics of the dermis of the skin are, however, in this research considered to have an especially

close affinity to the optical properties of the breast as the dermis has a high content of collagenous fibers (these fibers account for 70 percent of the dry weight of the dermis) (3:256). Anderson and Parrish state (2:17) with regard to Findlay's (16) optical measurements of pig dermis, "Summing Findlay's transmittance and remittance spectra gives values close to 1.0 (100 percent) across the entire visible spectrum, indicating that very little visible light was actually absorbed." Figure 5 shows spectral transmittance and remittance data (analogous to those of Findlay) for a 200 m thick section of human dermis in vitro. Figure 6 presents calculated values of the scattering coefficient S and the absorption coefficient K for human dermis in vitro. The coefficients S and K are calculated from the Kubelka-Munk theory of radiation transfer (22:106-116) and should not be confused with the scattering cross section σ_s or the absorption cross section σ_a which will be used in Chapter II in the development of the analytic and transport theories of scattering. The Kubelka-Munk theory is not employed in this research as it does not lend itself readily to interpretations relating to actual physical parameters of individual particles. This should not be construed, however, to imply that the Kubelka-Munk theory does not give valid quantitative results (22:106).

The data in Figure 6 indicate that absorption is indeed low over the visible spectrum and also in the near infrared region except at the prominent absorption bands of water. Figure 5 shows peak transmission occurs at about 1.23 μ m where, again, there is little absorption.

From the data presented, it is apparent that in the red and near infrared portion of the spectrum, a medium with a high percentage of collagenous fibers can be approximated as one having a low value of absorptance. Moreover, due to the fact that fatty tissues are low in

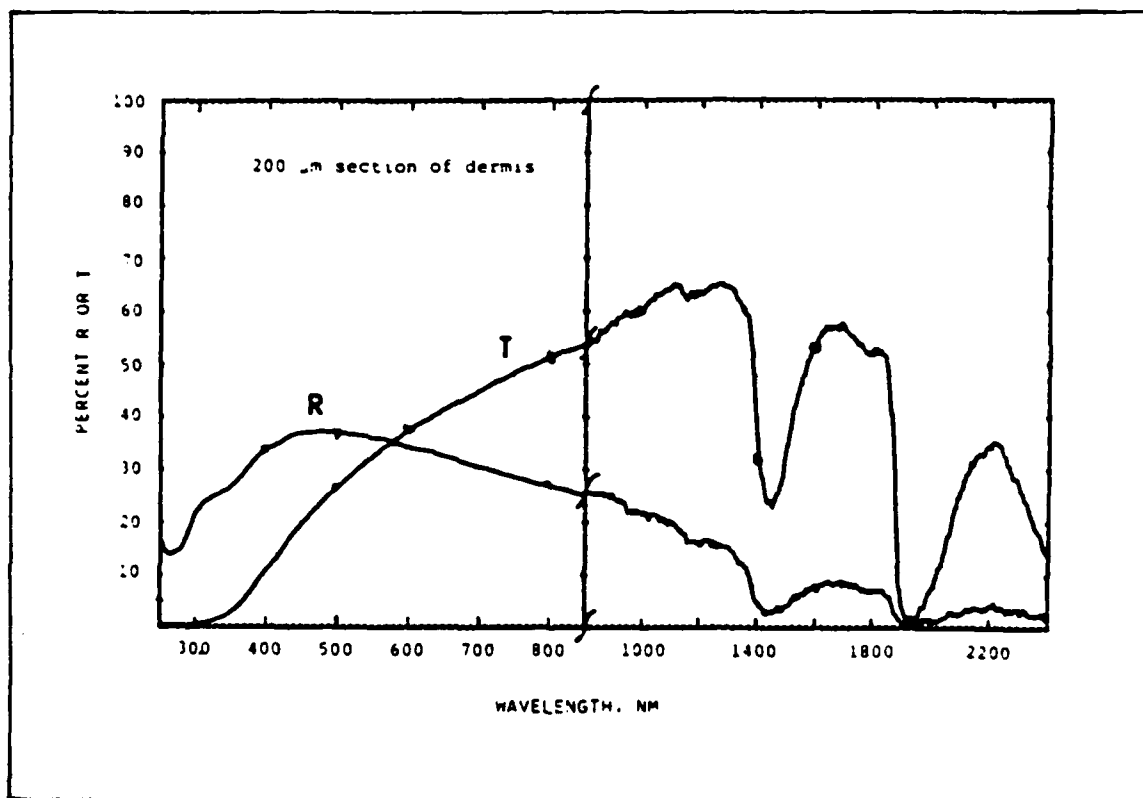


Figure 5 (2:17). Spectral Transmittance and Remittance of a 200 m Thick Section of Human Dermis. Data is given in percent remittance (R) or transmittance (T).

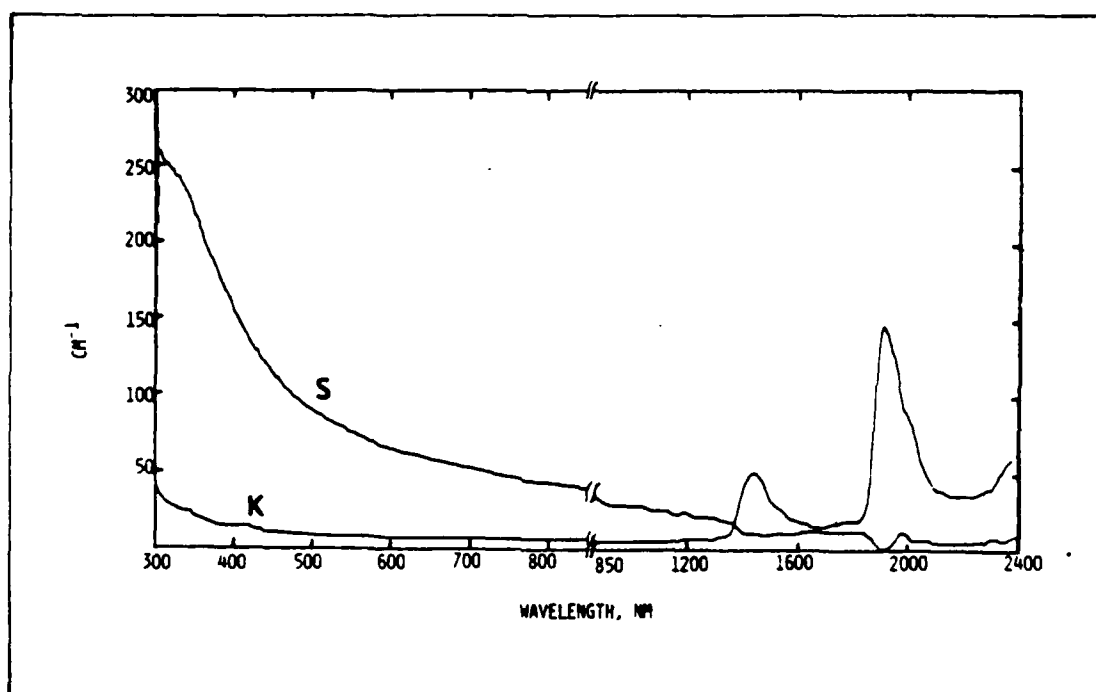


Figure 6. (2:17). Diffuse Scattering (S) and Absorption (K) Coefficients for Human Dermis. Data is calculated from the Kubelka-Munk theory of radiation transfer.

water content (21:695), one may conclude that these tissues, too, evidence relatively low absorption. It is not possible to determine the absolute absorptance of the fatty tissues at near μ m wavelengths (data in the literature seems to be concentrated in the microwave or ultraviolet region of the spectrum). Calculations to be done in Chapter III will show that total theoretical transmission based on a model assuming low absorptance is not at great variance with transmission data collected under actual transillumination. Consequently, the model of breast tissue adopted in this research considers breast tissues to exhibit low absorption of near infrared radiation except in areas where blood plasma is present.

Light Scattering Properties of the Breast.

In this section, the scattering properties of fatty tissues, collagen fibers, and whole blood are described.

However, before considering particular tissue types, it is convenient to describe some qualitative aspects of scattering, in general.

First, if the size of a particle is much smaller than a wavelength, the scattering cross section σ_s (a measure of the strength of scattering) is inversely proportional to the fourth power of the wavelength and directly proportional to the square of the volume of the particle (19:13) (see Appendix A for a definition of σ_s). This type of scattering is called Rayleigh scattering. It is generally isotropic (equal in all directions) in its radiation pattern and comparatively weak due to the λ^{-4} dependence. As particle size increases and becomes comparable to a wavelength, the scattering is much stronger than in Rayleigh scattering and is forward directed (or in a dipole pattern). When particle size greatly exceeds the wavelength, the

scattering cross section is proportional to λ^{-2} and is stronger than Rayleigh scattering but weaker than scattering from particles close to a wavelength in size. In this case, the scattering is more forward directed. This third classification of scattering will be referred to as large particle scattering.

Parrish, in discussing the types of scattering (as described above) which occur in skin stated, ". . .all these general types of scattering occur, but quantitatively, scattering by structure with dimensions on the order of optical wavelengths or somewhat larger must dominate over Rayleigh scattering." (2:14).

For wavelengths around 1μ m, Rayleigh scattering is not likely to occur in fatty tissues which are comparatively homogeneous on a scale of micrometers. This scattering would be due to fat molecules and be proportional to λ^{-4} and to V^2 where V is the volume of a molecule. This scattering should, therefore, be weak. Further, since breast tissue in younger persons tends to be more fibrous than fatty in nature, the contribution to scattering on the part of fatty tissues can be considered small in transillumination applications.

The situation is quite different, however, when the scattering properties of collagen fibers are considered. With regard to the transmission properties of these fibers in the dermis, Parrish writes:

"The data indicates that the Beer-Lambert relation is invalid for dermis, and that transmittance is both higher and more forward directed for longer wavelengths over the region between 0.5 and 1.23μ m. These observations suggest that scattering is of major importance in the dermis." (2:17)

In discussing Findlay's study of pig dermis, it was pointed out that collagenous material exhibited little absorption over the entire visible spectrum. Thus, from the above remarks, it may be concluded first of all, that collagen fibers represent a primarily scattering medium rather

than an absorptive one. It should be noted that, on a particle scale, collagen fibers exhibit an identity of structure not only throughout the body of an individual but across species as well (see Figures 7 and 8). Thus, it is considered here that scattering by collagen in the breast is, to a very good approximation, comparable to that found in dermal collagen.

So far, a discussion of the optical properties of fibrous breast tissue has led to the conclusion that this material is highly scattering and contributes very little to absorption. It remains to both quantify this conclusion (in so far as it is possible to do so given the comparative lack of data in this area) and to characterize the angular distribution of radiation scattered by collagen fibers. The problem of radiation distribution will be considered first to be followed by a discussion of the approximate dimensions of the scatterers.

It is possible, based on the data presented in Figure 9, to place some bounds on the distribution of scattered radiation from collagen fibers. The data in Figure 9 graph A for the thin sample of dermis of thickness $0.43\mu\text{m}$ shows that for longer wavelengths the scattering pattern of the tissue as a whole is concentrated in the forward direction. Compared to the thick sample of dermis, the thin sample reflects much more clearly the scattering properties of individual microscopic scattering centers. This is due to the fact that the light propagating through the thick sample is multiply scattered many times over effectively masking or averaging out the contributions of individual scatterers. The data previously presented in Figure 5 giving percent remittance (R) and transmittance (T) for a $200\mu\text{m}$ thick section of dermis is reproduced in Figure 9 as graph B. Graph B of Figure 9 gives absolute values of remittance and transmittance while graph A

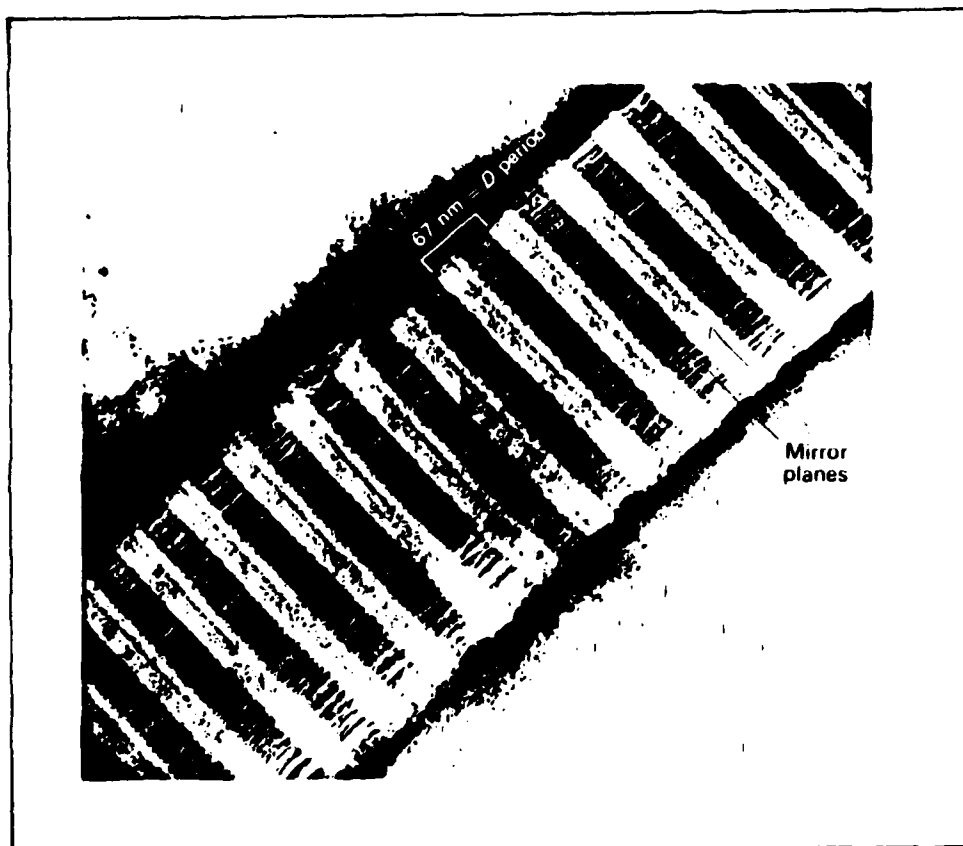


Figure 7. Rat tail tendon collagen fibril (39:16).

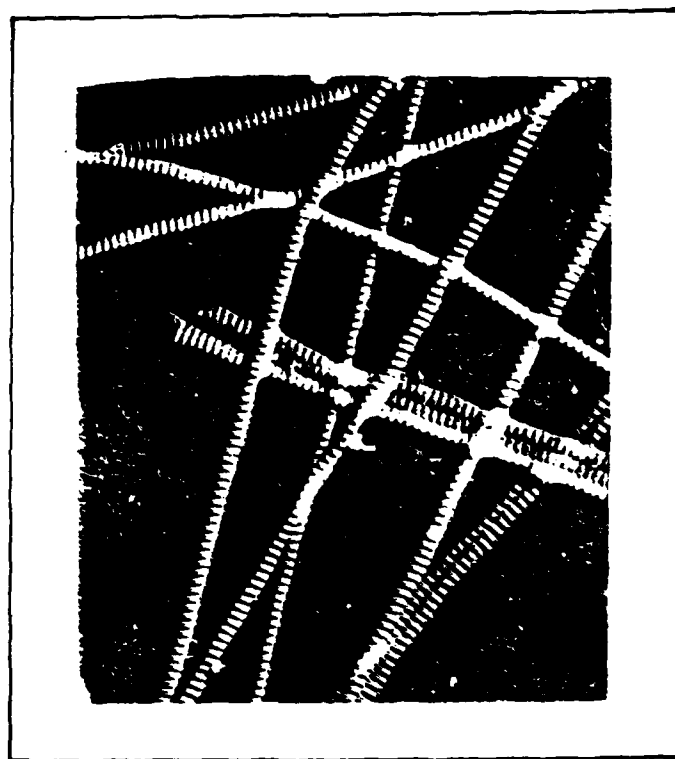
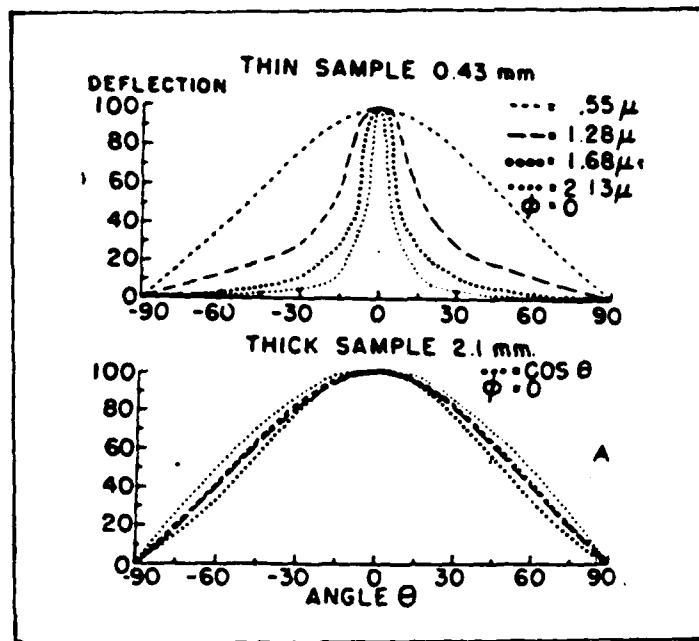
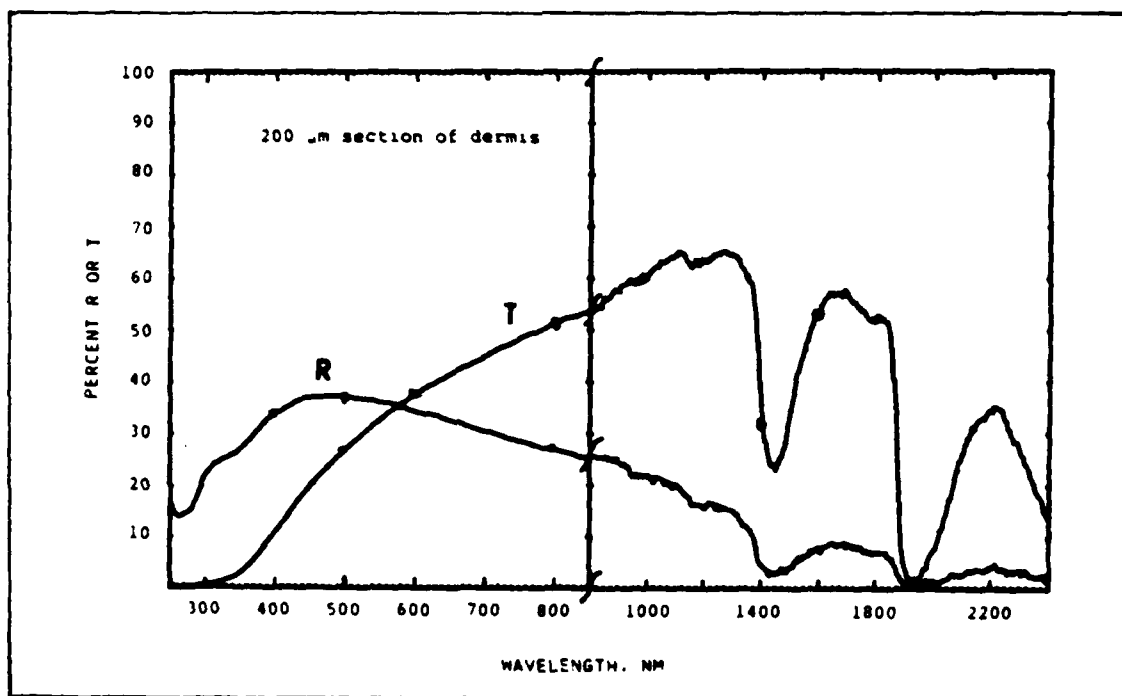


Figure 8. Collagen teased from a sample of human skin x 33,000 (37:53).



(A)



(B)

Figure 9. Graph A: Scattering Angle Dependence on Wavelength (17:259). Upper curves correspond to thin sample; lower curves to thick sample. Graph B: Spectral transmittance and remittance of a 200 μ m thick section of human dermis. Data is given in percent remittance (R) or transmittance (T).

represents percentage of total output scattered in a direction at the output plane. Of course, the data in graphs A and B of Figure 9 must be consistent with one another and an adequate theory of scattering in the breast must account for both sets of data.

An assumption that the microscopic scattering patterns of individual scattering centers are forward directed can be shown to be consistent with all the data presented in Figure 9. First, it is important to note that this data was collected from a gross sample of $200\mu\text{m}$ in thickness. The transmittance and remittance values, therefore, are the result of scattering contributions from a great many scattering centers. The fact that there are many scattering centers (consistent with the intense scattering known to characterize meshes of collagen fibers) implies that virtually all the photons are scattered during propagation through the tissue. Further, graph B of Figure 9 shows that at approximately $1.23\mu\text{m}$ where transmission is greatest, the ratio of transmitted to remitted light is about four to one. Therefore, the most likely explanation for the narrow output scattering pattern of the thin sample for longer wavelengths is that the individual scattering centers in the tissue scatter light in a primarily forward direction. In accordance with the general principles regarding size of particles, wavelength, and scattering outlined on pages 17 and 18, this forward directed scattering implies that the scattering centers are, on the average, larger than a wavelength of about $1\mu\text{m}$. The work of Hardy, et al. (17) supports this conclusion:

For thicknesses as great as 1mm scattering is maximal at all wavelengths although for the thinner specimens there is a wavelength dependence of scattering. This dependence, although varying inversely with wavelength, is far different from the Rayleigh scattering. This is to be expected as the 'particle size' of the scattering elements of the skin specimen is probably not less than that of a wavelength of light in the spectral range studied in these experiments (17:258).

At first glance, however, this conclusion regarding the scattered radiation patterns seems to be at variance with the fact that collagen fibers, though they may be a few micrometers in length, have an average diameter of approximately 100nm. This fact makes each fiber, in one dimension, at least 10 times smaller than a $1\mu\text{m}$ wavelength. Since the fibers are much smaller than a wavelength, one would expect the scattered radiation to be distributed almost equally in space at least about the axis of the fiber. To conclude that the scattered radiation is isotropic in the axial direction, would, however, be incorrect as the following will show.

Collagen fibers derive their collective strength as supportive structures from their high number density in a unit volume. Some idea of their density and arrangement may be gleaned from Figure 8 which shows a number of these fibers taken from a human specimen. As particles are packed closer together, the scattering properties they exhibit individually, or in small numbers, change dramatically (33:913-914). For dense particles, the scattering, in fact, decreases since, the denser the particles get, the more they begin to resemble a homogeneous medium. Under these circumstances, the product of the number density particles of ρ_n and the scattering cross section σ_s becomes $\rho_n \sigma_s = w(1 - w)\sigma_s/V_e$. Here, w is the fraction of the total volume of the gross medium which all the scattering particles take up and V_e is the volume of a single particle. The factor $w(1 - w)$ is parabolic with a maximum value at $w = 0.5$. This means that $\rho_n \sigma_s$ has the same value at $w = 0.95$ that it has at 0.05. However, the identity of the scatterers themselves may change from that of the particles at $w = 0.05$ to the interstitial gaps between particles at $w = 0.95$.

Considering Figure 8 and drawing upon the arguments above, one is

led to conclude that in a dense mesh of collagen fibers, the actual scattering centers are probably more accurately identified with the gaps between fibers or bundles of fibers with dimensions comparable to or perhaps larger than an optical wavelength. This estimate in size of the scattering centers should, in all likelihood, be revised upward to obtain a large particle approximation to scattering consistent with the transmittance and remittance data in Figure 5. Considering, again, the data in Figure 9, it may be felt that the angular spread of radiation for shorter wavelengths (such as $0.55\mu\text{m}$) is inconsistent with large particle scattering since these short wavelengths are smaller than the dimensions of gaps between fibers. A possible explanation for the phenomenon may be that the shorter wavelengths are exciting a different scattering species (perhaps the fibers themselves).

To close this section, a final comment regarding optimal transmittance through dermal tissue is called for. The reader will recall from Figure 5 that transmittance is greatest at a wavelength of about $1.23\mu\text{m}$. This suggests that, if internal fibrous tissue of the breast is similar to dermal collagen in structure, then a relatively good value of transmittance may be obtained in breast transillumination at $1.23\mu\text{m}$. At this wavelength absorption in the fibrous tissue is low (about 20 percent) and, therefore, light contrast due to differential absorption between cancers and surrounding tissues should be comparatively good. The suggestion to detect light of $1.23\mu\text{m}$ is made in view of the fact that detection in transillumination is now performed using silicon detectors whose responses extend to about $1.4\mu\text{m}$ but no further. Therefore, the transmission data so far collected in transillumination does not include transmittances for wavelengths beyond $1.4\mu\text{m}$.

Although transmittance maxima also occur at 1.7 and $2.2\mu\text{m}$, wavelengths in these regions suffer greater absorption and it can be expected that contrast in transillumination at these wavelengths would decrease somewhat from that at $1.23\mu\text{m}$.

Light Scattering in Whole Blood.

Whole blood consists of red blood cells and blood plasma. In normal blood tissue, the red blood cells account for approximately 40 percent of the total blood volume. Thus, 60 percent of blood is plasma which is almost entirely made up of water.

Considered in isolation, red blood cells which are about $7\mu\text{m}$ in diameter and $2\mu\text{m}$ in thickness, are highly scattering in a forward direction at near infrared wavelengths (19:63,66). However, because the cells are surrounded by plasma, radiation spanning the red and near infrared is absorbed in the plasma either before it reaches the cells or after scattering from them. This accounts for the shadows cast in transillumination by superficial blood vessels and by the mass of proliferated blood vessels which surround the highest percentage of tumors in the breast. Consequently, whole blood in breast tissue is considered primarily an absorptive medium vice a scattering one in transillumination.

Taking together, then, the data and arguments presented above, one may obtain a reasonable model of light interaction with breast tissues at red and near infrared wavelengths. The features of this model would include

- (1) Low absorption in tissues surrounding blood vessels and cancers,
- (2) High absorption in blood and blood vessels massed about cancers,

- (3) Low scattering in fatty and whole blood tissues, and
- (4) Intense highly forward directed scattering in the intralobular connective tissue made up of collagen fibers.

This model will be assumed in Chapter II in the development of the mathematical theory of multiple scattering as it applies to transillumination. There the reader will find the propagation of near infrared wavelengths through tissues surrounding breast tumors to be described by mathematical functions which provide for forward directed scattering, relatively large scattering cross section σ_s , and low absorption.

II. Scattering Theory

As will become clear in the discussion to follow, a central goal of the mathematical development of scattering theory as it applies to breast transillumination must be to calculate the correlation function (or mutual coherence function) for a scattering medium. The correlation function is an important quantity in the calculation of both the point spread function and the limitation of resolution of an imaging system in the presence of a random medium. It will become clear that the correlation function is the key to a quantitative determination of the quality of imaging that can be expected. From a knowledge of the point spread function, one can estimate the efficacy of the techniques of image processing such as phase retrieval which employ extrapolation from the Fourier modulus.

The mathematical development to follow proceeds along two differing lines of thought corresponding to the analytic and transport theories of scattering in a random medium. The analytic theory (also called multiple scattering theory) begins with Maxwell's equations or the wave equation and develops differential or integral equations for statistical quantities of interest. The transport theory, on the other hand, is not based on an electromagnetic wave approach but deals directly with the movement of energy through a medium containing scattering and absorbing particles. Since the transport theory does not develop from electromagnetic wave propagation, it does not directly include diffraction and interference effects--these effects enter indirectly through the scattering cross section (σ_s) and the absorption cross section (σ_a) (σ_s and σ_a being measurable quantities) (19:147).

Although the analytic and transport theories of scattering take

quite different points of view, it can be shown that the two theories are connected. Specifically, the correlation function of analytic theory and the specific intensity of transport theory are a Fourier transform pair (20:275). Thus, although the transport theory does not contain information as to fields, it is possible to calculate the correlation of fields via a Fourier transform. This concept will be exploited when the correlation function for a slab of tissue will be derived based on a knowledge of the specific intensity.

Twersky's multiple scattering theory is developed in Appendix A where the integral equation for the correlation function is obtained. This theory was chosen as it has been successfully applied by investigators to scattering problems in biological media (30). Twersky's correlation function is defined and its relation to the specific intensity of transport theory through a Fourier transform is shown.

A solution of the transport equation as tailored to the case of the plane-parallel slab of tissue is obtained. The slab configuration was chosen as it corresponds well to the clinical set-up for transillumination of the breast where the breast is itself compressed into the form of a plane-parallel medium (precisely as is done in X-ray mammography).

This chapter presents four topics: (1) the correlation function for analytic theory, (2) the connection between the analytic and transport theories, (3) the limitation on image resolution due to a scattering medium, and (4) the signal to noise ratio relevant to transillumination. It will be shown that according to scattering theory embodied in the four topics above, the image obtained via transillumination cannot be improved without first reducing the scattering by some physical means

before image processing is applied. This conclusion will lead in Chapter III to a consideration of time gating and spatial filtering- a method of imaging which attempts to reduce the effective scattering (and thus reduce noise) by temporal and spatial discrimination of photon paths.

The Correlation Function From Analytic Theory

The correlation function $\Gamma(\mathbf{r}_a, \mathbf{r}_b)$ of analytic theory for the scattered field at points \mathbf{r}_a and \mathbf{r}_b is presented here as it will be used later to calculate the limit of resolution one can expect to obtain when imaging through a random medium. This limitation of resolution is important to the transillumination problem as it will define the theoretical limits of the efficacy of transillumination and will provide quantitative methods for determining these limits.

Twersky's integral equation for the correlation of the field ψ^a at a point \mathbf{r}_a and ψ^b at a point \mathbf{r}_b in a random medium is (35:99)

$$\langle \psi^a \psi^{b*} \rangle = \langle \psi^a \rangle \langle \psi^{b*} \rangle + \int v_s^a v_s^{b*} \langle |\psi|^2 \rangle \rho(\vec{r}_s) d\vec{r}_s \quad (1)$$

where

$$v_s^a = u_s^a + \int u_t^a v_s^t \rho(\vec{r}_t) d\vec{r}_t \quad (2)$$

v_s^a and v_s^b are called multiple scattering operators. Their function is to convert a wave incident on a scatterer at a location \mathbf{r}_s into a scattered wave which is then subsequently observed at location \mathbf{r}_a (in the case of v_s^a) or \mathbf{r}_b (in the case of v_s^b). The function $\rho(\mathbf{r}_s)$ represents the number density of scatterers per unit volume as a function of position. In equation (2) the symbol u_s^a represents the

scattering of a wave incident on a scatterer at location \mathbf{r}_s and propagating through free space to a point \mathbf{r}_a . Thus, u_s^a is called the free space scattering operator. The form of the operators, v_s^a , v_s^b , and u_s^a are derived in detail in Appendix B. The brackets $\langle \rangle$ in equation (1) indicate the usual time average value and equation (1) is integrated over all scatterers in the medium. In order to complete the calculation of the correlation function given by equation (1), it would be necessary to find expressions for the quantity $\langle \psi^a \rangle \langle \psi^{b*} \rangle$ and $\langle |\psi^s|^2 \rangle$ using the analytic theory. But complete solutions for the Twersky integral equation for the correlation function have not appeared in the literature. However, as adumbrated at the beginning of this chapter, a methodology does exist for the complete calculation of the correlation function based on the fact that the correlation function of analytic theory and the specific intensity of the transport theory are a Fourier transform pair. It remains now to justify the assertion that this Fourier transform connection exists between the analytic and transport theories. Once this connection is established, it will be possible to depart from the analytic theory and calculate the correlation of fields from the specific intensity. The reader will find a description of the transport theory and specific intensity in Appendix C.

The Connection Between the Analytic and Transport Theories

Although solutions for Twersky's correlation function based on analytic theory have not yet appeared, various solutions for the specific intensity in radiation transport theory do exist. The reader is referred to Appendix C for a description and discussion of transport theory. In this section, the connection between the correlation function and specific intensity is described. With this knowledge in

hand, it will be possible to obtain information regarding correlation of fields despite the fact that radiation transport theory is not based on electromagnetic field equations. In later developments, it will be seen that the correlation function enters as an essential quantity in the calculation of the limit of resolution of an imaging system. Thus, the transport theory becomes a powerful tool in the analysis of imaging of the breast by transillumination. The specific intensity $I(\mathbf{r}, \mathbf{s})$ is measured in $\text{Wm}^{-2}\text{sr}^{-1}\text{Hz}^{-1}$ and is the average power flux density within a unit frequency band centered at frequency and radiating in the direction \mathbf{s} from a point \mathbf{r} on a radiating surface. See Figure 10.

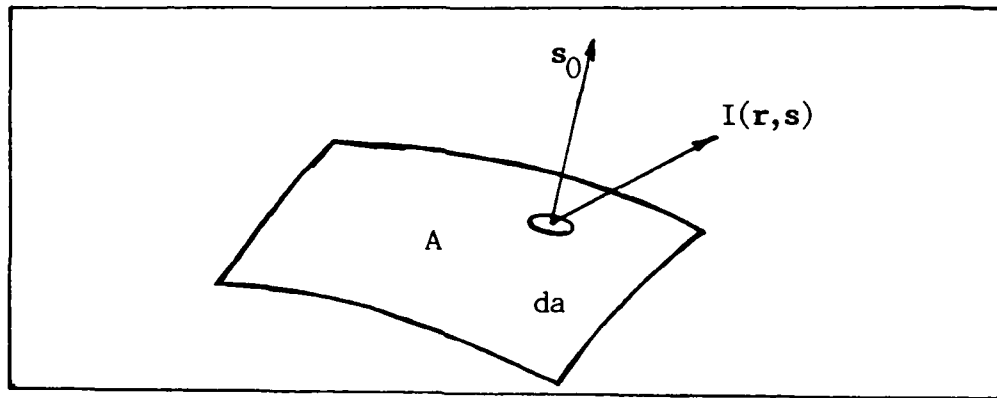


Figure 10. Flux through da on a surface A (19:150).

The correlation function presented in equation (1) and the specific intensity are related by (20:275)

$$\langle \psi(\vec{r}_a) \psi(\vec{r}_b) \rangle = \Gamma(\vec{r}_a, \vec{r}_b) = \Gamma(\vec{r}, \vec{r}_d) = \int I(\vec{r}, \hat{s}) \exp(iK_r \hat{s} \cdot \vec{r}_d) d\Omega \quad (3)$$

where $\mathbf{r} = 1/2(\mathbf{r}_a + \mathbf{r}_b)$ and $\mathbf{r}_d = (\mathbf{r}_a - \mathbf{r}_b)$, and K_r is the real part of the complex wave number for a scattering medium (see Appendix B for a description of K).

It can be shown that, assuming the validity of equation (3), the integral equation for the average intensity in transport theory can be derived (see Appendix D). Since this is the case, it follows that the

correlation function of analytic theory and the specific intensity of transport theory are a Fourier transform pair precisely as stated in equation (3).

Limitation on Image Resolution Due to a Scattering Medium

The reader will recall from Chapter I that, for the purposes of transillumination, the breast is compressed into a plane-parallel optical medium. In this section, the limit of resolution of an imaging system in the presence of a plane-parallel scattering medium is considered. The reason for calculating such a resolution limit is that it provides a measure for assessing the efficacy of imaging via transillumination. How this is the case will become clear as the discussion proceeds. Using the Fourier transform relation between the correlation function and the specific intensity, the correlation function for a plane wave (in the large particle scattering approximation) incident upon a scattering medium is presented. Figure 11 depicts the physical set up for the calculation of the limit of resolution.

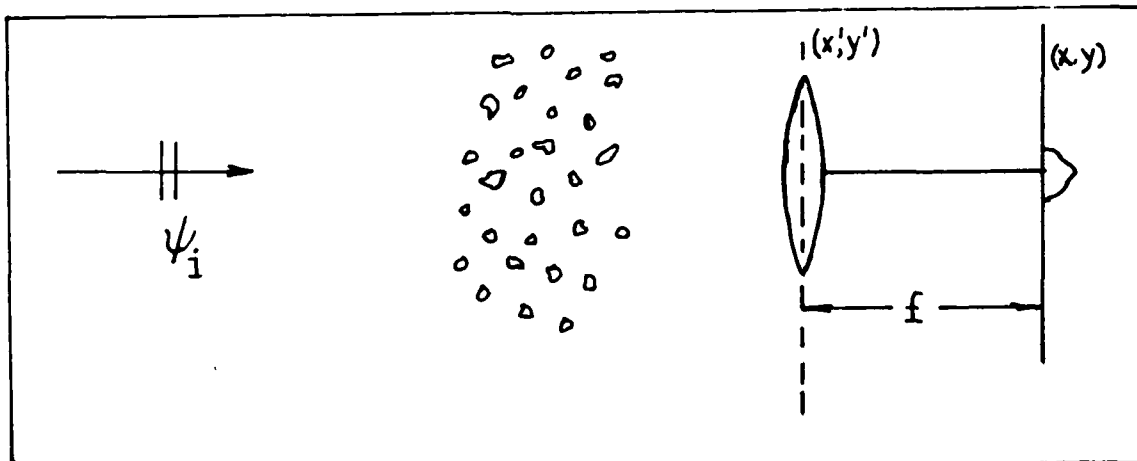


Figure 11. A monochromatic plane wave ψ_i propagating through a random distribution of scatterers (20:301). The resultant scattered wave is focused onto the x, y plane (Fourier transform plane). The lens has radius a and focal length f .

The assumption, based on the optical model presented in Chapter I,

that scattering is due primarily to particles larger than a wavelength in the near infrared implies that the scattering pattern of an individual particle is forward directed. A mathematical formulation of a forward scattering pattern may be obtained by means of a phase function $p(s)$ which describes the amount of power which is scattered into a direction s by a scatterer. A forward-directed scattering pattern may be approximated by giving $p(s)$ a Gaussian form:

$$p(\hat{s}) = 4\alpha_p W_0 \exp(-\alpha_p s^2) \quad (4)$$

where, for large scatterers $\alpha_p = 2.66 (D/\lambda)^2$ where D is the particle diameter and λ is the wavelength of incident radiation. W_0 is called the albedo of the scatterer and is defined as

$$W_0 = \sigma_s / (\sigma_s + \sigma_a) = \sigma_s / \sigma_t \quad (5)$$

where σ_s is the scattering cross section of a particle, σ_a is the absorption cross section, and σ_t (total cross section) is equal to $\sigma_s + \sigma_a$.

In appendices E and F, it is shown that the correlation function $\Gamma(z, q)$ for a plane-parallel medium with plane wave incidence is

$$\Gamma(z, \vec{q}) = I_0 \exp \left\{ -\rho_n \sigma_t z \left[1 - W_0 \exp(-q^2/4\alpha_p) \right] \right\} \quad (6)$$

where ρ_n is the number density of scatterers per unit volume. The quantity $q = K_r \vec{\rho}_d'$ where K_r is, again, the real part of the complex wave number for a scattering medium and $\vec{\rho}_d' = \vec{\rho}_1' - \vec{\rho}_2'$ where $\vec{\rho}_1'$ and $\vec{\rho}_2'$ are points in the x', y' plane as picture in Figure 11. Thus, $\Gamma(z, q)$ represents the correlation of fields originating at points $\vec{\rho}_1'$ and $\vec{\rho}_2'$

as measured a distance z in the horizontal direction in Figure 11.

The intensity in the focal plane of the lens pictured in Figure 11 is equal to the point spread function $P_f(\vec{\rho})$ for the system depicted since, in this case, the image is that of a point source at infinity. In physical terms, the point spread function describes the effect the scatterers have on the resultant image. Heuristically, the point spread function states that the point source is "spread out" in the focal plane. The reader will note the conspicuous absence of a cancer in the medium in Figure 11. The reason for this is that the goal of calculating the resolution limit is to gain an understanding of the effect of the scatterers on a propagating wave. The image that results from imaging an opaque object (in this case a cancer surrounded by blood vessels) through a non-scattering medium is well understood. Thus, it is only necessary to image the scatterers alone to obtain the required understanding of the effect of scattering on cancer detection by transillumination.

The point spread function $P_f(\vec{\rho})$ or intensity in the focal plane of Figure 11 can be shown to be (see Appendix G)

$$P_f(\rho) = \frac{k^2}{2\pi f^2} \int_0^{2a} \rho'_d d\rho'_d J_0\left(\frac{k}{f} \rho \rho'_d\right) \Gamma(z, \rho'_d) K(\rho'_d) \quad (7)$$

where $k = 2\pi/\lambda$, f = focal length of a lens, a = radius of lens, $K(\rho'_d)$ is the pupil function, and $\rho'_d = \rho'_1 - \rho'_2$. The quantity ρ is a point x, y at a distance $(x^2 + y^2)^{1/2}$ from the horizontal axis (see Figure 11).

In Appendix G it is shown that for an optically thick medium, the point spread function $P_f(\rho)$ may be expressed as the sum of a coherent (average) part and an incoherent (fluctuating) part:

$$P_f(\rho) = P_c(\rho) + P_i(\rho) \quad (8)$$

where $P_c(\rho)$ is the coherent portion of $P_f(\rho)$ and $P_i(\rho)$ is the incoherent portion. Also shown in Appendix G are expression for $P_c(\rho)$ and $P_i(\rho)$:

$$P_c(\rho) = I_0 \exp(-\tau) (a/\rho)^2 J_1^2(k\rho a/f) \quad (9)$$

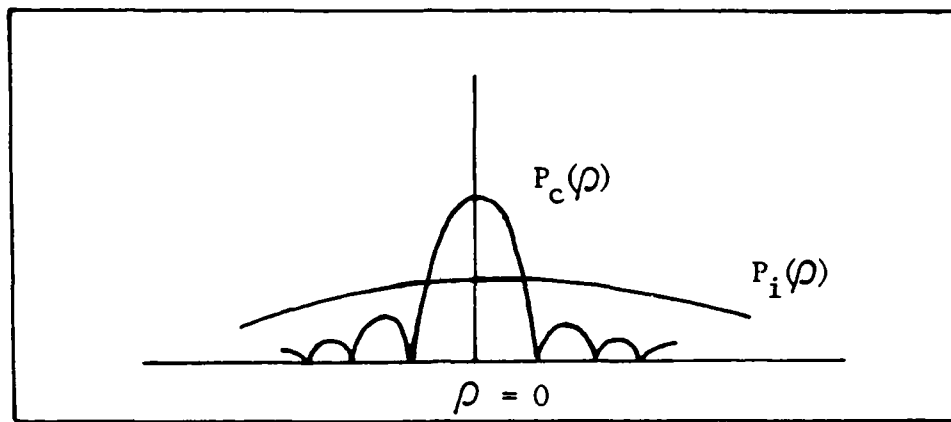
and

$$P_i(\rho) = I_0 (a/\rho_i)^2 \exp[-\tau(1 - W_0) - (\rho/\rho_i)^2] \quad (10)$$

where $\tau \equiv$ optical thickness $= \rho_n (\sigma_s + \sigma_a) z$. Again, ρ_n is the number density of scatterers per unit volume, σ_s and σ_a are the scattering and absorption cross sections, and

$$\rho_i^2 = (K_r f/k)^2 (\tau W_0 / \alpha_p) \quad (11)$$

The quantity z in the expression for τ is, for the transillumination problem, the physical thickness of a breast compressed for transillumination. The relationship between $P_c(\rho)$ and $P_i(\rho)$ is shown in Figure 12 where $P_i(\rho)$ is superimposed over $P_c(\rho)$.



(Distance across the focal plane).

Figure 12. $P_c(\rho)$ is the Airy pattern created by the imaging of the coherently propagating portion of the intensity (20:305). The incoherent intensity $P_i(\rho)$ is spread out over the focal plane and increases with increasing optical thickness T .

The coherent intensity is the image bearing component of the total intensity. If $P_i(\rho)$ is less than $P_c(\rho)$ around the point $\rho = 0$, it is possible to obtain an image of an object surrounded by a scattering medium. However, if $P_i(\rho)$ is greater than $P_c(\rho)$, the image is "washed out" by the incoherent intensity (20:305). Note, however, that even in cases where $P_i(\rho) < P_c(\rho)$, if $P_i(\rho)$ is significant, the contrast in the image may be quite poor. Under these circumstances some resolution may be possible but the image will still be difficult to see.

The Signal to Noise Ratio

Based on the development in the previous section it is possible to define a signal to noise ratio in terms of the coherent intensity $P_c(\rho)$ and the incoherent intensity $P_i(\rho)$. It should be understood at the outset that the noise (which will be defined as the incoherent intensity) is not additive. In fact, the incoherent noise is created directly from the coherently propagating intensity as it is scattered by the medium. Thus, as the incoherent intensity grows, the coherent intensity diminishes.

The signal to noise ratio will be defined as the ratio of the coherent to incoherent intensities:

$$\frac{P_c(\rho)}{P_i(\rho)} = \text{signal to noise ratio} = \frac{S}{N} \quad (12)$$

To simplify the calculation, consider the signal to noise ratio at the point $\rho = 0$:

$$\begin{aligned} \left. \frac{S}{N} \right|_{\rho=0} &= \frac{I_0 \exp(-\tau) (a/\rho)^2 J_1^2 \left(\frac{k \rho a}{f} \right)}{I_0 (a/\rho_i)^2 \exp[-\tau(1-W_0) - (\rho/\rho_i)^2]} \Big|_{\rho=0} \\ &= \lim_{\rho \rightarrow 0} \frac{(1/\rho)^2 J_1^2 \left(\frac{k \rho a}{f} \right)}{(1/\rho_i)^2 \exp(\tau W_0) \exp(\rho/\rho_i)^2} \end{aligned} \quad (13)$$

Expanding the numerator using the formula

$$J_1(x) = x/2 - x^3/2^2 \cdot 4 + x^5/2^2 \cdot 4^2 \cdot 6 - x^7/2^2 \cdot 4^2 \cdot 6^2 \cdot 8 + \dots ;$$

$$\left. \frac{S}{N} \right|_{\rho=0} = \frac{(\kappa^2 a^2 / 4 f^2)}{(1/\rho_i)^2 \exp(\tau W_0)} \quad (14)$$

and then recalling that

$$\rho_i^2 = (\kappa_r^2 f^2 / k^2) (\tau W_0 / \alpha_p) \quad (11)$$

the signal to noise ratio becomes

$$\left. \frac{S}{N} \right|_{\rho=0} = (K_r a / 2)^2 (\tau W_0 / \alpha_p) \exp(-\tau W_0) \quad (15)$$

It can readily be seen that the signal to noise ratio is strongly a function of $\tau = \rho_n (\sigma_s + \sigma_a) z$ as S/N falls exponentially with increasing optical thickness.

As an example of a calculation of S/N in a biological medium, the signal to noise ratio for a dilute blood medium will be obtained. The physical parameters employed are the same as those used by Maarek et al. (24) in a Monte Carlo simulation of photon propagation in a tissue medium (see the section entitled "Time Gating the Output" in Chapter V). This allows comparison of calculation techniques.

Before the calculation is attempted, however, a brief digression to discuss the relationship of the scattering cross section to particle density is required. As the number density of scatterers increases, the particles are packed closely together. As the ratio of total volume of scatterers to total volume of medium approaches 1, the particles are packed together in such a manner as to create a homogeneous medium of particles in which no scattering occurs. Thus, based on the argument above, one is led to the following approximation for the factor $\rho_n \sigma_s$:

$$\rho_n \sigma_s = [w(1-w)\sigma_s] / V_e \quad (16)$$

where w is the ratio of the total volume of particles to the total volume of the medium and V_e is the volume of a single particle.

Equation (16) was obtained by Twersky via a more mathematically rigorous approach (33:913). Incidentally, these considerations throw

some light on why transillumination can, in some instances, give better results for dense tissues than can x-ray mammography.

As in the study done by Maarek et al. (24) the following calculation assumes a hematocrit H (the ratio of blood cell content to whole blood where whole blood consists of blood cells and plasma) of 0.05. Thus, in this case, the quantity $H = w$. In addition to H , the equations listed below were substituted into equation (15) to calculate the signal to noise ratio:

$$W_0 = \sigma_s / \sigma_t = (1-H)(\sigma_s / (\sigma_s + \sigma_a)),$$

$$K_r = k + H/(1+H) k [n_1/n_0 - 1],$$

$$\alpha_p = 2.66 (D/\lambda)^2,$$

$$\tau = \rho_n (\sigma_s + \sigma_a) z = \left[\frac{w(1-w)\sigma_s}{V_e} \right] (z) + \rho_n \sigma_a z$$

and

$$V_e = \pi r^2 h$$

where r is the radius of a blood cell and h is its thickness. The equation for the real part of K (K_r) is taken from Twersky (32:168) and the ratio n_1/n_0 is the ratio of the index of refraction of a blood cell to that of water. As will be seen, the accuracy of the second term used in K_r are not critical as the signal to noise ratio is so strongly dependent on τ .

The numerical values chosen were

$$\begin{aligned}
H &= 0.05 \\
\sigma_s &= 32 \mu\text{m}^2 \\
\sigma_a &= 0.185 \mu\text{m}^2 \\
k &= \frac{2\pi}{\lambda} = 6.28 \mu\text{m}^{-1}; \lambda = 1 \mu\text{m} \\
D &= \text{diameter of blood cell} = 7 \mu\text{m} \\
h &= 2 \mu\text{m} \\
V_e &= 76.97 \mu\text{m}^3 \\
z &= \text{tissue thickness} = 4\text{cm}
\end{aligned}$$

The values for σ_s and σ_a are those supplied by Ishimaru (19:66) while blood cell dimensions (D,h) are taken from Johnson and Guy (21). The wavelength (λ) is consistent with Ishimaru's data on scattering and absorption cross sections.

Substitution of these numerical values into equation (11) gives the following result for the signal to noise ratio:

$$\begin{aligned}
\left. \frac{S}{N} \right|_{\rho=0} &= (2.21 \times 10^{10}) \exp(-746.16) \\
&\simeq 2.21 \times 10^{-334} \simeq 0
\end{aligned} \tag{17}$$

Equation (17) indicates that the coherent intensity has been completely turned into incoherent intensity by the scattering process. It might now be instructive to inquire at what point (in terms of optical thickness) one might expect to obtain a coherent image. This question

may be answered by setting the ratio $\frac{P_c(\rho)}{P_i(\rho)} = 0$ equal to unity and then solving for the optical thickness τ .

Using equation (15) one obtains

$$\left. \frac{P_c(\rho)}{P_i(\rho)} \right|_{\rho=0} = \frac{K_r^2 a^2 \tau W_0}{4\alpha_p} \exp(-\tau W_0) = 1$$

which implies that

$$\frac{K_r^2 a^2}{4} = [\exp(\tau W_0)] / \tau W_0 \quad (18)$$

The quantity α_p is proportional to $(D/\lambda)^2$ and $K_r \approx k$. Therefore, the left side of equation (18) is proportional to $(a/D)^2$ -- a quantity which is likely to be quite large in the case of transillumination. It may be concluded, then, that equation (18) is true only for large (i.e., either strong scattering and/or large thickness of medium).

Letting $\frac{(K_r a)^2}{4\alpha_p} = B$ and $\tau W_0 = x$, the following mathematical steps establish an equation for optical thickness wherein one may expect to obtain a reasonably good image in a scattering medium. First, following the definitions of B and x given above, equation (18) implies that

$$B = \exp(x)/x$$

Therefore,

$$\begin{aligned} \ln B + \ln(\ln B) &= \ln B + \ln(x - \ln x) \\ &= \ln[B(x - \ln x)] \\ &= \ln[Bx - B \ln x] \\ &= \ln[\exp(x) - (\exp(x)/x) \ln x] \\ &= \ln[e^x(1 - \ln x/x)] \end{aligned}$$

If $x \gg \ln x$, then

$$\ln B + \ln(\ln B) = \ln e^x = x \quad (19)$$

where $B = \frac{(K_r a)^2}{4\alpha_p}$ and $x = \tau W_0$.

Now if the diameter D of a scatterer is large compared to λ , then $\alpha_p = 2.66 (D/\lambda)^2$ (19:122). Substituting $\alpha_p = 2.66 (D/\lambda)^2$ into the equation for B yields

$$B = \frac{(K_r a)^2}{4\alpha_p} = 3.71 (a/D)^2 \quad (20)$$

Letting $a = 2\text{cm}$ and $D = 7\mu\text{m}$ (as in the example calculation for S/N) one obtains

$$B = 3.03 \times 10^7$$

Substituting this value of B into equation (19) one gets that

$$\ln(3.03 \times 10^7) + \ln(\ln 3.03 \times 10^7) = \tau W_0 \quad (21)$$

For a medium that is not highly absorbing (as is the case with breast tissues other than blood) $W_0 \approx 1$ and $\tau W_0 \approx \tau$. Therefore, from equation (21), $\tau = 20.08$ and

$$\rho_n (\sigma_s + \sigma_a) z \approx \rho_n \sigma_s z = 20.08 \quad (22)$$

Then using the fact that $\rho_n \sigma_s = \frac{H(1-H)\sigma_s}{V_e}$ and the same parameter values used before one obtains for z (thickness)

$$z = 1.019\text{mm}$$

This value for z , then, represents the upper limit on the thickness of tissue for which one would expect to be able to obtain a reasonable coherent image, i.e., an image which would still contain details of the object profile.

Interpretation of the Signal to Noise Ratio.

The calculation of S/N shows that, for the parameters chosen, the

coherent signal $P_c(\rho)$ is (for all intents and purposes) non-existent. The exponential factor (10^{-334}) may seem surprising since in many cases of noisy systems, although the signal to noise ratio may be quite low, equation (17) indicates an extremely weak signal, indeed (if it may be said to be there at all). However, if one considers the fact that the noise is not additive but derives from the scattering of the coherent signal itself, it is easier to see how the coherent intensity should be so overcome by the incoherent intensity that it "feeds". If the scattering cross section σ_s is at all significant, it does not take long as the wave propagation through the medium for the coherent portion of the intensity to be removed almost completely.

Given the analysis presented in this chapter, it does not appear that the optical processing techniques aimed at retrieving or enhancing the coherent intensity in order to improve imaging and are likely to succeed. Such methods as matched filtering or simple averaging of outputs to eliminate or reduce noise assume that the signal is present in the noise and is, therefore, retrievable, at least in principle. In the case of breast transillumination, however, the coherent or average signal is no longer present in the total wave. Therefore, a matched filter has virtually nothing to match. On the other hand, although averaging outputs (at, say, different angles) could theoretically reduce noise, the result would not be an enhanced coherent signal (since, in actuality, there virtually is none). Of course, the parameters chosen here for the calculation of the signal to noise ratio do not necessarily correspond exactly to those of breast tissue. The values of the parameters were chosen largely as they were simply because the scattering and absorption cross sections, density and other physical parameters for the breast were unavailable. Nevertheless, it is

reasonable to assume that breast tissue would not exhibit properties so different from those considered in this chapter that the conclusion implied by equation (17) would be changed in substance. The reader will also find that the calculation of the total intensity to be accomplished in Chapter III will show that the parameters used here yield results fairly close to those obtained under actual transillumination.

Further, one should consider that the assumption of a primarily forward scattering pattern for single scatterers constituted a "best possible" scattering medium for the retrieval of the coherent intensity. If, by chance, the single scatterers in the breast had scattered radiation patterns broader than that indicated by a Gaussian approximation to the phase function, the signal to noise ratio calculated under that circumstance could only be worse than that arrived at in the analysis presented. That is, the broader the scattering pattern of each scatterer, the more quickly would the coherent intensity be spread out through the medium and the more quickly would the coherent image bearing intensity disappear.

The development of scattering theory presented in this chapter has led to the conclusion that the coherent intensity is effectively destroyed by the intense scattering process in a biological medium of the kind considered here.

At this juncture, it is important to formulate the problem of transillumination imaging in the light of the theoretical results obtained. In particular, it is, of course, experimentally established that images of tumors are observed under transillumination despite the fact that the scattering theory presented here demonstrates an effective zero value of coherent image bearing intensity. A conclusion that may be drawn from this observation is that the imaging occurring in

transillumination is not obtained by means of the coherently propagating intensity. Instead, the shadow image cast by a tumor must be the result of differences in incoherent intensities. Therefore, to improve transillumination imaging in the near infrared, one should first concentrate on improving contrast in intensity over the image plane rather than attempting to resolve the details of the object of interest (a tumor) imbedded in the tissue.

In Appendix H, the reader will find, as an example of an attempt to recover the coherent signal, a description of the method of phase retrieval as it might be applied to breast transillumination. The results obtained in Appendix H show that the phase of the signal cannot be recovered by this method. Consequently, phase retrieval does not show promise of improving imaging by transillumination.

III. A Method for Improving Imaging in Transillumination

In this chapter a method for improving the contrast in transillumination will be presented. This technique, called Time Gating and Spatial Filtering (TGSF), concentrates on improving contrast by physically reducing the effects of scattering. The method does not attempt to retrieve a coherent signal but accentuates, instead, the contrast in incoherent intensity across the output plane.

Time Gating and Spatial Filtering of the Transmitted Radiation

Recent studies (24) based on a Monte Carlo model of propagation of light through thick (20 mm - 80 mm) heterogeneous biological samples have provided encouraging results suggesting that spatial and time discrimination of output radiation can, in some instances, significantly improve the contrast in transillumination. The work accomplished thus far has not been directed specifically toward the problem of cancer detection in the breast but the method used is certainly applicable to the problem.

Simulation of Laser Tomoscopy

This section is devoted to a description of the Monte Carlo simulation of photon propagation through a tissular medium performed by Maarek, et al. in 1986 (24). In this study, the researchers simulated the illumination of a tissular slab with a picosecond laser source. Inside the tissue there was considered to be a blood vessel which could be moved about to simulate the process of scanning the tissue with the source. At the output end of the slab was a simulated, collimated, ultrafast optical Kerr Shutter. Thus, at the shutter, both spatial and temporal discrimination of photons could be performed based on

scattering angle at the shutter and flight times of photons.

The advantage of using such an apparatus can be understood in terms of the source of noise in the imaging. As theory indicates (Chapter II) and experiment demonstrates, light scattering produces a reduction in contrast and resolution of an image. In terms of photon paths, the noise at the detector comes from photons which are first scattered far from the axis of illumination and are then eventually scattered back into the field of view of the detector. These photons cause light areas to appear where, imaging in the absence of scattering, there might otherwise be dark regions (24:207). Thus, a reduction in contrast and resolution occurs in the image. Now those photons which are scattered far from the axis of illumination and yet reach the detector travel distances greater (and have longer flight times) than those photons which tend to stay nearer the illumination axis. Consequently, a time gate at the output slab could remove noise from the total system by "discarding" those photons which take some time longer than a pre-set acceptance time to cross the tissular slab. The time gate would ensure that only those photons which tend to travel near the illumination axis would be detected.

Description of the Simulated Model

The tissular model which Maarek, et al. used is pictured in Figure 13. The tissue was a semi-infinite slab bounded by parallel planes at $x = 0$ and $x = x_{\text{max}}$. The tissue surrounding the blood vessel of radius R was assumed to be a homogeneous medium with optical characteristics equivalent to that of dilute blood with a hematocrit of 0.05 (indicating a ratio of total blood cell volume to blood cells and plasma of 0.05). The blood vessel of variable radius R centered at coordinate x_c, y_c as shown in Figure 13 contained blood with a hematocrit of 0.50. This

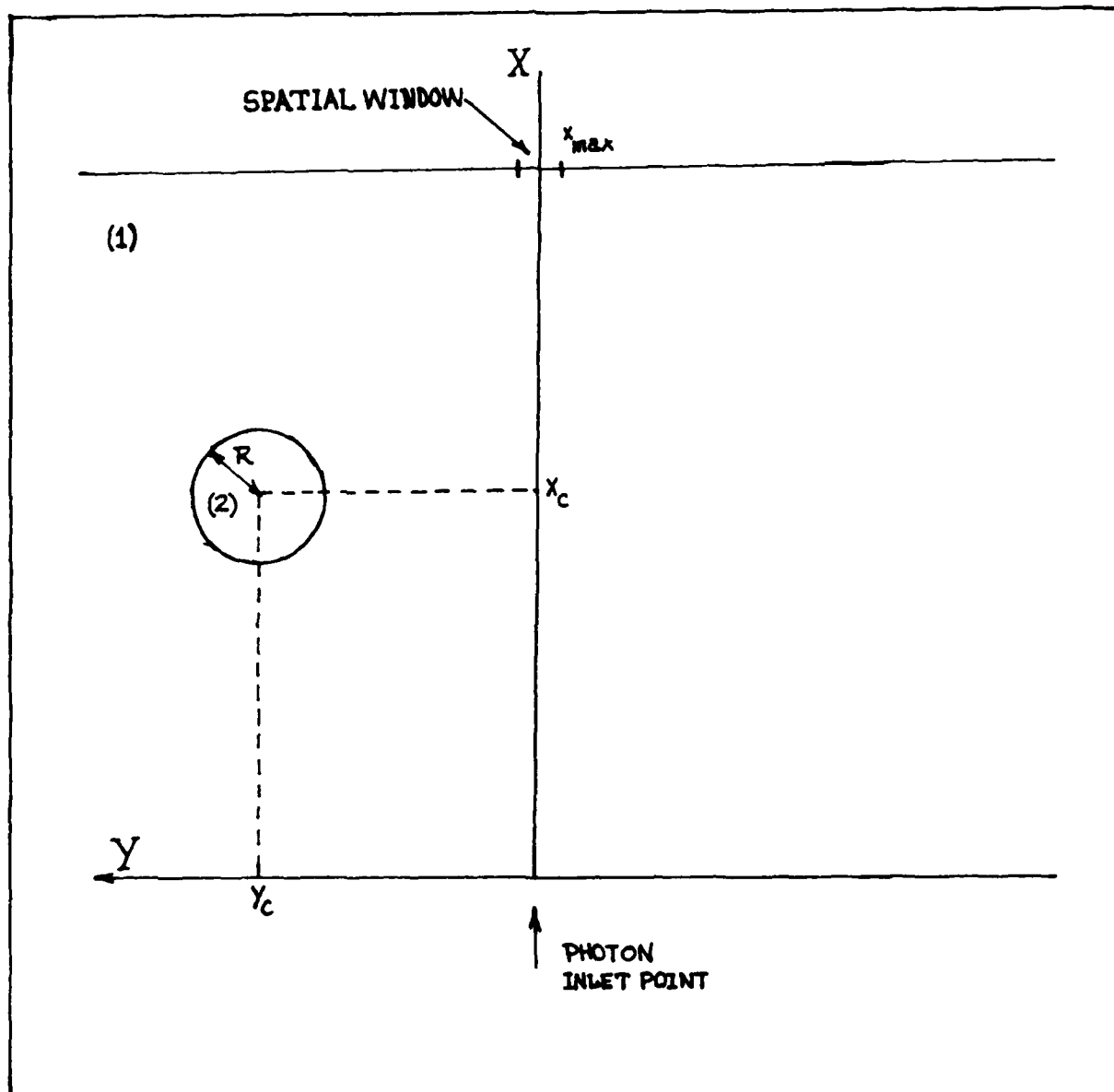


Figure 13 . Schematic representation of the heterogeneous tissue model constituted by a tissular slab (1) (thickness x_{max}) containing a blood vessel, (2) (radius R coordinates of the center x_c, y_c) (24:408).

model has some similarity to the model of the human breast described in Chapter I. It will be seen later in the description of the results of the simulation that the output intensity is, in terms of important qualitative features, very similar to that seen in transillumination of the breast. In both the surrounding medium and the blood vessel the oxygen saturation was assumed to be 100 percent and the refractive index 1.36 (4). In most cases the number of input photons was 30,000.

Optical Parameters Used in the Model

The optical parameters such as scattering and absorption coefficients S and K were calculated according to Zdrojkowski and Pisharoty (41). Path lengths between scattering events were based on work done by De Palma and Gasper (10).

Maarek, et al. reported that use of only an optical collimator is insufficient to select only those photons which travel near the axis of illumination:

It should be noted that for thin samples the probability of a photon's free path being greater than the sample thickness is fairly high and so photons can pass through without a single scattering event. It is for these situations that the use of an optical collimator can produce good image resolution using transillumination because a large number of detected photons will have travelled straight along the illumination axis (24:408).

The computation of scattering angles was the same for both the surrounding dilute blood medium and for the interior of the blood vessel and was based on experiments done by Maarek et al. on a dilute blood sample (24:408).

Transmittance and Reflectance Characteristics

To provide a baseline and normalization factor for the simulation of imaging, computations were carried out assuming a tissue sample not containing a light absorbing blood vessel. In addition, no detection aperture was included at the output end of the sample. Figure 14

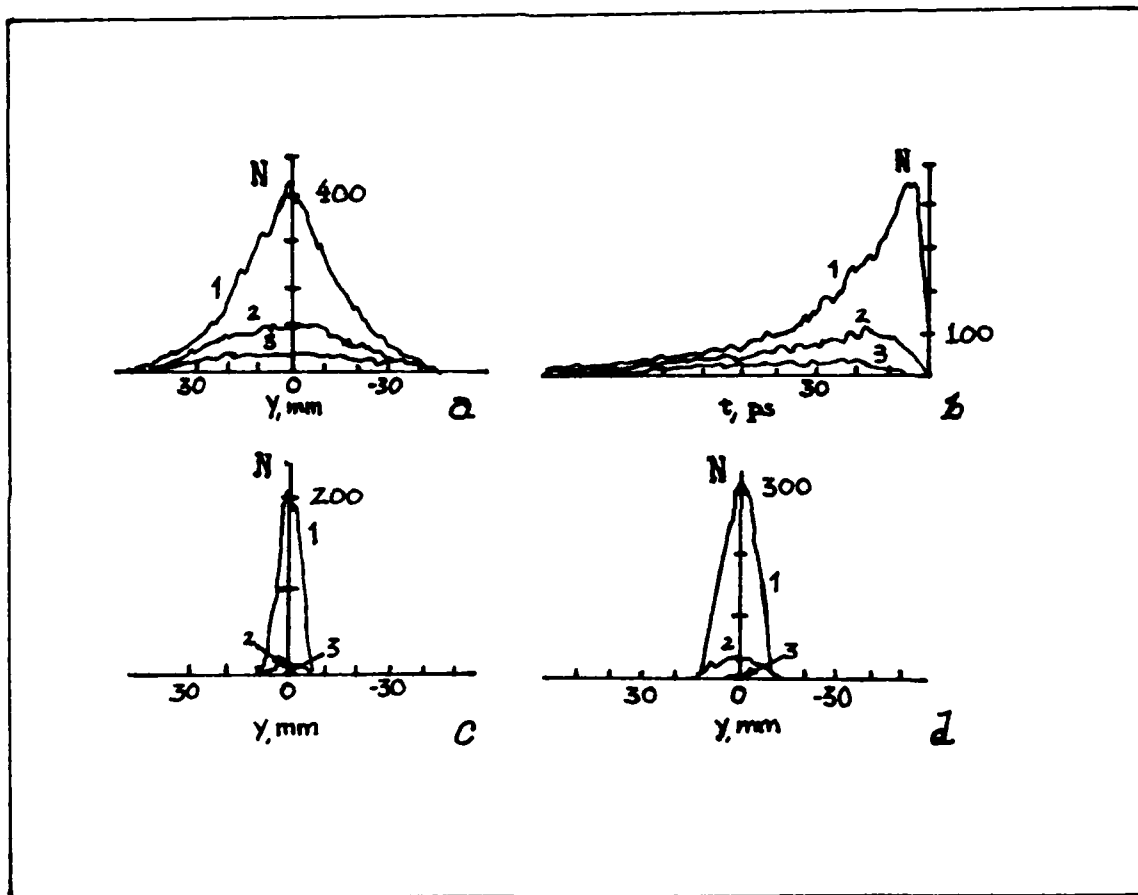


Figure 14. Variations of the number of transmitted photons (N) for three values of the medium thickness (x_{\max}); curves 1, 2, and 3 correspond to x_{\max} values of 40mm, 60mm, and 80mm, respectively (24:409). On graph (a) the number of diffusely transmitted photons is plotted as a function of emergence ordinate y (in mm). On graph (b) the same parameter is plotted as a function of emergence time t (in ps) and curves 1, 2, and 3 have been shifted to the same time origin considering that time zero corresponds to the straightforward crossing times of the media. The number of photons, N , detected with time gates of 5 ps and 10 ps have been plotted as a function of emergence ordinate y on graph (c) and (d), respectively (24:409).

depicts the results obtained for tissue thicknesses of 40mm, 60mm, and 80mm. Each of the graphs a, b, c, and d include results obtained with no time gate, a time gate of 5 ps, and a time gate of 10 ps. Figure 15 represents values of transmittance and reflectance obtained with varying thicknesses. Also included in Figure 15 are values of transmittance when a 1mm detection aperture only was used and when a 10 ps time gate only was employed.

Maarek, et al. stated that

Above sample thickness of about 50mm the reflectance R_e is approximately constant because the surface of the model has the greatest influence on the intensity of the reflected photons. Consequently, they contain no information about the deeper regions within the model (24:409).

Curve b in Figure 14 shows the flight times of photons assuming time zero corresponds to the straightforward crossing time. The curve shows that as thickness of tissue increases, an increasing number of photons have flight times greater than the straightforward crossing time t_s . In particular, for a 40mm thick sample, somewhat less than 100 photons of approximately 12,000 detected have a flight time close to t_s . In the band, for a sample 60mm thick or more virtually all photons detected have flight times greater than t_s .

Curve a in Figure 14 indicates that for a change from 40mm to 80mm thicknesses the transmittance is reduced from 21.4 percent to 3.18 percent when there is no time gate. A change in thickness from 40mm to 80mm with a time gate of 10 ps causes a decrease in transmittance from 5.8 to 0.08 percent. Under the same change in sample thickness, a reduction from 2.3 to 0.01 percent occurs with a time gate of 5 ps.

The input power required to obtain the transmittance indicated in Figure 14 can be calculated from a knowledge of the number of photons emerging from the sample and the total number of photons originally put

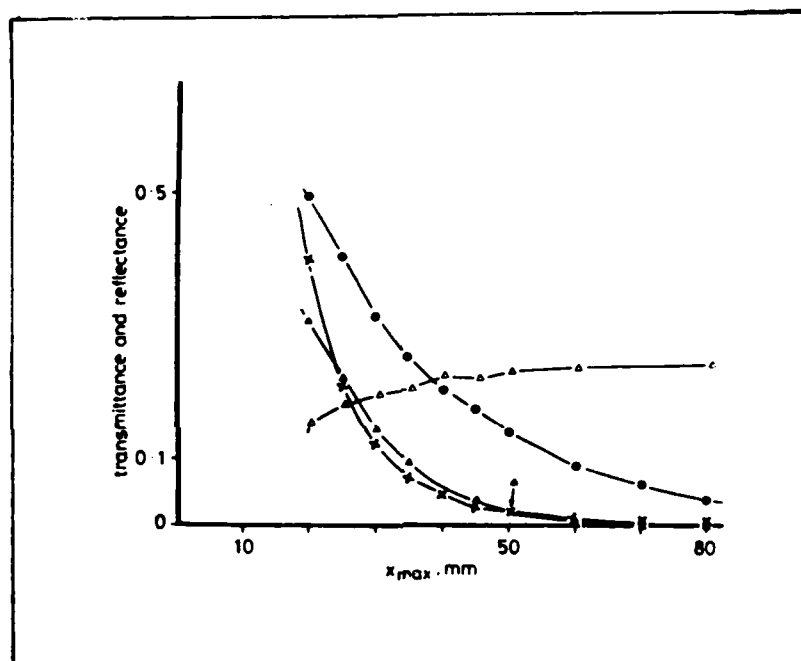


Figure 15. Variations of diffuse transmittance T_D , collimated transmittance T_{C1} through a 1mm aperture, transmittance T_{10} corresponding to a time gate of 10 ps and reflectance R_e as a function of medium thickness (x_{max}). The data are computed considering homogeneous tissular slabs (24:409).

$$T_D \times 10 \times T_{C1} = \text{diffuse transmittance through aperture dia.} = 1\text{mm.}$$

$$T_{10} = \text{transmittance with time gate of 10 ps.}$$

$$10 \times R_e = \text{reflectance}$$

into the medium. Considering graph a in Figure 14 and a tissue thickness of 40mm, the total number of photons received is the area under the graph. This is

$$N_R = \text{number of photons received} \\ \approx (1/2) N \Delta y$$

where $N = 400$ is the number of photons received on axis and $\Delta y \approx 60\text{mm}$ is the width of the curve at its base. Since the transmittance for this curve was 21.4 percent the number of input photons required is given approximately by

$$N_I = \text{number of input photons} \\ = \frac{(1/2)(400)(60\text{mm})}{0.214} \\ = 56,100 \text{ photons}$$

This approximation is reasonable considering that blood cells have an absorption cross section of approximately 0.06 m^2 at $\lambda = .6328 \mu\text{m}$ which is much smaller than the scattering cross section σ_s ($\sigma_s \approx 60 \mu\text{m}^2$ at the same wavelength). Thus, the probability of scattering is much greater than the probability of absorption.

From these considerations, one obtains for the input power P:

$$P = \frac{N_I h \nu}{t} \\ = \frac{(56,100 \text{ photons})(6.63 \times 10^{-34} \text{ J}\cdot\text{s})(4.74 \times 10^{14} \text{ Hz})}{5 \times 10^{-12} \text{ s}} \\ = 3.53 \text{ mW}$$

Since Maarek, et al. assumed He-Ne laser λ was set equal to $.6328\mu\text{m}$. The Monte Carlo study also assumed an instantaneous pulse which was approximated in the above calculation by a time of 5 ps.

Simulation of Imaging by Transillumination

The following is a summary of the results which Maarek, et al. obtained for two tissue thicknesses and varying location of a blood vessel of radius R.

The first case assumes a 40mm thick sample with a 2mm radius blood vessel. Figure 16 depicts the transmittance graphed against y_c which is the y coordinate of the center of the blood vessel. The movement of y_c simulated scanning of the sample with the source. All transmittances are normalized by the total transmittance obtained with no blood vessel present. The symbol T_D represents the transmittance without regard to either the time or position at which photons emerged from the sample. The symbol T_n indicates the transmittance received with a time gate of n picoseconds and $T_{n,m}$ represents a transmittance with a time gate of n picoseconds and a detecting aperture diameter of m millimeters. The detecting aperture allowed for spatial resolution. In all cases the aperture or "window" was centered on the illumination axis.

From Figure 16 one can see that transmittance decreases as the blood vessel is moved closer to the axis of illumination. Based on a formula for the contrast (C) given as

$$C = 1 - \frac{\text{minimum of transmittance}}{\text{maximum of transmittance}}$$

the contrast for T_D was

$$C_{TD} = 1 - \frac{0.80}{1.00} = 0.2$$

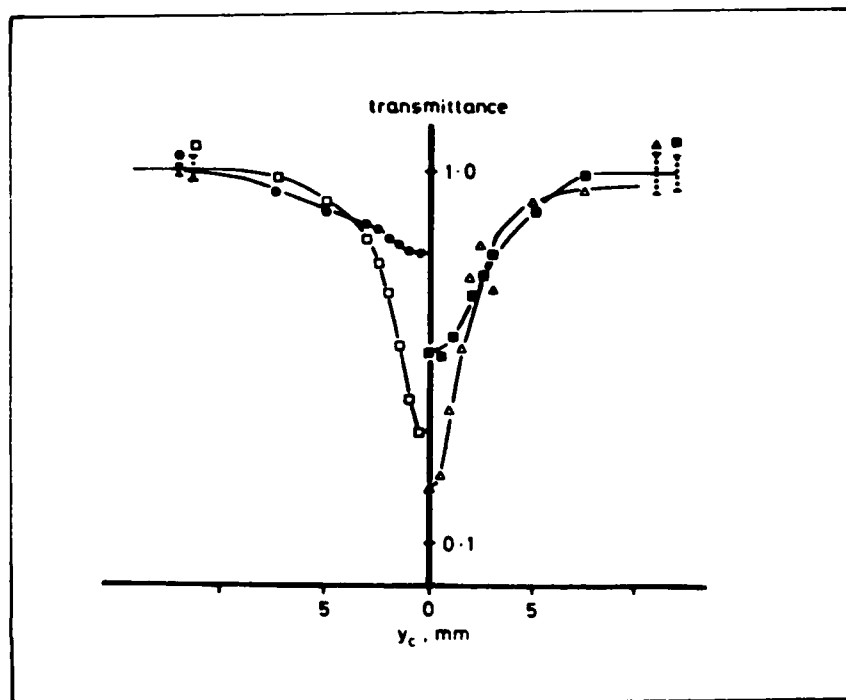


Figure 16. Variations of normalized transmittance values as a function of ordinate of the vessel center y_c when a small vessel ($R = 2\text{mm}$) is displaced in the core of a thin tissular slab ($X_{\text{max}} = 40\text{mm}$) (24:311). Curves are plotted for values of transmittance T_D , T_5 , T_{10} , and $T_{5,2.4}$ (see text for explanation of symbols).

Legend for graph:

● T_D	$X_{\text{max}} = 40\text{mm}$
□ T_5	$X_c = 20\text{mm}$
■ T_{10}	$R = 2\text{mm}$
△ $T_{5,2.4}$	Time Gate = 5ps Aperture Diameter = 2.4mm

$X_c = 20\text{mm}$ indicates blood vessel was at constant depth in the middle of the sample.

With a time gate of 5 picoseconds (without filtering with an aperture), the contrast was

$$C_5 = 1 - \frac{0.37}{1.00} = 0.63$$

Similarly, for a time gate of 10 picoseconds (no aperture),

$$C_{10} = 1 - \frac{0.52}{1.00} = 0.48$$

The curve in Figure 16 denoted by a diamond symbol \diamond represents transmittance values obtained with a time gate of 5 picoseconds and an aperture window of 2.4 mm. In this case the contrast increased to

$$C_{5,2.4} = 1 - \frac{0.23}{1.00} = 0.77$$

The second case of simulated transillumination assumed a tissue thickness of 80mm and a blood vessel of radius $R = 4\text{mm}$. Figure 17 depicts the transmittance values obtained when the blood vessel was moved laterally across the middle of the tissular slab. Contrast values obtained were $T_D: C_D = 0.20$, $T_{10}: C_{10} = 0.65$, $T_{15}: C_{15} = 0.50$, $T_{20}: C_{20} = 0.45$.

Figure 18 represents the transmittances when the blood vessel was at a distance away from the source of 60mm (20mm from the unilluminated end of the tissular slab). The contrast values obtained in this instance were $T_D: C_D = 0.11$, $T_{10}: C_{10} = 0.40$, $T_{15}: C_{15} = 0.37$, $T_{20}: C_{20} = 0.29$.

In addition to the cases detailed above, Maarek, et al. also simulated the transillumination of an 80mm thick slab with a 2mm radius blood vessel located at the center of the slab. The researchers

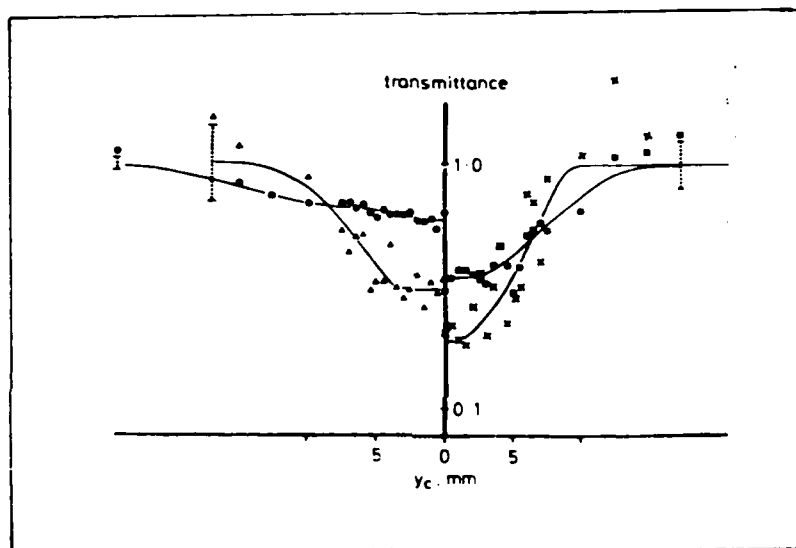


Figure 17. Variations of normalized transmittance values as a function of ordinate of the vessel center y_c when a medium-sized vessel ($R = 4\text{mm}$) is displaced in the core ($X_c = 40\text{mm}$) of a thick tissular slab ($X_{\text{max}} = 80\text{mm}$) (24:411).

Legend for graph:

● T_D	$X_{\text{max}} = 80\text{mm}$
× T_{10}	$X_c = 40\text{mm}$
△ T_{15}	$R = 4\text{mm}$
■ T_{20}	

$X_c = 40\text{mm}$ indicates blood vessel was at a constant depth in the middle of the sample.

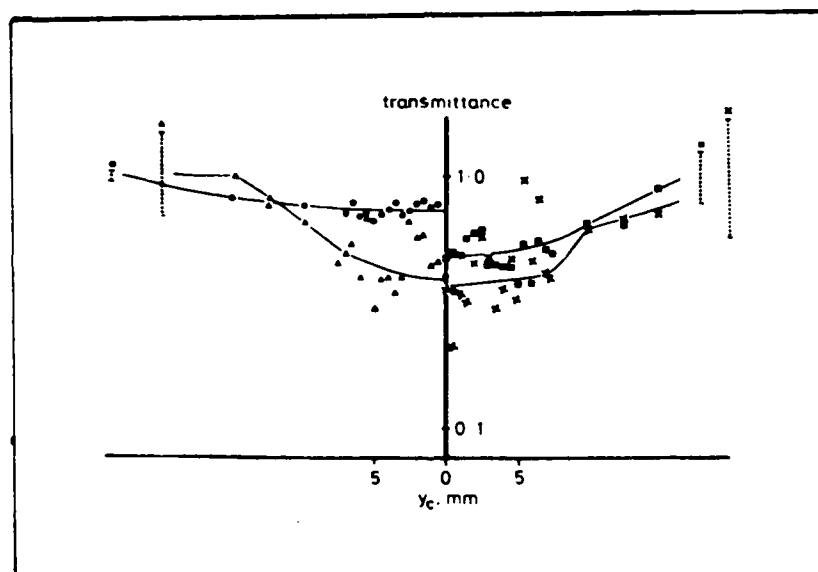


Figure 18. Same caption as for Figure 17 (24:412). The medium-sized blood vessel has been shifted towards the unilluminated side of the tissular slab ($X_c = 60\text{mm}$). Contrast is degraded from the case where $X_c = 40\text{mm}$.

Legend for graph:

- | | | |
|---|----------|--------------------------|
| ● | T_D | $X_{\max} = 80\text{mm}$ |
| × | T_{10} | $X_c = 60\text{mm}$ |
| △ | T_{15} | $R = 4\text{mm}$ |
| ■ | T_{20} | |

reported that, in this case, there was only a very slight decrease in transmittance as the vessel was moved laterally with respect to the source. The contrast obtained without time gating or spatial filtering with an detecting aperture was only 0.08. It was reported that time discrimination could not be used because of "uncertainties in the computed results." (24:412).

Discussion of Results Obtained by Simulated Transillumination

The contrast values obtained by Maarek, et al. incorporate the same general features one sees in transillumination of a breast containing a tumor attended by a proliferation of blood vessels. Notably, Figures 16 through 18 indicate a transmittance gradient across the y ordinate which to the eye would present a shallow region encompassed by a light area.

Maarek, et al. have succeeded in showing that, for the optical parameters used and the model chosen, the technique of time gating coupled with spatial filtering by a detection aperture may be able to increase the contrast obtained under actual conditions of transillumination. The best improvement in contrast obtained with time gating and spatial filtering was 57% over that obtained without time and spatial discrimination (see Figure 14).

Maarek, et al. caveat their study with the remark that "...Because of the present lack of experimental data on the optical parameters of biological samples other than blood, we have used a model with the assumption that only intratissular blood cells interact with photons, which could have resulted in overoptimistic results." (24:412).

It will be shown below that, though the Monte Carlo study gives somewhat higher transmittance values than those obtained experimentally in diaphanography, the difference is certainly not so great as to throw fundamental suspicion on the Monte Carlo results. It will also be shown

that the results obtained theoretically in Chapter II show a close agreement with the Monte Carlo results described in this section when the same optical parameters and thicknesses of tissue are used.

As an analytical tool, the Monte Carlo simulation technique has several advantages and some disadvantages when compared to the theoretical approach presented in Chapter II. The simulation allows one to keep track of paths traversed through the scattering medium thus leading to the possibility of time domain analysis of the scattering process. This feature led to the time discrimination technique which resulted in the noted improvements in contrast. The Monte Carlo method also gives one the capability of determining the probability density of path times and lengths from an output such as that pictured on graph b in Figure 14. Thus, one again gets greater insight into the effect of the scattering process on path lengths. The theoretical analysis (Chapter II), however, provides for a more general conceptual understanding of the relationships between multiple scattering and transport processes (eg. the Fourier transform relation between the correlation function and the specific intensity). The mathematical approach also allows for a quicker calculation of the effect of changes in optical parameters, wavelength, and thicknesses of media.

Comparison of Transmittances Obtained by Monte Carlo Simulation and Theoretical Calculation

To provide some comparison between the results obtained by the Monte Carlo simulation of Maarek, et al. and the theoretical approach in Chapter II, the calculated value of the angular spectrum of the specific intensity $I(\tau, \theta)$ will be obtained for the same optical parameters and tissue thicknesses considered in the Monte Carlo method.

The calculations of the angular spectrum $I(z, \theta)$ are based on the formula

$$I(\tau, \theta) = I_0 \exp(-\tau) \delta(\theta) + I_0 \alpha_p / (\pi W_0 \tau) \exp \left\{ -\tau(1-W_0) - \frac{\sin^2 \theta \alpha_p}{W_0} \right\} \quad (23)$$

which is valid for large optical thickness τ (20:300). To obtain the total intensity received in 2π steradian in the forward direction, $I(\tau, \theta)$ must be integrated over values of θ from zero to $\pi/2$. Knowing that

$$d\Omega = \sin \theta \cos \theta d\theta$$

and neglecting the small quantity $I_0 \exp(-\tau) \delta(\theta)$ one gets from equation (23):

$$I(\tau, \theta) = I_0 \alpha_p / (\pi \tau) \int_0^{\pi/2} \exp[-\alpha_p \sin^2 \theta / \tau] \sin \theta \cos \theta d\theta \quad (24)$$

The albedo W_0 has been set equal to unity as the particles (blood cells) are virtually non-absorbing at $\lambda = .6328 \mu$.

From equation (24),

$$\begin{aligned} I(\tau, \theta) &= I_0 \alpha_p / (\pi \tau) \left(-1/2\tau / \alpha_p \right) \exp[-\alpha_p \sin^2 \theta / \tau] \Big|_0^{\pi/2} \\ &= - \frac{I_0}{2\pi} \exp[-\alpha_p / \tau - 1] \end{aligned} \quad (25)$$

The quantity $\alpha_p = 2.66(D/\lambda)^2$ for large particles where D is the diameter of a particle and λ is the wavelength of radiation. The scattering

blood cells have a diameter of approximately $7\mu\text{m}$ and τ is calculated from the formula:

$$\tau = \rho_n \sigma_s z = \frac{H(1-H)\sigma_s}{V_e} (z)$$

where H is the hematocrit, V_e is the volume of a single scatterer (blood cell) and z is the tissue thickness. The volume of a blood cell is

$$\begin{aligned} V_e &= \pi (D/2)^2 t \\ &= (7/2\mu\text{m})^2 (2\mu\text{m}) \\ &= 76.97\mu\text{m}^3 \end{aligned}$$

where t is the thickness of a blood cell which is approximately $2\mu\text{m}$. (19:63). The scattering cross section σ_s is obtained by linear extrapolation from data published by Ishimaru (19:66) on the scattering cross section of blood cells. For $\lambda = .6328\mu\text{m}$, $\sigma_s = 60.6\mu\text{m}^2$. Substituting these parameters into equation (25) gives

$$\begin{aligned} I &= (I_0/2\pi) \exp\left(-\frac{325.50}{1495.9} - 1\right) \\ &= 0.196 I_0/2\pi \end{aligned}$$

Then, since intensity is measured per steradian, one obtains for a flux P in 2π steradians:

$$P = 0.196 I_0$$

for a transmittance value of 19.6 percent. This value is in fairly

close agreement with the transmittance obtained in the Monte Carlo simulation of 21.4 percent. Accomplishing the same steps for a tissue thickness of 60mm one obtains a transmittance of 13.5 percent according to scattering theory. The Monte Carlo method obtained a transmittance of approximately 10 percent if it is assumed that the number of input photons was 30,000. For an 80mm thick sample the calculated transmittance is 10.3 percent while the reported Monte Carlo value was only 3.8 percent. In the case of the 80mm thick sample, the number of input photons must have been approximately

$$N_I \approx \frac{(1/2)(38)(60) \text{ photons received}}{0.038}$$

$$= 30,000 \text{ photons}$$

It is difficult to assess the exact nature of the relationship between the theory developed in Chapter II and the Monte Carlo method. Nevertheless, it is clear that the two approaches agree fairly well as long as tissue thicknesses do not become too large.

The reader should note that conclusions based on the comparison given here between the theoretical and Monte Carlo approaches should not be carried too far. The comparison does, however, support the notion of a general agreement in results of the two methods. In particular, the Gaussian approximation to the phase function for forward scattering seems to be essentially valid based on the analysis given above. Again, it must be noted, however, that for very thick biological samples the results of the methods diverge.

To conclude this section, a comparison of the transmittances obtained in the Monte Carlo tissue model with those obtained under

actual breast transillumination would be useful. Table II presents optical densities (38:V-9) obtained under actual transillumination. The values D_g and D_r are the optical densities obtained using narrow band filters with transmission peaks at 540 and 650 nm, respectively.

The mean value (\bar{X}) of D_r of 0.83 given for 25 women with normal breast tissue gives a transmittance value $T = 10^{-0.83} = 14.8$ percent. It is possible to compare this value with transmittances obtained via Monte Carlo simulation and scattering theory despite the fact that the Monte Carlo tissue model had only a 0.05 value for the fraction of volume taken up by scatterers (and is therefore, not a dense medium) and yet breast tissue is relatively dense. Recall that the equation for scattering strength

$$\rho_n \sigma_s = \frac{w(1-w)\sigma_s}{V_c}$$

is symmetric about its maximum value of $w = 1/2$ (w = volume of scatterers as a fraction of total sample volume).

The equation for $\rho_n \sigma_s$ shows that the values of $w = 0.05$ and $w = 0.95$ gives the same values of scattering strength. Thus, a comparison between transmittances obtained by Monte Carlo simulation and actual transillumination of breast tissues is not unfounded. In particular, the approximate agreement of transmittances obtained by simulation, theory, and actual transillumination lend further support to the contention that scattering in the breast is primarily forward directed and is due to particles somewhat larger than red or near infrared wavelengths.

TABLE II

OPTICAL DENSITIES

Optical density values. D_g and D_r , obtained from diaphanograms of 110 women with breast cancer and 10 women with benign breast disorders. The miscellaneous group consisted of two women who had lymph nodes and one woman who had a lipoma. \bar{X} = mean value and SD = standard deviation.

Histologic classification	Visual interpretation of diaphanograms	No. of patients	Optical density*			
			D_g		D_r	
			\bar{X}	SD	\bar{X}	SD
Cancer	Dark-shaded area	42	2.87	0.42	2.03	0.86
	Light-shaded area	52	2.25	0.49	1.12	0.56
	No shaded area	16	2.16	0.58	1.19	0.75
Fibroadenoma	No shaded area	37	2.01	0.58	0.84	0.53
Mastitis	Light-/dark-shaded area	7	2.38	0.43	0.93	0.46
Miscellaneous	No shaded area	3	1.69	0.40	0.56	0.07
Mammary duct ectasia/Fibrocystic disease	No shaded area	82	2.08	0.47	0.68	0.24
Normal breast tissue	No shaded area	25	2.02	0.59	0.83	0.50

*Expressed in density units

(38:V-9)

Implementing Monte Carlo Simulation Using the Gaussian Approximation to the Phase Function.

It would be useful to implement a Monte Carlo simulation of the scattering process in a way which ties Monte Carlo results closely to the scattering theory presented in Chapter II. The motivation for doing so comes from the consideration that the improvement in contrast experienced by time gating and spatial filtering (TGSF) of the transillumination output could then be translated mathematically into a reduced optical thickness \mathcal{T}_R . This reduced optical thickness of a tissue medium with the same transmission characteristics of a medium of thickness τ where the scattering cross section σ_s is reduced in magnitude. In other words, TGSF effectively produces a "new" medium with reduced optical thickness \mathcal{T}_R . It is suggested that, using this reduced optical thickness, one could again apply the scattering theory of Chapter II to determine the feasibility of mathematical image processing on the new \mathcal{T}_R medium.

As a first step in this direction, the following is presented to show how a Monte Carlo simulation can be created incorporating the Gaussian approximation to the phase function $p(s)$ which describes the distribution of scattered radiation.

In capsule form the steps involved to implement the simulation are

- (1) Introduce a photon into the medium at position $(x, y, z = 0)$,
- (2) Calculate the path length l to the location where the next scattering or absorption event takes place,
- (3) Determine if the photon is absorbed or scattered after traversing path length l ,
- (4) If the photon is absorbed, stop and input a new photon,
- (5) If the photon is scattered, calculate the direction (θ, ϕ) which

the photon takes, and

(6) Compute the position (x, y, z) of the photon to track its progress through the medium.

The probability density functions needed to calculate l , θ , and φ at each scattering event are

$$p_l(l) = \exp\left(-\frac{1}{l}\right) \frac{1}{l} ; 0 < l < \infty,$$

$$p_\theta(\theta) = \frac{1}{2(\alpha_p)^{1/2} W_0} \exp(-\alpha_p^2) ; 0 < \theta < \infty,$$

$$p_\varphi(\varphi) = 1/2\pi ; 0 < \varphi < 2\pi$$

where $l = 1/n\sigma_s$ is the mean free path length (n is the total number of scatterers). Note that the integration to arrive at $p_\theta(\theta)$ was over limits from 0 to ∞ which is a valid approximation since the contributions to the integral for large θ are negligible. For $p_l(l)$ and $p_\theta(\theta)$ exponential and Gaussian random variables would have to be generated from a random variable uniformly distributed over the interval from 0 to 1 as generated by a computer. The values of l may be calculated from the equation

$$l = -l \ln[1/(u-1)] \quad (26)$$

where u is a uniform random variable distributed over the interval $0 < u < 1$. The values of θ can be calculated from an approximation listed by Abramowitz and Stegun (1:932).

To tie the results of the Monte Carlo method outlined above to scattering theory as developed in Chapter II, the output flux as predicted by the angular spectrum of the specific intensity could be

fitted mathematically to the output flux of the obtained by Monte Carlo simulation with TGSF. If all the same optical parameters are used in the simulation and in the scattering theory, the difference in the fluxes predicted by simulation and theory becomes a function of optical thickness \mathcal{T} .

To accomplish this mathematical fit, however, the output fluxes of the Monte Carlo simulation with and without TGSF must be normalized relative to each other to insure that a reduction in $\mathcal{T}(\mathcal{T} \rightarrow \mathcal{T}_R)$ is actually obtained. To see this, consider typical transmission curves in Figure 19 for the same medium with and without TGSF. If one does not normalize the outputs in graphs (a) and (b) in Figure 19 it can be seen that a medium corresponding to graph (b) without TGSF would be one with a larger optical thickness than in graph (a) because of the reduction in total transmission. However, one would expect that if effective scattering is reduced (artificially by TGSF) then graph (b) would represent a medium with reduced \mathcal{T} .

Therefore, the areas under graphs (a) and (b) in Figure 19 should be normalized relative to one another to produce equivalent transmission values as shown in Figure 20. The areas under the graph (c) and (d) in Figure 20 are equal and, consequently, represent outputs with equal total transmission. It can be seen that with transmission normalization, graph (d) must correspond to a medium with reduced optical thickness \mathcal{T}_R because the spread of intensity in graph (d) is decreased with respect to that in graph (c). If one fixes particle density ρ_n and physical thickness Z , then the reduction in the spread of intensity reflected in graph (d) corresponds to a reduced scattering cross section produced by removing scattered photon noise by TGSF. Consequently, the actual

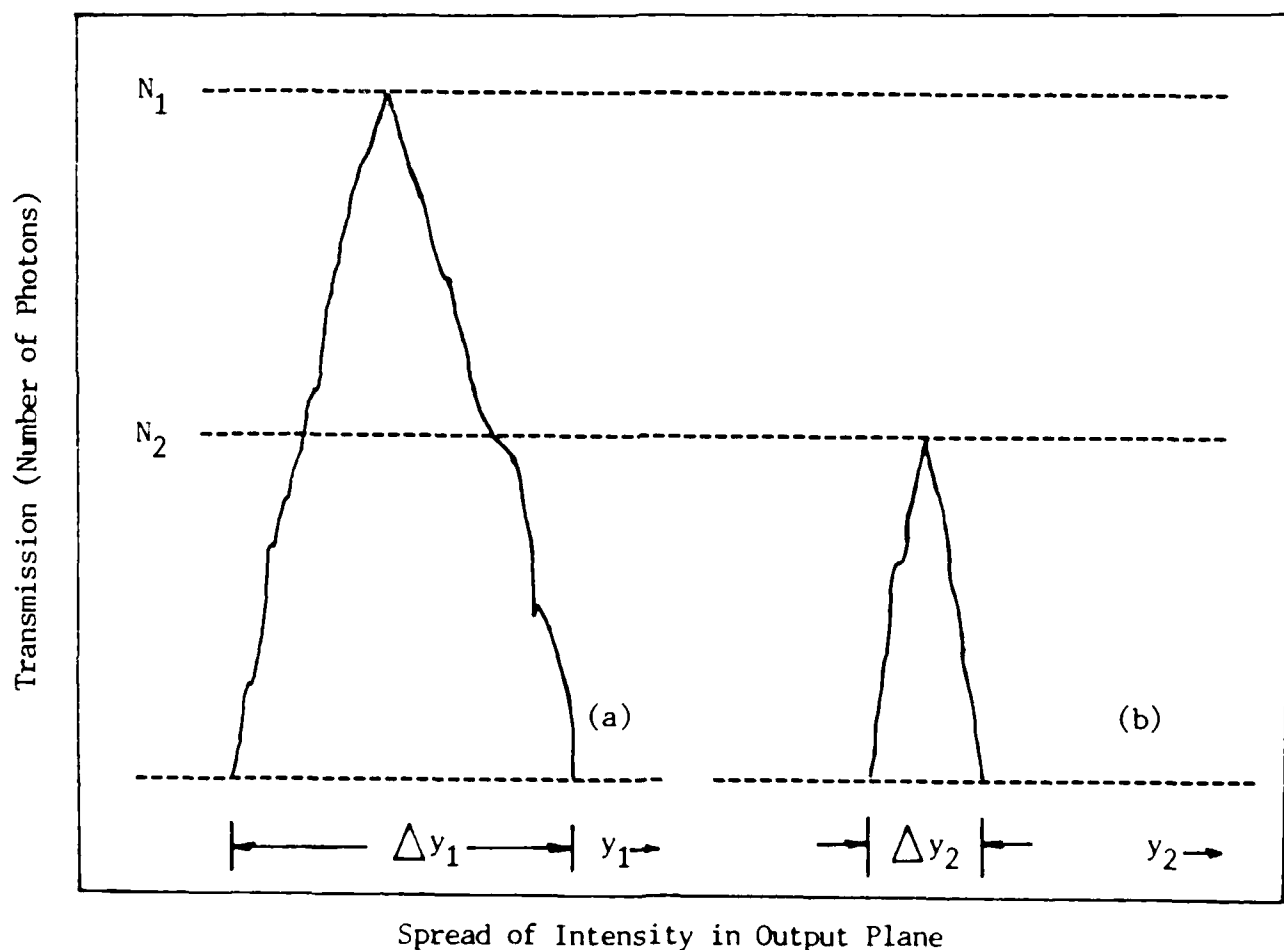


Figure 19. Typical transmission curves obtained via Monte Carlo simulation. Graph (a) shows the transmission obtained without time gating or spatial filtering at the output (note the large spread in photon intensity Δy_1). Graph (b) shows transmission obtained with time gating and spatial filtering (note total transmission is reduced as well as the spread of intensity Δy_2).

Transmission (Number of Photons)

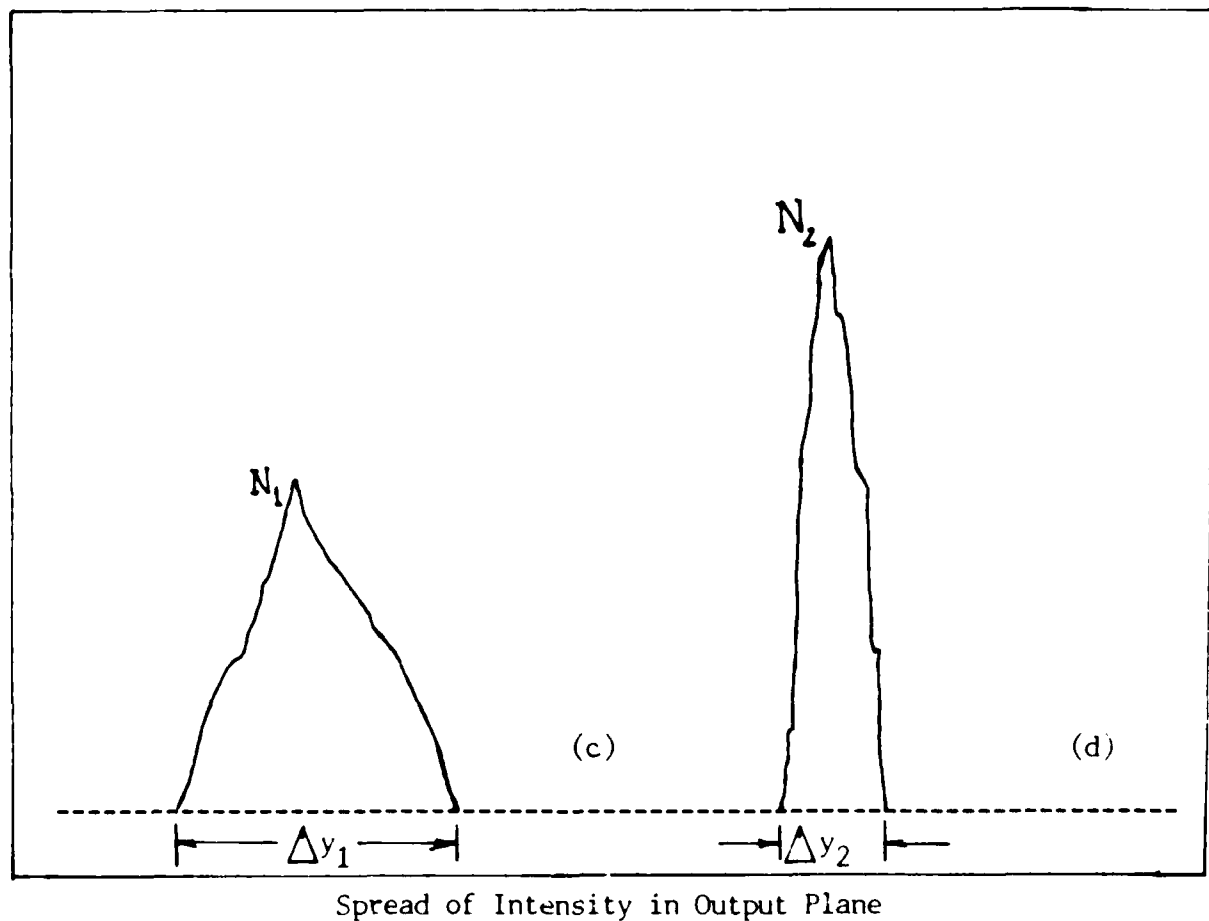


Figure 20. Normalized transmission curves obtained by Monte Carlo simulation. Areas under the graphs are equal (identical total transmission values). Graph (c) shows transmission obtained without time gating or spatial filtering. Graph (d) shows transmission obtained with time gating and spatial filtering.

optical thickness τ_a

$$\tau_a = \rho_n(\sigma_s + \sigma_a)Z \quad (27)$$

becomes the reduced optical thickness τ_R :

$$\tau_R = \rho_n(\sigma_s' + \sigma_a)Z \quad (28)$$

where $\sigma_s' < \sigma_s$. It remains to show how the value of σ_s' may be obtained from the equation for the angular spectrum of specific intensity $I(\tau, \theta)$:

$$I(\tau, \theta) = (I_0/2\pi) \int_0^\infty q dq J_0(q \sin \theta) \exp \left\{ -\tau \left[1 - W_0 \exp \left(-\frac{q^2}{4\alpha_p} \right) \right] \right\} \quad (29)$$

which is obtained by Fourier transformation of the correlation function.

Let the total transmission (or flux) obtained without TGSF be denoted by T_1 , then

$$T_1 = \int_{\Delta\theta_1} N_1(\theta_1) d\theta_1 \quad (30)$$

where $N_1(\theta_1)$ is the number of photons received in the output plane as a function of $\theta_1 = \tan^{-1}(y_1/z)$. The integration is carried out over the angle θ_1 , (the angular extent of the intensity in the output plane). The subscript 1 in equation (30) identifies quantities corresponding to an experimental arrangement without TGSF. The symbol y_1 is the coordinate axis in the output plane perpendicular to the illumination axis.

Similarly, let T_2 be the total transmission in the output plane with TGSF, then

$$T_2 = \int_{\Delta\theta_2} N_2(\theta_2) d\theta_2 \quad (31)$$

where the subscript 2 identifies a quantity obtained with TGSF. If F_N is the normalization factor, then

$$T_1 = F_N T_2(\tau_R) \quad (32)$$

where T_1 is a quantity determined by simulation. The total transmission (flux) T_2 has been integrated over θ_2 leaving a quantity which is now a function of τ_R alone. From equation (29) one obtains

$$I_2(\tau_R) = \frac{I_0}{2\pi} \int_{\Delta\theta_2}^{\infty} q dq J_0(q \sin\theta) \exp \left\{ -\tau_R \left[1 - W_0 \exp \left(-\frac{q^2}{4\alpha_p} \right) \right] \right\} \quad (33)$$

where τ_R is

$$\tau_R = \rho_n (\sigma_s + \sigma_a) Z \quad (34)$$

Since ρ_n , σ_a , and Z have been set the same values for cases with and without TGSF, τ_R is a function of σ_s' (a scattering cross section reduced by TGSF). Therefore, equation (33) for the specific intensity states that $I(\tau_R) = I(\sigma_s')$.

Finally, since $T_1 = 2 I_1$, and $T_2 = 2 I_2$, σ_s' may be determined by solving the equation

$$I_2(\sigma_s') = I_1 / F_N \quad (35)$$

for σ_s' where

$$I_2(\sigma_s') = \frac{I_0}{2\pi} \int_{\Delta\theta_2}^{\infty} q dq J_0(q \sin\theta) \exp \left\{ -\rho_n \sigma_s' Z \left[1 - W_0 \exp \left(-\frac{q^2}{4\alpha_p} \right) \right] \right\} \quad (36)$$

and σ_a has been set equal to zero for a (relatively) non-absorbing medium. Equation (36) can be solved numerically.

Once σ_s' , the reduced scattering cross section is obtained, one is then presented with (or, so it may turn out) a new imaging problem to which the equations for the limit of resolution may be applied. Of course, the hope would be that the reduced optical thickness τ_R is low enough that either a reasonable image may be obtained, or that mathematical imaging processing could be reapplied with reasonable expectations of success.

IV. Conclusions and Recommendations

Imaging tumors of the breast by transillumination proves to be a challenging problem - and this for principally two reasons:

- (1) Noise generated by the scattering process is not additive, and
- (2) Breast tissue has an extremely high optical thickness.

Point (1) above sets fundamental limitations on methodology.

Because the coherent or average signal is physically converted into noise by scattering, matched filtering or averaging techniques are not likely to succeed in improving image quality. A highly scattering medium very quickly destroys the average signal bearing wave and, consequently, after a short propagation distance, there is little or no signal left to match. Also, techniques based on averaging various outputs suffer from the lack of a coherent field so that although a sum of outputs (perhaps at different illumination angles) could in principal reduce noise, the result of averaging would not be an enhancement of the coherent image since any coherency is virtually gone.

Point (2) addresses the high degree of scattering which light undergoes as it propagates in breast tissue. The optical thickness determines the severity of the scattering and, therefore, the minimum physical thickness through which one might obtain a reasonable coherent image. For the aperture and focal length of lens chosen, the value of τ for which a coherent image could be expected to be obtained was 20.08 while for the biological medium used in the Monte Carlo simulation was nearly 750. It is believed that the τ for the human breast would likewise be very large.

Thus, one is led to conclude that because of the lack of a coherent signal in optically thick tissues, the image obtained by

transillumination can be improved only if some physical process to mitigate the scattering is first applied. A technique designed to do this is time gating and spatial filtering (TGSF). Using TGSF it was found, that under some circumstances, an improvement in contrast of 77 percent is theoretically possible.

Since the Monte Carlo simulation done by Maarek et al. used a dilute blood sample as the scattering medium, it can be expected that some differences would exist between the results obtained by the Maarek et al. Monte Carlo simulation and a Monte Carlo simulation of breast transillumination. Thus, a Monte Carlo simulation designed specifically for breast transillumination could prove to be of value.

Such a study could be used in principal to test the applicability various models and model parameters. Also, following the implications of the last section of Chapter III, it might be found that a particular time gate and spatial filter could produce a reduced optical thickness \mathcal{T}_R for which mathematical image processing is a feasibility. Of course, before any such scheme can be entertained as a possibility, it is essential that experimental data be obtained for important optical parameters of breast tissue such as scattering and absorption cross sections, and particle densities, concentrations and dimensions. It is recommended that if further research is conducted on improving imaging in breast transillumination, that it be done in three phases. The first phase should concentrate on gathering data as described above. The second phase of the research should conduct Monte Carlo simulations to determine the reduced optical thickness \mathcal{T}_R which can be theoretically, achieved by TGSF. The third and final phase should be devoted to determining the feasibility of and quantitative efficacy of mathematical image processing using the medium with an optical thickness \mathcal{T}_R reduced

by TGSF.

Finally, the reader will recall that one result of the discussion of the scattering model in Chapter I was that improvement in transillumination imaging could occur by simply detecting photons at 1.23μ m. There is a transmission peak at this wavelength in human collagen of the dermis. Since the fibrous material in the breast is also collagenous, it is reasonable to suggest that experimentation on breast transillumination at 1.23μ m would show increased transmission through structures surrounding cancers while yet retaining the feature of high absorption in the water-bearing plasma of vessels massed about cancers. An increase in contrast, then, should be detectable in the image plane. It is recommended, therefore, that transillumination with detection at 1.23μ m be attempted.

Appendix A: Multiple Scattering Theory

The following development of Twersky's theory is based on Ishimaru's formulation. Consider a random distribution of N particles located at point vectors $\mathbf{r}_1, \mathbf{r}_2, \dots, \mathbf{r}_N$ in a volume V . At this point, no specific assumptions are made concerning the size or shape of the individual particles. Also consider a scalar field ψ^a at \mathbf{r}_a (\mathbf{r}_a being a point in space between scatterers). The field ψ^a satisfies the wave equation

$$(\nabla^2 + k^2)\psi = 0 \quad (37)$$

where $k = 2\pi/\lambda$ is the wave number describing the propagation characteristic of the medium surrounding the particles (20:254).

If φ_i^a is an incident wave ("i" meaning incident and "a" indicating location \mathbf{r}_a) in the absence of any particles, the field ψ^a is then the sum of φ_i^a and the contributions U_s^a from all N particles located at some point \mathbf{r}_s , $s = 1, 2, \dots, N$.

$$\psi^a = \varphi_i^a + \sum_{s=1}^N U_s^a \quad (38)$$

The symbol U_s^a indicates the field contributions at a point \mathbf{r}_a (upper index of U) from scatterers located at various points \mathbf{r}_s (lower index of U) (20:254).

The sum over U_s^a ($\sum_s U_s^a$) is, then, the wave at \mathbf{r}_a due to all scatterers in the volume V . This wave may be expressed in terms of a wave φ^s incident upon a scatterer located at \mathbf{r}_s and a scattering characteristic u_s^a of the scatterer located at \mathbf{r}_s as observed at a location (between scatterers \mathbf{r}_a). In mathematical form U_s^a is

$$U_s^a = u_s^a \varphi^s \quad (39)$$

where u_s^a is taken to be an operator so that the symbol u_s^a does not indicate a product (in general) (20:254).

The "effective field" field incident upon a scatterer located at a point r_s is (20:255)

$$\varphi^s = \varphi_i^s + \sum_{\substack{t=1, \\ t \neq s}}^N u_t^s \quad (40)$$

The case $s = t$ is excluded from the sum in equation (40) since a scatterer does not contribute to the wave incident upon it. Figures 21 and 22 depict the quantities thus far described.

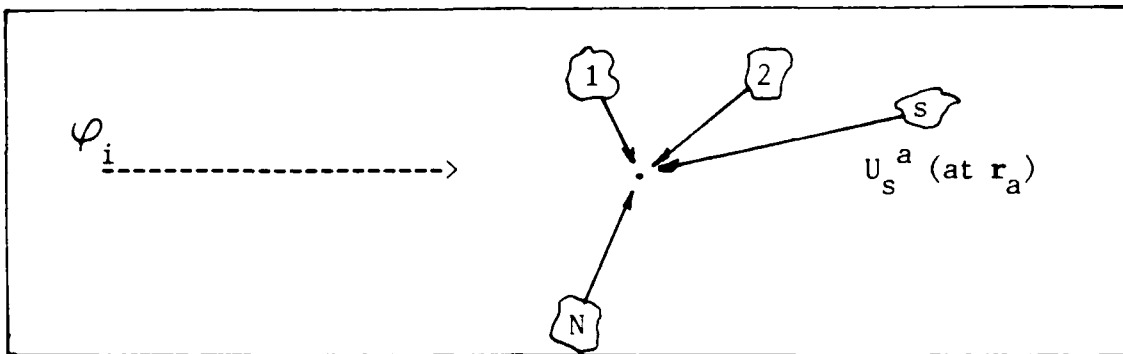


Figure 21. The wave u_s^a as the sum of the contributions from an incident wave φ_i and scattered waves from particles 1, 2, ..., s, ..., N (20:255).

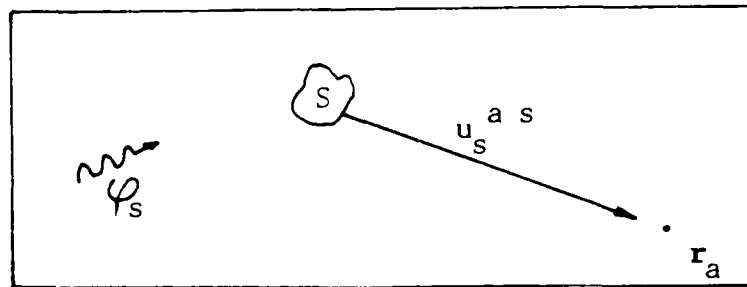


Figure 22. The wave $u_s^a \varphi^s$ at r_a due to the scattering of wave φ^s by a single particle S (20:255).

Combining equations (38), (39), and (40) results in the following expression for the field ψ^a :

$$\psi^a = \varphi_i^a + \sum_{s=1}^N u_s^a \left(\varphi_i^s + \sum_{\substack{t=1, \\ t \neq s}}^N u_t^s \varphi^t \right) \quad (41)$$

Equation (41) may be iterated over φ and thereby include the effects

of an ever increasing number of scatterers. If such an iteration is carried out, ψ^a becomes (20:256)

$$\psi^a = \varphi_i^a + \sum_{s=1}^N u_s^a \varphi_i^s + \sum_{s=1}^N \sum_{\substack{t=1, \\ t \neq s}}^N u_s^a u_t^s \varphi_i^t + \sum_{s=1}^N \sum_{\substack{t=1, \\ t \neq s}}^N \sum_{\substack{m=1, \\ m \neq s, m \neq t}}^N u_s^a u_t^s u_m^t \varphi_i^m \quad (42)$$

The first term in equation (42) is the incident wave at r_a . The second term is the contribution to ψ^a from all single scatterings from all the scatterers $s = 1, 2, \dots, N$. The third term represents the scattering contribution to ψ^a from all double scatterings. The terms in equation (42), then represent the scattering contributions from all the single, double, triple and multiple scatterings that occur in the random medium. See Figure 23 for a depiction of various multiples of scattering.

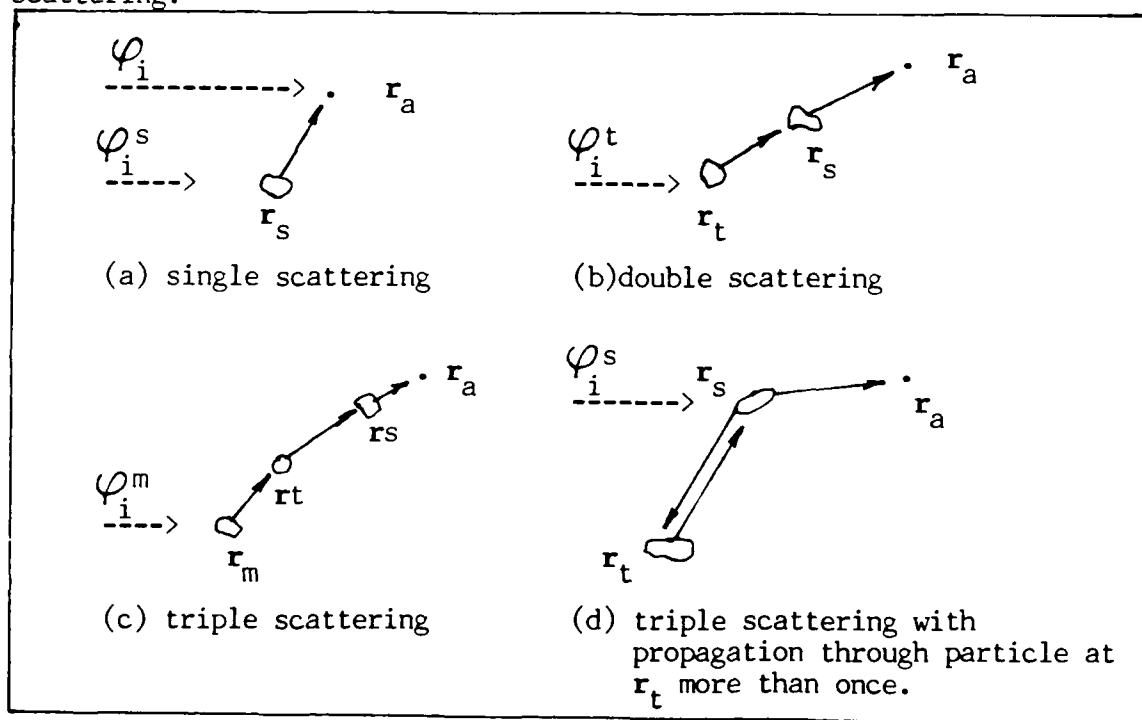


Figure 23. Multiple scattering (20:257).

Note that the term corresponding to $s = m$ is not excluded from equation (42). The case of $s = m$ represents paths that go through a given scatterer more than once. To mathematically illustrate the

concept of multiple scattering through one particle the fourth term in equation (42) may be written as

$$\sum_{s=1}^N \sum_{t=1}^N \sum_{m=1}^N u_s^a u_t^s u_m^t \varphi_i^m = \sum_{s=1}^N \sum_{t=1}^N \sum_{m=1}^N u_s^a u_t^s u_m^t \varphi_i^m + \sum_{s=1}^N \sum_{t=1}^N u_s^a u_t^s u_s^t \varphi_i^s \quad (43)$$

The second term on the right side of equation (43) has conflated to a double sum since the sum is over s and t and m = s (20:256).

Twersky's theory does not include scattering through a single particle more than once. As Ishimaru states, ". . . Twersky's theory should give excellent results when the backscattering is insignificant compared to scattering in other directions" (20:257). Even so, in other cases where backscattering is present to a more pronounced degree, the difference between the Twersky scattering process and an exact process (including multiple paths through a single particle) becomes small as the number N of particles grows large (20:258).

TABLE III

EXACT THEORY AND TWERSKY'S THEORY

Shown in the table are the number of terms included in the exact scattering process and the Twersky process. As N (the number of particles) grows large, the difference between the exact process and the Twersky process becomes very small.

	E = Exact	T = Twersky	Difference $\frac{E - T}{E}$
φ_i^a	1	1	0
Single Scattering	N	N	0
Double Scattering	$N(N - 1)$	$N(N - 1)$	0
Triple Scattering	$N(N - 1)^2$	$N(N - 1)(N - 2)$	$\frac{1}{N - 1}$
Quadruple Scattering	$N(N - 1)^3$	$N(N - 1)(N - 2)(N - 3)$	$\frac{3N - 5}{(N - 1)^2}$

(20:258)

For convenience, the mathematical form of the Twersky process is written here explicitly.

$$\psi_a = \varphi_i^a + \sum_{s=1}^N u_s^a \varphi_i^s + \sum_{s=1}^N \sum_{\substack{t=1, \\ t \neq s}}^N u_s^a u_t^t \varphi_i^t + \sum_{s=1}^N \sum_{\substack{t=1, \\ t \neq s}}^N \sum_{\substack{m=1, \\ m \neq t, \\ m \neq s}}^N u_s^a u_t^s u_m^t \varphi_i^m \quad (44)$$

Integral Formulation

The development so far presented is useful for a conceptual understanding of the multiple scattering process but does not lend itself to use as a tool for determining quantities in practical problems (20:259).

To make the theory practical, Twersky derived an integral formulation of his theory. Consider a random medium consisting of particles all of which have the same statistical characteristics described by a weighting function $w(\underline{s})$. "The variable \underline{s} designates all of the characteristics of a scatterer s such as location (\mathbf{r}_s), shape, orientation, and dielectric constant" (20:259). Since all the scatterers have the same statistical characteristics, $w(\underline{s})$ may be written as

$$w(\underline{s}) = w(\vec{\mathbf{r}}_s, \xi_s) \quad (45)$$

where ξ_s represents all the characteristics of the particles with the exception of location (20:259).

If we now have some random function f which depends on all the scatterers we can express f as (20:259)

$$\langle f \rangle = \iiint \cdots \int \langle f(\xi) \rangle w(\underline{1}) w(\underline{2}) \cdots w(\vec{\mathbf{r}}_s) \cdots w(\vec{\mathbf{r}}_n) d\vec{\mathbf{r}}_1 \cdots d\vec{\mathbf{r}}_n \quad (46)$$

where $\langle f(\xi) \rangle$ represents the average of f corresponding to scatterer characteristics other than location. One can then write

$$w(\vec{r}_s) d\vec{r}_s = \frac{\text{Number of scatterers within volume } V: d\vec{r}_s = dx_s dy_s dz_s}{\text{total number of scatterers in } V}$$

$$= \frac{\rho(\vec{r}_s) d\vec{r}_s}{N} \quad (47)$$

where $\rho(\vec{r}_s)$ is the number of scatterers per unit volume (20:260).

The average of f is (20:260)

$$\begin{aligned} \langle f \rangle &= \iiint \dots \int \langle f(\xi) \rangle \frac{\rho(\vec{r}_1)}{N} \cdot \frac{\rho(\vec{r}_2)}{N} \dots \frac{\rho(\vec{r}_s)}{N} \dots \frac{\rho(\vec{r}_n)}{N} d\vec{r}_1 \dots d\vec{r}_n \\ &= \iiint \dots \int \langle f(\xi) \rangle \frac{\rho(\vec{r}_1) \rho(\vec{r}_2) \dots \rho(\vec{r}_s) \dots \rho(\vec{r}_n)}{N^n} d\vec{r}_1 \dots d\vec{r}_n \quad (48) \end{aligned}$$

In the development above, it is assumed that the scatterers are (to within a good approximation) statistically independent of one another. For a biological medium, investigators assume this to be the case for wavelengths in the visible and near infrared. This assumption may be supported by a consideration of the far field of a particle. For a collagen fiber (diameter $\equiv D \approx 100\text{nm}$) the far field is $D^2/\lambda = 0.01\mu\text{m}$ for a value of $\lambda = 1\mu\text{m}$. To put this in perspective, a distance of $0.01\mu\text{m}$ is 700 times smaller than the average diameter of a red blood cell. Thus, the fibers do not have to be a significant distance from each other for the far field approximation to be accurate. In this case it may be concluded that statistical independence is a good approximation. Later, it will be shown both qualitatively and quantitatively that when the density of scatterers becomes large (and the distance between scatterers is small), the character of the scattering process changes significantly (scattering, in fact, decreases).

Given the expression for $\langle f \rangle$ in equation (48), an equation for the

various scattering terms in Twersky's equation may be written. First, from the equation for ψ^a

$$\langle \psi^a \rangle = \varphi_i^a + \sum_{s=1}^N \langle u_s^a \varphi_i^s \rangle + \sum_{s=1}^N \sum_{\substack{t=1, \\ t \neq s}}^N \langle u_s^a u_t^s \varphi_i^t \rangle + \sum_{s=1}^N \sum_{\substack{t=1 \\ t \neq s}}^N \sum_{\substack{m=1 \\ m \neq s, t}}^N \langle u_s^a u_t^s u_m^t \varphi_i^t \rangle \quad (44)$$

consider the second term. This term has the integral form (see equation 48)

$$\begin{aligned} \sum_{s=1}^N \langle u_s^a \varphi_i^s \rangle &= \sum_{s=1}^N \int [u_s^a \varphi_i^s \frac{\rho(\vec{r}_s)}{N} d\vec{r}_s] \\ &= \int (u_1^a \varphi_i^1 + u_2^a \varphi_i^2 + \dots + u_N^a \varphi_i^N) \frac{\rho(\vec{r}_s)}{N} d\vec{r}_s \\ &= \int N u_s^a \varphi_i^s \frac{\rho(\vec{r}_s)}{N} d\vec{r}_s \\ &= \int u_s^a \varphi_i^s \rho(\vec{r}_s) d\vec{r}_s \end{aligned} \quad (49)$$

The third term in equation (44) becomes (20:260)

$$\sum_{s=1}^N \sum_{\substack{t=1, \\ t \neq s}}^N \langle u_s^a u_t^s \varphi_i^t \rangle = \sum_{s=1}^N \sum_{\substack{t=1, \\ t \neq s}}^N \iint u_s^a u_t^s \varphi_i^t \frac{\rho(\vec{r}_s) \rho(\vec{r}_t)}{N^2} d\vec{r}_s d\vec{r}_t \quad (50)$$

Since there is one less term in the sum over t as compared to the sum over s , equation (50) results in

$$\begin{aligned} \sum_{s=1}^N \sum_{\substack{t=1, \\ t \neq s}}^N \langle u_s^a u_t^s \varphi_i^t \rangle &= \iint N(N-1) u_s^a u_t^s \frac{\rho(\vec{r}_s) \rho(\vec{r}_t)}{N^2} d\vec{r}_s d\vec{r}_t \\ &= \frac{N-1}{N} \iint u_s^a u_t^s \varphi_i^t \rho(\vec{r}_s) \rho(\vec{r}_t) d\vec{r}_s d\vec{r}_t \end{aligned} \quad (51)$$

For large N (which is the case in breast transillumination) equation (51) becomes

$$\iint u_s^a u_t^s \varphi_i^t \rho(\vec{r}_s) \rho(\vec{r}_t) d\vec{r}_s d\vec{r}_t$$

In general, the terms in equation (44) generate multipliers of the integrals of the form

$$M = \frac{N(N-1)(N-2) \cdots (N-(n-2))}{N^{n-1}} \quad (52)$$

where n indicates the n th term in equation (44). Since the highest degree terms in the numerator and the denominator of equation (44) are N^{n-1} ,

$$\lim_{N \rightarrow \infty} M = 1 \quad (53)$$

Therefore, the integral expression for $\langle \psi^a \rangle$ is

$$\begin{aligned} \langle \psi^a \rangle = & \varphi_i^a + \int u_s^a \varphi_i^s \rho(\vec{r}_s) d\vec{r}_s + \iint u_s^a u_t^s \varphi_i^t \rho(\vec{r}_s) \rho(\vec{r}_t) d\vec{r}_s d\vec{r}_t \\ & + \iiint u_s^a u_t^s u_m^m \varphi_i^m \rho(\vec{r}_s) \rho(\vec{r}_t) \rho(\vec{r}_m) d\vec{r}_s d\vec{r}_t d\vec{r}_m \\ & + \cdots \end{aligned} \quad (54)$$

Recalling that $\langle \psi^s \rangle = \varphi_i^s + \int u_t^s \varphi_i^t \rho(\vec{r}_t) d\vec{r}_t$ one can write equation (54) as

$$\langle \psi^a \rangle = \varphi_i^a + \int u_s^a \langle \psi^s \rangle \rho(\vec{r}_s) d\vec{r}_s \quad (55)$$

Iteration of equation (55) results in equation (54).

Equation (55) represents the fundamental equation for the coherent (average) field in Twersky's multiple scattering theory and is the major result of this section.

Appendix B: The Correlation Function

Twersky's integral equation for the correlation of the field in a random medium at points \mathbf{r}_a and \mathbf{r}_b is consistent with equation (55) developed in last section (20:263). The correlation function $\langle \psi^a \psi^{b*} \rangle$ as derived by Twersky is (35:99)

$$\langle \psi^a \psi^{b*} \rangle = \langle \psi^a \rangle \langle \psi^{b*} \rangle + \int v_s^a v_s^{b*} \langle |\psi|^2 \rangle \rho(\vec{r}_s) d\vec{r}_s \quad (1)$$

where

$$v_s^a = u_s^a + \int u_t^s v_t^a \rho(\vec{r}_t) d\vec{r}_t \quad (2)$$

v_s^a will be referred to as the multiple scattering operator.

If equation (1) is iterated in accordance with equation (2) the following expansion results:

$$\begin{aligned} \langle \psi^a \psi^{b*} \rangle = & \langle \psi^a \rangle \langle \psi^{b*} \rangle + \int v_s^a v_s^{b*} \langle |\psi^s|^2 \rangle \rho(\vec{r}_s) d\vec{r}_s \\ & + \iint v_s^a v_s^{b*} v_t^s v_t^{b*} \langle |\psi^t|^2 \rangle \rho(\vec{r}_s) \rho(\vec{r}_t) d\vec{r}_s d\vec{r}_t \\ & + \iiint v_s^a v_s^{b*} v_t^s v_t^{b*} v_m^t v_m^{b*} \langle |\psi^m|^2 \rangle \rho(\vec{r}_s) \rho(\vec{r}_t) \rho(\vec{r}_m) \\ & \quad \times d\vec{r}_s d\vec{r}_t d\vec{r}_m \\ & + \dots \end{aligned}$$

The first term of equation (56) is the product of the wave at \mathbf{r}_a and the complex conjugate of the coherent wave at \mathbf{r}_b . The second term represents the wave at \mathbf{r}_a scattered by the field at \mathbf{r}_s through the mechanism v_s^a and the complex conjugate of the wave at \mathbf{r}_b generated by the complex conjugate of the field at \mathbf{r}_s through the mechanism of v_s^{b*} . The third term

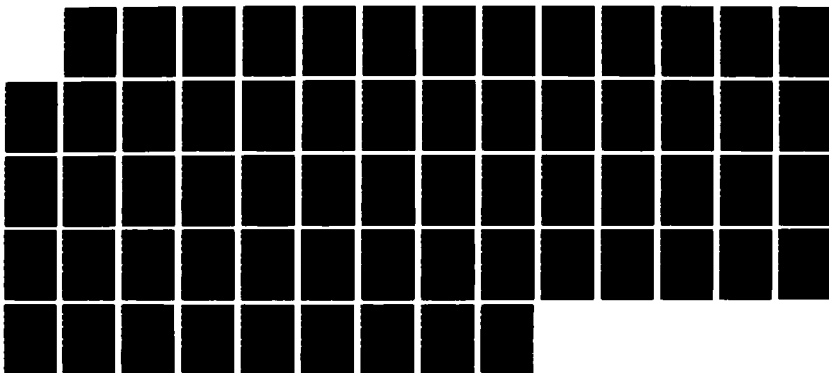
AD-A189 858

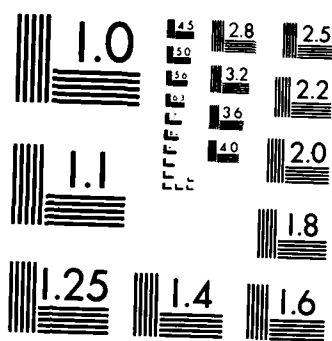
THEORETICAL ANALYSIS OF CANCER DETECTION IN THE HUMAN
BREAST BY TRANSLUMINATION(U) AIR FORCE INST OF TECH
WRIGHT-PATTERSON AFB OH SCHOOL OF ENGI D W SANDERS
DEC 87 AFIT/GEO/ENP/87D-4 F/G 6/5

2/2

UNCLASSIFIED

NL





MICROCOPY RESOLUTION TEST CHART
NATIONAL BUREAU OF STANDARDS-1963-A

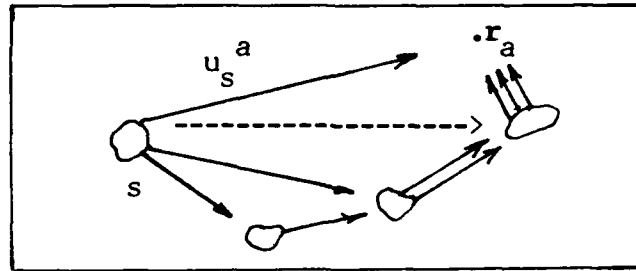
$v_s^a.$


Figure 24. The v_s^a scattering processes giving rise to the field at r_a (20:264).

Based on the development thus far, the relation between the scattering operators u_s^a and v_s^a becomes clear. In heuristic terms, the scattering operator u_s^a represents the radiation from r_s to r_a through free space, whereas v_s^a represents the radiation from r_s to r_a through multiple scattering (20:270). In order for the theory to become useful the mathematical form of v_s^a (the multiple scattering operator) must be obtained. Consequently, the next stage of the mathematical formulation of the scattering problem will be devoted to a determination of v_s^a based upon (1) a reasonable approximation to the form of u_s^a (the free space scattering operator and (2) the relation between u_s^a and v_s^a given by equation (2) (20:264).

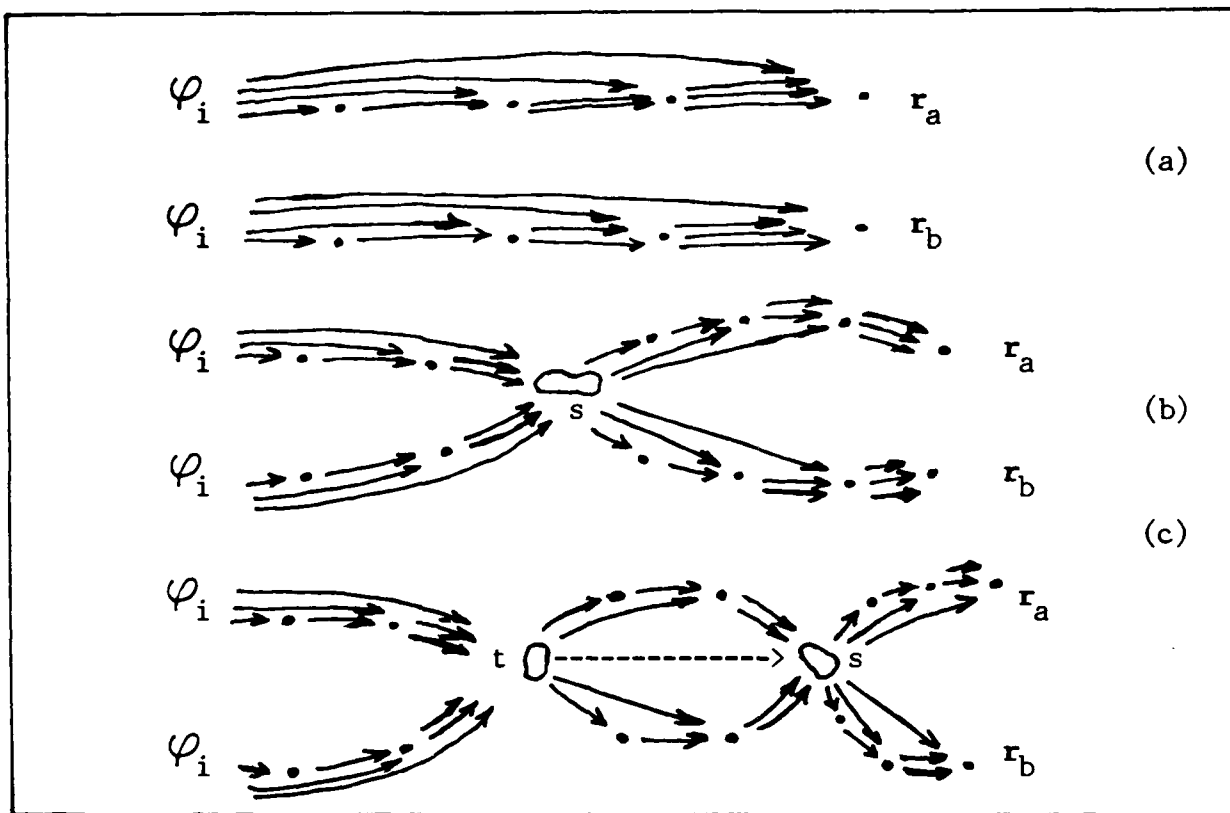


Figure 25. Scattering process for equation (22) (20:264)
 (a) represents scattering for the first term, (b) for the second, and
 (c) the scattering for the third term.

The reader will recall that the far field approximation was assumed for the scattered field. Invoking this same approximation the wave $u_s^a \langle \psi^s \rangle$ may be written as (20:266)

$$u_s^a \langle \psi^s \rangle = f(\hat{o}, \hat{i}) \frac{\exp(ik|\vec{r}_a - \vec{r}_s|)}{|\vec{r}_a - \vec{r}_s|} \langle \psi^s \rangle \quad (57)$$

where $f(\hat{o}, \hat{i})$ is the amplitude scattering coefficient for a single scatterer. $f(\hat{o}, \hat{i})$ represents the amplitude of the \hat{o} component a field $\langle \psi^s \rangle$ incident upon a scatterer from the direction \hat{i} and scattered into the direction \hat{o} (the symbol \hat{o} is chosen to indicate a direction of observation). Given the expression in equation (57) and the relation between u_s^a and v_s^a [equation (2)] it is possible to calculate the form

of v_s^a . First, from equation (57) write u_s^a as (20:266)

$$u_s^a = f(\hat{o}, \hat{i}) \frac{\exp(ik|\vec{r}_a - \vec{r}_s|)}{|\vec{r}_a - \vec{r}_s|} \quad (58)$$

and by extension, for the radiation from another scatterer at r_t to location r_a one gets

$$u_t^a = f(\hat{i}_{at}, \hat{i}_{ts}) \frac{\exp(ik|\vec{r}_a - \vec{r}_t|)}{|\vec{r}_a - \vec{r}_t|} \quad (59)$$

Figure 26 illustrates the physics of the problem. The solution to the problem of finding v_s^a consists of solving the following equation

$$v_s^a = u_s^a + \int u_t^a v_s^t \rho(r_t) dr_t \quad (2)$$

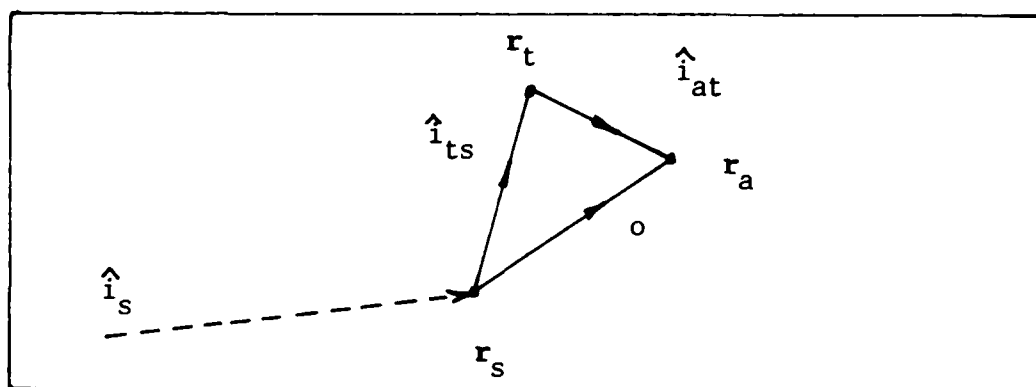


Figure 26. The scattering process for determining the operator v_s^a (20:269). The problem consists of integrating over all contributions v_s^t to v_s^a from scatterers located at all positions r_t .

To proceed, it is first assumed that $\rho(r_t)$ in equation (57) is constant. This assumption can be seen to be valid if one considers that over a given macroscopic region in the tissue medium surrounding a cancer the density is relatively isotropic (primarily fibrons with little fat).

The operator v_s^t in equation (2) may be written as

$$V_s^t = u_s^t \xi_{ts} \quad (60)$$

where ξ_{ts} is some unknown function expressing the results of multiple scattering. Then, substituting equation (60) into equation (2) the following equation results (20:269)

$$u_s^a \xi_{as} = u_s^a + \int_0^d dz_t \int_{-\infty}^{\infty} dx_t \int_{-\infty}^{\infty} dy_t u_t^a u_s^t \xi_{ts} \rho \quad (61)$$

The integral in equation (61) may be evaluated by the method of stationary phase (20:287-291) to yield (20:269)

$$\begin{aligned} & \int_{-\infty}^{\infty} dx_t \int_{-\infty}^{\infty} dy_t u_t^a u_s^t \xi_{ts} \\ &= \int_{-\infty}^{\infty} dx_t \int_{-\infty}^{\infty} dy_t f(\hat{i}_{at}, \hat{i}_{ts}) f(\hat{i}_{ts}, \hat{i}_s) \\ & \quad \times \frac{\exp[ik(r_1 + r_2)]}{r_1 r_2} \xi_{ts} \\ & \approx f(\hat{o}, \hat{o}) f(\hat{o}, \hat{i}_s) \exp(ik|\vec{r}_a - \vec{r}_s|) \frac{2\pi i}{k|\vec{r}_a - \vec{r}_s|(\hat{o} \cdot \hat{i}_s)} \xi_{ts} \end{aligned} \quad (62)$$

where $r_1 = |\vec{r}_t - \vec{r}_s|$, $r_2 = |\vec{r}_a - \vec{r}_t|$, and ξ_{ts} is evaluated at the stationary phase point. The contributions from the regions $z_t < z_s$ are neglected (20:269).

Substituting equations (58), (59), and (62) into equation (61) one gets

$$\xi_{as} = 1 + \frac{2\pi i f(\hat{o}, \hat{o}) \rho}{k(\hat{o} \cdot \hat{i}_s)} \int_{z_s}^{z_a} \xi_{ts} dz_t \quad (63)$$

It must be the case that ξ_{as} and ξ_{ts} have the same functional form such that $\xi_{as} = \xi_{ts}|_{z_t = z_s}$. The following will show that the form for

ξ_{ts} which satisfies the condition just mentioned as well as equation (63) is

$$\xi_{ts} = \frac{2\pi i \rho f(\hat{o}, \hat{i})}{k(\hat{o}, \hat{i}_z)} (z_t - z_s) \quad (64)$$

Substituting equation (64) into equation (63) one gets

$$\begin{aligned} \xi_{as} &= 1 + \frac{2\pi i \rho f(\hat{o}, \hat{o})}{k(\hat{o}, \hat{i}_z)} \int_{z_s}^{z_a} \exp\left[\frac{2\pi i \rho f(\hat{o}, \hat{o})}{k(\hat{o}, \hat{i}_z)} (z_t - z_s)\right] dz_t \\ &= 1 + \frac{2\pi i \rho f(\hat{o}, \hat{o})}{k(\hat{o}, \hat{i}_z)} \exp\left[\frac{2\pi i \rho f(\hat{o}, \hat{o})}{k(\hat{o}, \hat{i}_z)} z_s\right] \\ &\quad \times \int_{z_s}^{z_a} \exp\left[\frac{2\pi i \rho f(\hat{o}, \hat{o})}{k(\hat{o}, \hat{i})} z_t\right] dz_t \\ &= 1 + \exp\left[\frac{-2 i f(\hat{o}, \hat{o}) z_s}{k(\hat{o}, \hat{i})}\right] \left\{ \exp\left(\frac{2\pi i \rho f(\hat{o}, \hat{o}) z_a}{k(\hat{o}, \hat{i})}\right) - \exp\left(\frac{2\pi i \rho f(\hat{o}, \hat{i})}{k(\hat{o}, \hat{i})}\right) \right\} \\ &= \exp\left[\frac{2\pi i \rho f(\hat{o}, \hat{o}) (z_a - z_s)}{k(\hat{o}, \hat{i})}\right] \\ &= \xi_{ts} \Big|_{z_t=z_a} \end{aligned} \quad (65)$$

It is now possible to calculate v_s^a by noting, first, that by extension from equation (60)

$$v_s^a = u_s^a \xi_{as} \quad (66)$$

Then, substituting equations (58) and (65) into equation (66) one obtains

$$\begin{aligned}
v_s^a &= f(\hat{o}, \hat{i}) \frac{\exp(ik|\vec{r}_a - \vec{r}_s|)}{|\vec{r}_a - \vec{r}_s|} \exp\left[\frac{2\pi i \rho f(\hat{o}, \hat{o})(z_a - z_s)}{K(\hat{o}, \hat{i})}\right] \\
&= f(\hat{o}, \hat{i}) \frac{\exp(ik|\vec{r}_a - \vec{r}_s|)}{|\vec{r}_a - \vec{r}_s|} \exp\left[\frac{2\pi i \rho f(\hat{o}, \hat{o})|\vec{r}_a - \vec{r}_s| \cos\theta_{as}}{K \cos\theta_{as}}\right] \\
&= f(\hat{o}, \hat{i}) \frac{\exp[i|\vec{r}_a - \vec{r}_s|(k + \frac{2\pi \rho f(\hat{o}, \hat{o})}{K})]}{|\vec{r}_a - \vec{r}_s|}
\end{aligned}
\tag{67}$$

Defining $K \equiv k + \frac{2\pi \rho f(\hat{o}, \hat{o})}{K}$ equation (67) becomes

$$v_s^a = f(\hat{o}, \hat{i}) \frac{\exp(iK|\vec{r}_a - \vec{r}_s|)}{|\vec{r}_a - \vec{r}_s|}
\tag{68}$$

At this point the formulation presented in this section has arrived at (1) an expression for the correlation function (equation (1)), and (2) an expression for the multiple scattering operator v_s^a (equation (68)).

Appendix C: The Transport Theory

The transport theory is described by a basic differential equation which is equivalent to the Maxwell-Boltzmann collision equation used in the kinetic theory of gases. The usefulness of the theory is not limited to photon transport but has been applied to many physical phenomena ranging from underwater visibility and neutron transport, to the propagation of radiant energy in the atmospheres of planets, stars, and galaxies (19:148).

The fundamental quantity in the transport theory is the specific intensity $I(\mathbf{r}, \hat{\mathbf{s}})$ (also called the radiance). $I(\mathbf{r}, \hat{\mathbf{s}})$ is measured in $\text{Wm}^{-2}\text{sr}^{-1}\text{Hz}^{-1}$ and is the average power flux density within a unit frequency band centered at frequency ν and radiating in the direction $\hat{\mathbf{s}}$ from a point \mathbf{r} . See Figure 27.

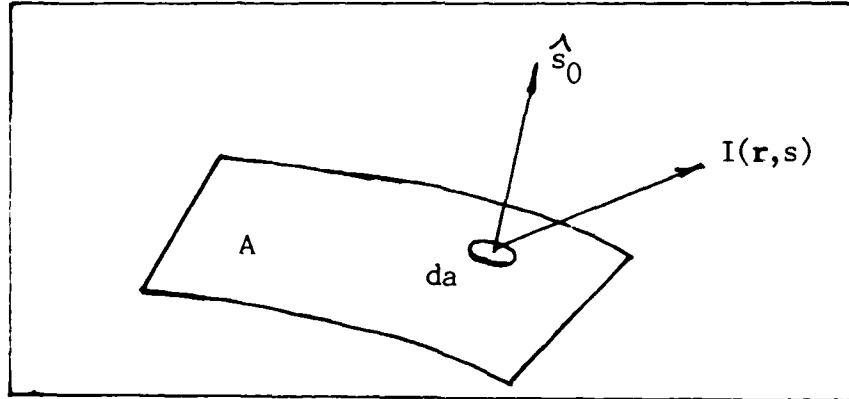


Figure 27. Flux through da on a surface A (19:150).

The amount of power dP flowing within a solid angle $d\omega$ through an elementary area da (with vector $\hat{\mathbf{s}}_0$) in a frequency interval ν to $\nu + d\nu$ is (19:149)

$$dP = I(\mathbf{r}, \hat{\mathbf{s}}) \cos\theta da d\omega d\nu \quad (\text{watts}) \quad (69)$$

It is also convenient to define the average intensity $U(\mathbf{r})$ in terms of the specific intensity:

$$U(\mathbf{r}) = (1/4\pi) \int_{4\pi} I(\mathbf{r}, \hat{s}) d\omega$$

where the integration is taken over all 4π of solid angle (19:152).

If the specific intensity is independent of \hat{s} , the radiation is isotropic. On the other hand, if $I(\mathbf{r}, \hat{s})$ depends on \hat{s} , the specific intensity scattered by ρds particles in a volume ds can be expressed in terms of the amplitude scattering coefficient by (19:156)

$$I(\mathbf{r}, \hat{s})_{\text{scattered}} = \int_{4\pi} \rho ds |f(\hat{s}, \hat{s}')|^2 I(\mathbf{r}, \hat{s}') d\omega' \quad (70)$$

See Figure 28.

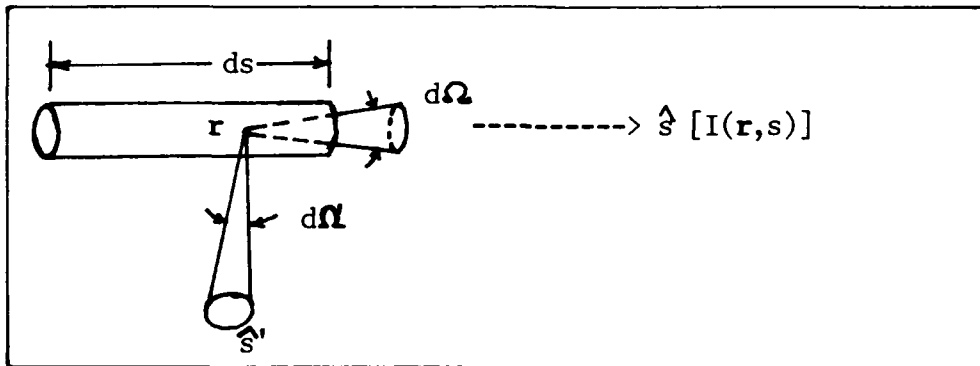


Figure 28. Scattering of specific intensity incident from direction \hat{s}' into direction \hat{s} (19:156).

where $f(\hat{s}, \hat{s}')$ indicates the amplitude of radiation incident in direction \hat{s}' and scattered into direction \hat{s} .

It is convenient to define the phase function $p(\hat{s}, \hat{s}')$ according to the following equation:

$$p(\hat{s}, \hat{s}') = \frac{4\pi}{\sigma_s + \sigma_a} |f(\hat{s}, \hat{s}')|^2 \quad (71)$$

This phase function provides a quantitative description of the directional scattering characteristic of a single scatterer (from \hat{s} into \hat{s}'). It represents the amount of scattered power in a particular direction and has no relation to the phase of the wave (the terminology "phase function" has its origin in astronomy). The albedo of a particle

$$W_0 \equiv \frac{\sigma_s}{\sigma_t} \quad (\text{where } \sigma_t = \sigma_s + \sigma_a) \text{ is dependent on the phase function}$$

(19:11):

$$W_0 = \frac{\sigma_s}{\sigma_t} = (1/4\pi) \int_{4\pi} P(\hat{s}, \hat{s}') d\omega \quad (72)$$

Using the terminology and symbology just presented the differential equation for the specific intensity takes the form

$$\frac{dI(\vec{r}, \hat{s})}{ds} = -\rho\sigma_t I(\vec{r}, \hat{s}) + \frac{\rho\sigma_s}{4\pi} \int_{4\pi} P(\hat{s}, \hat{s}') I(\vec{r}, \hat{s}') d\omega' \quad (73)$$

in the absence of sources inside the scattering medium (19:157). In general a source term $\epsilon(\vec{r}, s)$ would have to be added to the right side of equation (73).

Consider the terms in equation (73). The first term on the right side of the equation is due simply to the losses in a volume ds from scattered and absorbed power and has the form of the Lambert-Beer law. The second term represents the added contributions to the specific intensity from all scatterers in the volume ds .

It is possible to write equation (73) in terms of a nondimensional "optical thickness" defined by

$$\tau = \int \rho\sigma_t ds \quad (74)$$

whereupon equation (39) becomes (19:157)

$$\frac{dI(\tau, \hat{s})}{d\tau} = -I(\tau, \hat{s}) + (1/4\pi) \int p(\hat{s}, \hat{s}') I(\tau, \hat{s}') d\omega' \quad (75)$$

The optical thickness will be used extensively in sections to follow and in the calculation of the limit of resolution of an imaging system in the presence of a scattering medium.

The integral form of equation (73) will be used in the following section to derive the relationship between the analytic and transport theories. Therefore, the integral equation based on the specific intensity is presented here. Its derivation is provided by Ishimaru (19:161-162). After integration over the total volume V of the medium, the following equation is obtained (19:162):

$$U(\vec{r}_a) = U_{ri}(\vec{r}_a) + \int d\vec{r}_s \left[\left(\frac{\rho \sigma_t}{4\pi} \right) \int_{4\pi} p(\hat{s}, \hat{s}') I(\vec{r}_s, \hat{s}') d\omega' \right] \times \frac{\exp[-|\vec{r}_a - \vec{r}_s|]}{4\pi |\vec{r}_a - \vec{r}_s|^2} \quad (76)$$

where

$$U(\vec{r}_a) \equiv \text{average intensity} = (1/4\pi) \int_{4\pi} I(\vec{r}_a, \hat{s}) d\omega \quad (77)$$

and

$$U_{ri}(\vec{r}_a) \equiv \text{average reduced intensity} = (1/4\pi) \int_{4\pi} I_{ri}(\vec{r}_a, \hat{s}) d\omega \\ = (1/4\pi) \int_{4\pi} I_{ri}(\vec{r}_a, \hat{s}) \exp(-|\vec{r}_a - \vec{r}_0|) d\omega \quad (78)$$

where I_{ri} is the reduced intensity which is the result of power losses from the incident intensity $I_i(\hat{r}_0, \hat{s})$ (\hat{r}_0 = point of incidence on the medium) due to absorption and scattering in accordance with the Lambert-Beer law of propagation. This reduced intensity propagates along a straight line connecting r_0 and r_a , the point of interest. Figure 29 illustrates the quantities involved in equation (76).

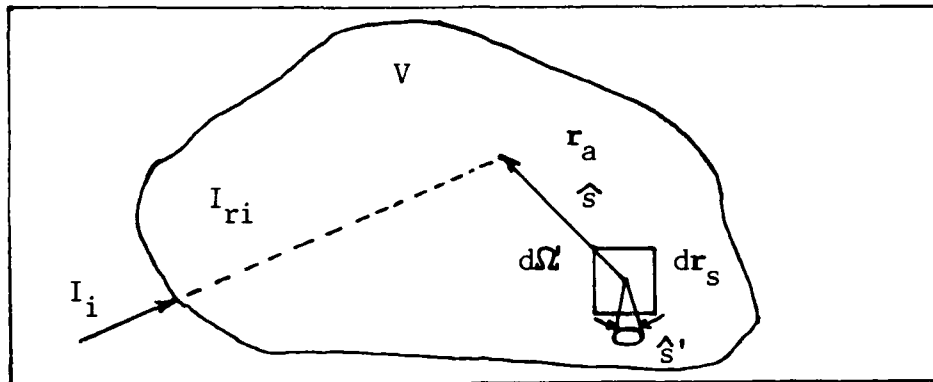


Figure 29. Physical quantities appearing in equation (76) (19:162).

The first term in equation (76) is the average intensity which results from the intensity reduced in strength and by losses due to scattering and absorption. The second term represents additive contributions to the average intensity at r_a due to radiation scattered to that point from all scatterers in the volume V . Note that these contributions due to scattering are each diminished by spherical expansion (indicated by

$\frac{1}{r_a - r_s}$ factor) and by attenuation (indicated by the $\exp[-\mu(r_a - r_s)]$ factor) (19:162).

Appendix D: The Connection Between the Analytic and Transport Theories

From the correlation function of analytic theory the intensity may be written as

$$\langle |\psi^a|^2 \rangle = |\psi^a|^2 + \int |v_s^a|^2 \langle |\psi^s|^2 \rangle \rho(\vec{r}_s) d\vec{r}_s \quad (79)$$

$$v_s^a = u_s^a + \int u_t^a v_s^t \rho(\vec{r}_t) d\vec{r}_t \quad (80)$$

where ψ^{b*} has been set equal to ψ^a to calculate the intensity at \vec{r}_a .

Again, the form of v_s^a is given by

$$v_s^a = f(\hat{o}, \hat{i}) \frac{\exp(iK|\vec{r}_a - \vec{r}_s|)}{|\vec{r}_a - \vec{r}_s|} \quad (68)$$

where $K = k + [2\pi\rho f(\hat{o}, \hat{o})/k]$ and \hat{i} is a unit vector in the direction of the incident wave. The term $|v_s^a|^2 \langle |\psi^s|^2 \rangle$ in equation (79) represents the contribution to the intensity from all incident directions i .

To demonstrate that the correlation function and the specific intensity constitute a Fourier transform pair, it will be assumed that the Fourier relation exists and that the equation for the average intensity (equation (76)) follows from this assumption. Consequently, the correlation function takes the form (20:275)

$$\langle \psi(\vec{r}_a) \psi^*(\vec{r}_b) \rangle = \Gamma(\vec{r}_a, \vec{r}_b) = \Gamma(\vec{r}, \vec{r}_d) = \int I(\vec{r}, \hat{s}) \exp(ik_r \hat{s} \cdot \vec{r}_d) \frac{d\omega}{(3)}$$

where $\vec{r} = 1/2(\vec{r}_a + \vec{r}_b)$ and $\vec{r}_d = \vec{r}_a - \vec{r}_b$, and K_r is the real part of K given in equation (68).

The intensity at a point \vec{r} can now be written as

$$\langle |\psi(\vec{r})|^2 \rangle = \Gamma(\vec{r}, 0) = \int I(\vec{r}, \hat{s}) d\omega \quad (81)$$

Following equation (81) and operating on $\langle |\psi^s|^2 \rangle$ with $|v_s^a|^2$ the equation for the scattered wave from a particle may be derived. First, the operator $|v_s^a|^2$ is calculated:

$$|v_s^a|^2 = v_s^a v_s^{a*} = |f(\hat{s}, \hat{s}')|^2 \frac{\exp(iK|\vec{r}_a - \vec{r}_s|)}{|\vec{r}_a - \vec{r}_s|} \frac{\exp(-iK^*|\vec{r}_a - \vec{r}_s|)}{|\vec{r}_a - \vec{r}_s|} \quad (82)$$

Using the relation $2 \operatorname{Im} K = i^{-1}(K - K^*) = \rho \sigma_t$ (Im denotes "imaginary part of") equation (82) becomes

$$|v_s^a|^2 = |f(\hat{s}, \hat{s}')|^2 \frac{\exp(-\rho \sigma_t |\vec{r}_a - \vec{r}_s|)}{|\vec{r}_a - \vec{r}_s|^2} \quad (83)$$

where \hat{o} and \hat{i} have been replaced by \hat{s} and \hat{s}' . The equation $2 \operatorname{Im} K = \rho \sigma_t$ is a result of the forward scattering theorem (19:14). Having obtained $|v_s^a|^2$ the quantity $(|v_s^a|^2, \langle |\psi^s|^2 \rangle)$ may be evaluated to give

$$|v_s^a|^2 \langle |\psi^s|^2 \rangle = \int d\omega |f(\hat{s}, \hat{s}')|^2 \frac{\exp(-\rho \sigma_t |\vec{r}_a - \vec{r}_s|)}{|\vec{r}_a - \vec{r}_s|^2} I(\vec{r}_s, \hat{s}') \quad (84)$$

Now using the equation for the phase function $p(\hat{s}, \hat{s}')$:

$$p(\hat{s}, \hat{s}') = (4\pi/\sigma_t) |f(\hat{s}, \hat{s}')|^2 \quad (85)$$

and the average intensity

$$U(\vec{r}) = (1/4\pi) \int_{4\pi} I(\vec{r}, \hat{s}) d\omega \quad (86)$$

the integral in equation (79) may be written as

$$\int d\vec{r}_s \frac{\exp(-\rho\sigma_t |\vec{r}_a - \vec{r}_s|)}{4\pi |\vec{r}_a - \vec{r}_s|^2} \int \frac{\rho\sigma_t}{4\pi} p(\hat{s}, \hat{s}') I(\vec{r}_s, \hat{s}') d\omega'$$

As for the first term in equation (79) it should be recognized that the coherent intensity $\langle |\psi^a|^2 \rangle$ attenuates in just the same manner as the reduced intensity incident on the scattering medium. Thus, the following equation is finally obtained

$$U(\vec{r}_a) = U_{ri}(\vec{r}_a) + \int d\vec{r}_s \frac{\exp(-\rho\sigma_t |\vec{r}_a - \vec{r}_s|)}{4\pi |\vec{r}_a - \vec{r}_s|^2} \int \frac{\rho\sigma_t}{4\pi} p(\hat{s}, \hat{s}') I(\vec{r}_s, \hat{s}') d\omega' \quad (87)$$

which is identical to the equation for average intensity arrived at by the transport theory. Equation (87) was obtained by making the assumption expressed by equation (3) which relates to the correlation function to the specific intensity. Thus, equation (87) establishes the result that the correlation function and the specific intensity are related by a Fourier transform.

Appendix E: Plane Wave Illumination of a Plane-Parallel Medium

A critical question to ask is to what extent, if any, it is possible to use image processing techniques to obtain or improve an image of a breast cancer. As an approach to this question, the problem of plane wave illumination of a medium bounded by parallel planes oriented perpendicular to the direction of incident radiation will be considered.

The first step towards a solution to the problem of plane wave incidence is to calculate the specific intensity using the transport theory under what will be referred to as the small angle approximation. In this approximation, a single scatterer is considered comparable to or larger than the wavelength of illuminating radiation and so scatters incident radiation in primarily the forward direction. This approximation is in accordance, then, with the model presented in Chapter 1.

Once the specific intensity has been calculated, the result of the last section will be evoked in order to obtain the correlation function and finally, the limit of image resolution.

Using the relation

$$\frac{dI(\vec{r}, \hat{s})}{ds} = \hat{s} \cdot \text{grad } I(\vec{r}, \hat{s}) \quad (88)$$

the equation of transfer (transport equation) may be written as

$$\hat{s} \cdot \text{grad } I(\vec{r}, \hat{s}) = -\rho\sigma_t I(\vec{r}, \hat{s}) + \frac{\rho\sigma_t}{4\pi} \int_{4\pi} P(\hat{s}, \hat{s}') I(\vec{r}, \hat{s}') d\omega' \quad (89)$$

in the absence of a source inside the medium (19:235).

In Cartesian coordinates $\vec{r} = x\hat{x} + y\hat{y} + z\hat{z}$ where \hat{x} , \hat{y} , and \hat{z} are unit

vectors in the x,y, and z directions, respectively. The direction \hat{s} (the direction of scattered light) in terms of direction cosines (l,m,n) is given by (19:234)

$$\hat{s} = l\hat{x} + m\hat{y} + n\hat{z} \quad (90)$$

where

$$l = \sin\theta \cos\varphi \quad (91)$$

$$m = \sin\theta \sin\varphi \quad (92)$$

and

$$n = \cos\theta \quad (93)$$

Also, the differential element $dl dm$ which is set equal to ds where $\hat{s} = l\hat{x} + m\hat{y}$ has the form

$$d\hat{s} = dl dm = \cos\theta \sin\varphi d\theta d\varphi = n d\omega \quad (94)$$

Under the small angle approximation, the angle should always be small and, therefore, $n = \cos\theta \approx 1$. Further, although the limits of integration on l and m should be $l^2 + m^2 \leq 1$, the contribution to the specific intensity from regions where $l^2 + m^2 \approx 1$ is small and, therefore, the limits of integration on l and m can be extended to $\pm\infty$:

$$\int_{4\pi} d\omega \approx \int_{-\infty}^{\infty} dl \int_{-\infty}^{\infty} dm = \int d\hat{s} \quad (95)$$

It is also assumed that the phase function $p(\hat{s}, \hat{s}')$ is a function of $\hat{s} - \hat{s}'$.

Using the above approximations the transport equation becomes

$$\begin{aligned} \frac{\partial}{\partial z} I(\mathbf{r}, \vec{\rho}, \hat{s}) + \hat{s} \cdot \nabla_{\vec{\rho}} I(\mathbf{r}, \vec{\rho}, \hat{s}) \\ = -\rho_n \sigma_t I(\mathbf{r}, \vec{\rho}, \hat{s}) + \frac{\rho_n \sigma_s}{4\pi} \iint p(\hat{s} - \hat{s}') I(\mathbf{r}, \vec{\rho}, \hat{s}') d\hat{s}' \end{aligned} \quad (96)$$

where

$$\vec{r} = x\hat{x} + y\hat{y} + z\hat{z}, \quad \nabla_t \equiv \frac{\partial}{\partial x} + \frac{\partial}{\partial y}, \quad \vec{s} \equiv l\hat{x} + m\hat{y}$$

The quantity ρn designates the number density of scatterers.

At $z = 0$ (the boundary of the medium) the specific intensity is

$$I(0, \rho, \vec{s}) \equiv I_0(\rho, \vec{s}) \quad (97)$$

The general solution to equation (96) was obtained by Ishimaru using Fourier transform method. The detailed solution to this problem is presented in Appendix J. The final solution for the specific intensity is given by (19:238)

$$I(\vec{z}, \vec{s}) = \frac{1}{(2\pi)^4} \int d\vec{\kappa} \int d\vec{q} \exp(-i\vec{\kappa} \cdot \vec{\rho} - i\vec{s} \cdot \vec{q}) E_0(\vec{\kappa}, \vec{q} + \vec{\kappa} z) K(\vec{z}, \vec{\kappa}, \vec{q}) \quad (98)$$

where

$$K(\vec{z}, \kappa, q) = \exp\left[-\int_0^z \rho_n \sigma_t \left\{1 - (1/4\pi) P(\vec{q} + \vec{\kappa}(z-z'))\right\} dz'\right] \quad (99)$$

where $\vec{q} = K_T(\rho_1 - \rho_2) = K_T \rho_d$

The vector κ is a spatial frequency and the Fourier transform of the specific intensity with respect to $\rho = x\hat{x} + y\hat{y}$ is

$$\mathcal{F}\{I(\vec{z}, \vec{\rho}, \vec{s})\} \equiv I_1(\vec{z}, \kappa, \vec{s}) = \int I(\vec{z}, \vec{\rho}, \vec{s}) \exp(i\vec{\kappa} \cdot \vec{\rho}) d\vec{\rho} \quad (100)$$

where $\mathcal{F}\{\cdot\}$ indicates the Fourier transform operation. The inverse Fourier transform of $I_1(\vec{z}, \kappa, \vec{s})$ is

$$I(\vec{z}, \vec{\rho}, \vec{s}) = \frac{1}{(2\pi)^2} \int_{-\infty}^{\infty} I_1(\vec{z}, \kappa, \vec{s}) \exp(i\vec{\kappa} \cdot \vec{\rho}) d\kappa \quad (101)$$

In addition, the Fourier transforms of the phase function $p(s)$ and the flux density are given by

$$P(\vec{q}) = \int_{-\infty}^{\infty} p(\vec{s}) \exp(i\vec{s} \cdot \vec{q}) d\vec{s} \quad (102)$$

and

$$F(z, \kappa, q) = \int_{-\infty}^{\infty} I_2(z, \kappa, \vec{s}) \exp(i\vec{s} \cdot \vec{q}) d\vec{s} \quad (103)$$

(for the definition of $I_2(z, \vec{\kappa}, \vec{s})$ see Appendix J).

Consider now the case of plane wave incidence on a tissue medium bounded by parallel planes located at $z = 0$ and $z = d$. At the boundary $z = 0$ the incident specific intensity can be written as

$$I_0(\vec{\rho}, \vec{s}) = I_0 \delta(\vec{s}) \quad (104)$$

and the flux at $z = 0$ is (see Appendix J).

$$F_0(\kappa, q) = (2\pi)^2 I_0 \delta(\kappa) \quad (105)$$

To approximate forward scattering a Gaussian form for the phase function may be assumed whereupon the phase function $p(s)$ becomes

$$p(\vec{s}) = 4\alpha_p W_0 \exp(-\alpha_p s^2) \quad (106)$$

where α_p is proportional to $(D/\lambda)^2$ and D is the particle diameter and λ is the wavelength of illuminating radiation.

If equation (105) and the Fourier transform of equation (106) are substituted into equations (98) and (99) respectively, one gets for $K(z, \vec{\kappa}, q)$ and $I(z, \vec{\rho}, s)$ the following solutions:

$$K(z, \vec{\kappa}, q) = \exp \left\{ - \int_0^z \rho_n \sigma_t [1 - W_0 \exp(q^2/4\alpha_p)] dz' \right\} \quad (107)$$

and

$$I(z, \vec{\rho}, \vec{s}) = \frac{\alpha_P I_0}{\pi \rho_{nt} \sigma_z W_0} \exp \left[-\rho_{nt} \sigma_z z - \frac{\alpha_P s^2}{\rho_{nt} \sigma_z W_0} \right] \quad (108)$$

The steps that lead to equations (107) and (108) may be found in Appendices J and K. Appendix J presents the general solution of equation (96) leading to equation (108). Appendix K describes the steps required to calculate the Fourier transform of the phase function to arrive at equation (107).

Appendix F: The Correlation Function in the Small Angle Approximation:
Plane Wave Solution

The general solution for the specific intensity is:

$$I(\vec{z}, \vec{s}) = [1/(2\pi)^4] \int d\vec{\kappa} d\vec{q} \exp(-i\vec{\kappa} \cdot \vec{\rho} + i\vec{s} \cdot \vec{q}) E_0(\vec{\kappa}, \vec{q} + \vec{\kappa} \vec{z}) K(\vec{z}, \vec{\kappa}, \vec{q}) \quad (98)$$

where

$$E_0(\vec{\kappa}, \vec{q}) = \iint I_0(\vec{\rho}, \vec{s}) \exp(-i\vec{\kappa} \cdot \vec{\rho} + i\vec{s} \cdot \vec{q}) d\vec{\rho} d\vec{s} \quad (109)$$

$$K(\vec{z}, \vec{\kappa}, \vec{q}) = \exp\left[-\int_0^z \rho_n \sigma_t \left\{1 - \frac{1}{4\pi} P(\vec{q} + \kappa(\vec{z} - \vec{z}'))\right\} dz'\right] \quad (110)$$

$$P(\vec{q}) = \iint p(\vec{s}) e^{i\vec{s} \cdot \vec{q}} d\vec{s} \quad (111)$$

For plane wave incidence, the specific intensity at $t = 0$ is

$$I_0(\vec{\rho}, \vec{s}) = I_0 \delta(\vec{s}) \quad (112)$$

and, therefore the flux density at $z = 0$ becomes

$$E_0(\vec{\kappa}, \vec{q}) = (2\pi)^2 I_0 \delta(\vec{\kappa}) \quad (113)$$

To approximate forward scattering, the phase function is written in Gaussian form:

$$p(s) = 4\alpha_p W_0 \exp(-\alpha_p s^2) \quad (4)$$

where α_p is proportional to $(D/\lambda)^2$ and $W_0 = \sigma_s/\sigma_t$. By equation (111)

$P(q)$ becomes

$$P(\vec{q}) = 4\pi W_0 \exp(-q^2/4\alpha_p) \quad (111)$$

The Fourier transform calculation to derive equation (111) from equation (4) may be found in Appendix K.

Substituting equations (112), (113), and (111) into equation (98) one gets

$$I(\mathbf{z}, \mathbf{\bar{s}}) = \frac{1}{(2\pi)^4} \int_{-\infty}^{\infty} d\vec{\kappa} \int_{-\infty}^{\infty} d\vec{q} \exp(i\vec{\kappa} \cdot \vec{\rho} - i\vec{s} \cdot \vec{q}) (z)^2 I_0 \delta(\kappa) K(\mathbf{z}, \vec{\kappa}, \vec{q}) \quad (114)$$

$$= \frac{1}{(2\pi)^2} \int I_0 \delta(\vec{\kappa}) \exp(i\vec{\kappa} \cdot \vec{\rho}) K(\mathbf{z}, \vec{\kappa}, \vec{q}) d\kappa \int e^{i\vec{s} \cdot \vec{q}} d\vec{q} \quad (115)$$

Evaluating equation (115) for $\rho = 0$ yields

$$I(\mathbf{z}, \mathbf{\bar{s}}) = \frac{I_0}{(2\pi)^2} \int K(\mathbf{z}, \vec{q}) e^{i\vec{s} \cdot \vec{q}} d\vec{q} \quad (116)$$

Since the correlation function and the specific intensity are Fourier transform pairs and equation (116) is an inverse Fourier transform, it follows that

$$\begin{aligned} \Gamma(\mathbf{z}, \vec{q}) &= \mathcal{F}\{I(\mathbf{z}, \mathbf{\bar{s}})\} \\ &= \mathcal{F}\left\{I_0 \left[\frac{1}{(2\pi)^2} \int K(\mathbf{z}, \vec{q}) e^{-i\vec{s} \cdot \vec{q}} d\vec{q} \right]\right\} \\ &= I_0 \mathcal{F}\mathcal{F}^{-1}\{K(\mathbf{z}, \vec{q})\} \\ &= I_0 K(\mathbf{z}, \vec{q}) \end{aligned} \quad (117)$$

However, by equation (106),

$$\begin{aligned}
 K(z, \vec{q}) &= \exp \left[- \int_0^z \rho_t \sigma_t \left[1 - \frac{1}{4\pi} P(\vec{q}) \right] dz' \right] \\
 &= \exp \left\{ - \rho_t \sigma_t z \left[1 - W_0 \exp(-q^2/4\alpha_p) \right] \right\}
 \end{aligned} \tag{118}$$

Therefore, by equation (117) the correlation function becomes

$$\Gamma(z, \vec{q}) = I_0 \exp \left\{ - \rho \sigma z \left[1 - W_0 \exp(-q^2/4\alpha_p) \right] \right\} \tag{6}$$

where

$$\begin{aligned}
 \Gamma(z, \rho_d) &= \Gamma(z, \vec{q}) \Big|_{\vec{q} = K_T \rho_d} \\
 &= \langle \psi(z, \rho_1) \psi^*(z, \rho_2) \rangle
 \end{aligned} \tag{119}$$

Appendix G: Image Resolution Limit in a Random Medium

Consider a monochromatic plane wave normally incident upon a medium consisting of randomly distributed scatterers with absorption cross section σ_a and scattering cross section σ_s and optical thickness $\tau = \rho_n(\sigma_s + \sigma_a) \cdot d$ where d is the physical thickness of the medium.

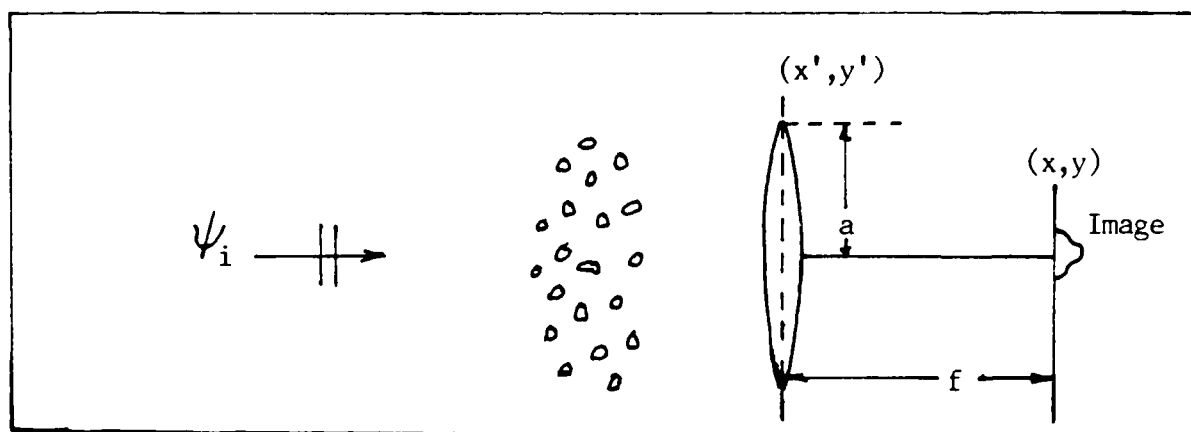


Figure 30. A monochromatic plane wave ψ_i propagating through a random distribution of scatterers (20:301). The resultant scattered wave is focused onto the x, y plane (Fourier transform plane). The lens has radius a and focal length f .

The resultant scattered wave is focused by a lens of radius a and focal length f onto the x, y plane as shown in Figure 30. Since, in the absence of scattering, the lens would produce the Airy pattern in the x, y plane (representing the diffraction limit), the actual intensity distribution that results from scattering can be compared with the diffraction limited case to get a sense of attainable resolution for an arbitrary object.

In the x', y' plane (the plane where the lens is located) the field is $\psi(z, \rho')$ ($\rho' = x'\hat{x} + y'\hat{y}$). The field at the focal plane (x, y) can be written in general terms using the Kirchoff formula (20:302):

$$\psi_f(\rho) = \frac{k}{2\pi i} \int_S \frac{\exp(ikr + i\varphi)}{r} \psi(z, \rho') d\rho' \quad (120)$$

where the integration is taken of the area S of the lens and r is the distance between the point on the aperture (lens) and the point on the focal plane (2:302).

Using the Fresnel approximations

$$\frac{e^{ikr}}{r} \approx (1/f) \exp ik \left[f + \frac{(x' - x)^2 + (y' - y)^2}{2f} \right]$$

and

$$\varphi \approx -\frac{k}{2f} (x'^2 + y'^2)$$

and substituting these approximations into equation (116) one obtains

$$\psi_f(\rho) = (k/2\pi f i) \exp(ikf + \frac{ik\rho^2}{2f}) \int_S \exp(\frac{ik}{f} \vec{\rho} \cdot \vec{\rho}') \psi(z, \vec{\rho}') d\vec{\rho}' \quad (121)$$

where $\vec{\rho} = x\hat{x} + y\hat{y}$ and $\vec{\rho}' = x'\hat{x} + y'\hat{y}$.

To get the intensity in the focal plane the quantity $\psi_f \psi_f^*$ = $|\psi_f(\rho)|^2$ must be calculated. This is done in the following manner:

$$\begin{aligned} \psi_f(\rho) \psi_f^*(\rho) &= \frac{k}{2\pi i} \exp(ikf + \frac{ik\rho^2}{2f}) \int_S \exp(\frac{ik}{f} \vec{\rho} \cdot \vec{\rho}_1') \psi(z, \vec{\rho}_1') d\vec{\rho}_1' \\ &\times \left(\frac{k}{2\pi i} \right)^* \exp(ikf - \frac{ik\rho^2}{2f}) \int_S \exp(-\frac{ik}{f} \vec{\rho} \cdot \vec{\rho}_2') \psi^*(z, \vec{\rho}_2') d\vec{\rho}_2' \end{aligned} \quad (122)$$

Carrying out the indicated multiplication results in

$$|\psi_f(\vec{\rho})|^2 = \iint_S \exp\left[\frac{ik}{f} \vec{\rho}(\vec{\rho}'_1 - \vec{\rho}'_2)\right] \psi(z, \vec{\rho}'_1) \psi^*(z, \vec{\rho}'_2) d\vec{\rho}'_1 d\vec{\rho}'_2 \quad (123)$$

If, following Ishimaru (2:302), the identifications $\vec{\rho}_d' = \vec{\rho}'_1 - \vec{\rho}'_2$, $\vec{\rho}_c' = 1/2 (\vec{\rho}'_1 + \vec{\rho}'_2)$, and $d\vec{\rho}'_1 d\vec{\rho}'_2 = d\vec{\rho}_d' d\vec{\rho}_c'$ are made, equation (123) may be written as

$$|\psi_f(\rho)|^2 = \iint_S \exp\left[\frac{ik}{f} \vec{\rho} \vec{\rho}_d'\right] \Gamma(z, \vec{\rho}_d') d\vec{\rho}_d' d\vec{\rho}_c' \quad (124)$$

Note that the equation $d\vec{\rho}_d' d\vec{\rho}_c' = d\vec{\rho}'_1 d\vec{\rho}'_2$ is not, strictly speaking, mathematically true. However, under the integration indicated, the end result is the same whether one uses $d\vec{\rho}'_1 d\vec{\rho}'_2$ or $d\vec{\rho}_d' d\vec{\rho}_c'$ since all points in the aperture are included in either case.

Using the result obtained in the last section for the correlation function, namely that

$$\begin{aligned} \Gamma(z, \vec{\rho}_d') &= \langle \psi(z, \vec{\rho}'_1) \psi^*(z, \vec{\rho}'_2) \rangle \\ &= I_0 \exp\left\{-\tau \left[1 - w_0 \exp\left(-\frac{K_T^2 \rho_d'^2}{4\alpha_p}\right)\right]\right\} \end{aligned} \quad (125)$$

where $\tau = \rho_n \sigma_t z$, it can be seen that equation (124) takes the form

$$\begin{aligned} P_f(\rho) &= \langle |\psi_f(\rho)|^2 \rangle \\ &= \frac{k^2}{(2\pi f)^2} \iint_S \exp\left(\frac{ik}{f} \rho \cdot \rho_d'\right) \Gamma(z, \rho_d') d\rho_d' d\rho_c' \end{aligned} \quad (126)$$

The quantity $P_f(\rho)$ is called the point spread function, and in the case of plane wave illumination, is the intensity in the focal plane as the result of imaging a point source at a large distance from the scattering

medium. An evaluation of the point spread function provides information as to how the scattering (random) medium "breaks up" the forward propagating plane wave into a myriad of phase fronts propagating in various and constantly changing directions as the wave strikes particle after particle in the medium. It can be seen from equation (126) that the correlation function Γ determines the behavior of the point spread function and is, therefore, from a mathematical point of view, the quantity representative of the scattering process.

To carry out the integration indicated in equation (126) it is useful to define a function $F(\vec{\rho})$ (20:302):

$$F(\vec{\rho}) = \begin{cases} 1 & , \quad |\vec{\rho}| < a \\ 0 & , \quad |\vec{\rho}| > a \end{cases} \quad (127)$$

Given equation (122), $P_f(\rho)$ becomes

$$P_f(\rho) = \frac{k^2}{(2\pi f)^2} \iint_{-\infty}^{\infty} \exp\left(\frac{ik}{f} \vec{\rho} \cdot \vec{\rho}_d\right) \Gamma(z, \vec{\rho}_d') F(\vec{\rho}_1') F(\vec{\rho}_2') d\vec{\rho}_d' d\vec{\rho}_c' \quad (128)$$

Using the relation $\vec{\rho}_d' = \vec{\rho}_1' - \vec{\rho}_2'$ and $\vec{\rho}_c' = 1/2(\vec{\rho}_1' + \vec{\rho}_2')$, the integration of $F(\vec{\rho}_1') F(\vec{\rho}_2')$ can be written as

$$K(\rho_d') = \iint_{-\infty}^{\infty} F\left(\rho_c' + \frac{\rho_d'}{2}\right) F\left(\rho_c' - \frac{\rho_d'}{2}\right) d\rho_c' \quad (129)$$

The quantity $K(\rho_d')$ is the area of the intersection of two circles of radius a and whose centers are separated by ρ_d' . The solution to equation (129) can be obtained geometrically resulting in (20:303)

$$K(\vec{\rho}_d) = K(\rho_d) = \begin{cases} 2a^2 \left[\cos^{-1} \left(\frac{\rho'_d}{2a} \right) - \frac{\rho'_d}{2a} \left(1 - \frac{\rho_d'^2}{4a^2} \right) \right], & \rho'_d < 2a \\ 0 & \rho'_d > 2a \end{cases} \quad (130)$$

Now equation (128) may be written as

$$\begin{aligned} P_f(\vec{\rho}) &= P_f(\rho) \\ &= \frac{k^2}{(2\epsilon)^2} \int_{-\infty}^{\infty} \exp(i \frac{k}{f} \vec{\rho} \cdot \vec{\rho}'_d) \Gamma(z, \vec{\rho}'_d) K(\vec{\rho}'_d) d\vec{\rho}'_d \end{aligned} \quad (131)$$

Note that

$$\begin{aligned} \rho \cdot \rho'_d &= (x\hat{x} + y\hat{y}) \cdot [(x_1 - x_2)\hat{x} + (y_1 - y_2)\hat{y}] \\ &= x(x_1 - x_2) + y(y_1 - y_2) \end{aligned} \quad (132)$$

Transforming equation (129) to polar coordinates by the relations

$$\begin{aligned} x &= \rho \cos \varphi & y &= \rho \sin \varphi \\ x_1 &= \rho_1 \cos \theta & y_1 &= \rho_1 \sin \theta \\ x_2 &= \rho_2 \cos \theta & y_2 &= \rho_2 \sin \theta \end{aligned} \quad (133)$$

$$d\rho'_d d\rho'_c = \rho'_d d\rho'_d d\theta$$

and substituting equation (133) into equation (132) one obtains after algebraic manipulation:

$$\vec{\rho} \cdot \vec{\rho}'_d = \rho \rho_d [\cos(\theta - \varphi)] \quad (134)$$

Then equation (131) becomes

$$P_f(\rho) = \frac{k^2}{(2\pi f)^2} \iint \rho_d' d\rho_d' d\theta \exp(i \frac{k}{f} \rho \rho_d' \cos(\theta - \varphi)) \Gamma(z, \rho_d') K(\rho_d') \quad (135)$$

Upon interchanging the order of integration one gets

$$P_f(\rho) = \frac{k^2}{(2\pi f)^2} \int_0^{2a} \left\{ \int_0^{2\pi} \exp\left[\frac{ik}{f} \tilde{\rho} \cdot \tilde{\rho}_d' \cos(\theta - \varphi)\right] d\theta \right\} \Gamma(z, \tilde{\rho}_d') K(\tilde{\rho}_d') \tilde{\rho}_d' d\tilde{\rho}_d'$$

And using the identity

$$J_0(a) = \frac{1}{2\pi} \int \exp[-ja \cos(\theta - \varphi)] d\theta$$

$P_f(\rho)$ can be written as

$$P_f(\rho) = \frac{k^2}{(2\pi f)^2} \int_0^{2a} [2\pi \rho_d' J_0(\frac{k}{f} \tilde{\rho} \tilde{\rho}_d')] \Gamma(z, \tilde{\rho}_d') K(\tilde{\rho}_d') d\tilde{\rho}_d'$$

and, therefore,

$$P_f(\rho) = \frac{k^2}{2\pi f^2} \int_0^{2a} \rho_d' d\rho_d' J_0(\frac{k}{f} \rho \rho_d') \Gamma(z, \rho_d') K(\rho_d') \quad (7)$$

where $\Gamma(z, \rho_d')$ is given in equation (125) and $K(\rho_d')$ is given in equation (130).

Equation (7) (the point spread function) gives the intensity in the focal plane. Note that, in the case of no scattering, ρ_n in $\rho_n \sigma_t z$ is zero and $\Gamma(z, \rho_d')$ (equation (125)) becomes equal to I_0 . Therefore, in the absence of scattering, from equation (126) the intensity in the focal plane is (20:302)

$$P_d(\rho) = \frac{k^2 I_0}{(2\pi f)^2} \left[2\pi \int_0^a J_0(\frac{k}{f} \rho \rho') \rho' d\rho' \right]^2 \quad (136)$$

Letting $r' = \frac{k}{f}\rho'$ one obtains $d\rho' = \frac{f}{k}dr'$ and equation (136) becomes

$$\begin{aligned} P_a(\) &= \frac{k^2 I_0}{(2\pi f)^2} \left[2\pi \int_0^{(k/f)\rho a} r' \frac{f}{k} J_0(r') \frac{f}{k} dr' \right]^2 \\ &= \frac{k^2 I_0}{(2\pi f)^2} (2\pi)^2 (f/k)^4 \int_0^{(k/f)\rho a} r' J_0(r') dr' \end{aligned}$$

Then using the relation

$$\int_0^x \xi J_0(\xi) d\xi = x J_1(x)$$

one obtains

$$\begin{aligned} P_a(\) &= \frac{I_0 f^2}{k^2 \rho^4} \left[\left(\frac{k\rho a}{f} \right)^2 J_1^2 \left(\frac{k\rho a}{f} \right) \right] \\ &= I_0 (a^2/\rho^2) J_1^2 \left(\frac{k\rho a}{f} \right) \end{aligned} \quad (137)$$

Equation (137) is the Airy pattern created by a lens of radius a and focal length f .

Equation (7) is the major result of this section and will constitute the basis for the following analysis of the limit of resolution one can expect from an imaging system in the presence of a scattering medium.

To arrive at a useful interpretation of equation (7), it is convenient to consider the case of large optical thickness ($\tau \gg 1$) corresponding to a situation in which there is strong scattering (large σ_s) and/or a large physical thickness. In this case, the correlation function Γ takes the form

$$\Gamma(\vec{z}, \vec{q}) \approx I_0 \exp(-\tau) [1 - W_0 + W_0(q^2/4\alpha_p)] \quad (138)$$

where the approximation

$$\exp(-q^2/4) \approx 1 - (q^2/4)$$

has been used.

To equation (138) may be added $I_0 \exp(-\tau)$ since, if τ is large, this additional term can contribute only a small amount to the value for Γ .

If these approximations are made, equation (125) becomes

$$\Gamma(z, q') \approx I_0 \exp(-\tau) + I_0 \exp \left\{ (-\tau) [1 - W_0 + W_0 (q'^2/4\alpha_p)] \right\} \quad (139)$$

With Γ expressed in this form, it becomes clear that the first term ($I_0 \exp(-\tau)$) represents a coherent component of the correlation function propagating through a medium in accordance with the Lambert-Beer law.

The second term, then, represents an incoherent component of Γ indicating the presence of scattering. By equation (139), then, it has become possible to separate Γ into coherent and incoherent parts (20:304).

Given the form of Γ in equation (139) and considering equation (137) (the Airy pattern under no scattering) it can be seen that equation (7) has a solution for large τ which is the sum of coherent and incoherent components.

Accordingly, replacing I_0 with $I_0 \exp(-\tau)$ in equation (137) one gets the coherently propagating portion of $P_f(\rho)$:

$P_c(\rho) \equiv$ coherent component of the intensity

$$= I_0 \exp(-\tau) (a/\rho)^2 J_1^2 \left(\frac{k\rho a}{f} \right) \quad (9)$$

The incoherent part of the intensity is unchanged from its form in

equation (7) (in accordance with the approximation indicated in equation (139)), and therefore

$P_i(\rho) \equiv$ incoherent component of the intensity

$$= \frac{k^2}{2f^2} \int \rho_d' d\rho_d' J_0\left(\frac{k\rho}{f} \rho_d'\right) \Gamma_i(z, \rho_d') K(\rho_d') \quad (140)$$

where

$$\Gamma_i(z, \rho_d') \equiv I_0 \exp\left\{-\tau\left[1 - W_0 + W_0 \frac{K^2 \rho_d'^2}{4\alpha_p}\right]\right\} \quad (141)$$

and $q' = Kr\rho_d'$. Using equations (9) and (140), the intensity in the focal plane can be written as

$$P_f(\rho) = P_c(\rho) + P_i(\rho) \quad (8)$$

At this point it is convenient to define the correlation distance- a concept which will be employed later to recast equation (140) into a form which lends itself to gaining a clearer understanding of limitations on resolution.

The correlation distance ρ_0 is the distance from the axis of illumination at which the correlation function fall to e^{-1} of its value at $\rho_d = 0$.

The incoherent portion of the correlation function Γ_i (equation 139) at $\rho_d = 0$ is

$$\Gamma_i(z, \rho_d) = I_0 \exp\{-\tau(1 - W_0)\} \quad (142)$$

Taking e^{-1} of Γ_i one obtains

$$[I_0 \exp(-\tau(1 - W_0))]e^{-1} = I_0 \exp\left[-\tau\left(1 - W_0 + W_0 \frac{K^2 \rho_0^2}{4\alpha_p}\right)\right] \quad (143)$$

where ρ_d has been set equal to ρ_0 . After eliminating the factor $I_0 \exp[-\tau(1 - w_0)]$ from both sides of equation (143) one arrives at the results (20:304)

$$\rho_0 = \left(\frac{4\alpha_p}{\tau W_0 K_r^2} \right)^{1/2} \quad (144)$$

It may be assumed that, due to intense scattering (large τ), the correlation distance in the case of transillumination is much smaller than the size of the aperture. Under these circumstances, $K(\rho_d')$ in equation (140) may be set equal to $K(0) = \pi a^2$ and equation (140) may be integrated from 0 to ∞ . Consequently, (20:304)

$$P_i(\rho) = \frac{k^2}{2\pi f^2} \int \rho_d' d\rho_d' J_0\left(\frac{k\rho}{f}\rho_d'\right) \Gamma_i(z, \rho_d') \pi a^2 \quad (145)$$

This equation may be solved using the integral formula

$$\int J_\nu(at) \exp(-p^2 t^2) t^{\nu+1} dt = \frac{a^\nu}{(2p)^{\nu+1}} \exp\left(-\frac{a^2}{4p^2}\right)$$

to get

$$P_i(\rho) = a^2 (k^2/f^2) [\alpha_p / \tau W_0 K_r^2] \exp\left(-\frac{\alpha_p}{\tau W_0 K_r^2} \frac{k^2}{f^2} \rho^2\right) I_0 \exp[-\tau(1-w_0)]$$

Then defining the quantity (20:304)

$$\rho_i^2 = \left(\frac{K_r f}{k} \right)^2 \left(\frac{\tau W_0}{\alpha_p} \right) = (f/k)^2 (4/\rho_0)^2$$

one obtains

$$P_i(\rho) = I_0 (a/\rho_i)^2 \exp[-\tau(1-w_0) - (\rho/\rho_i)^2] \quad (10)$$

Using equations (9) and (10) it is possible to gain a clearer understanding of the imaging process in the presence of scatterers. Equation (9) indicates that the coherent portion of the intensity propagates with the same pattern as in free space except for the Lambert-Beer type of attenuation. According to equation (10), on the other hand, the incoherent intensity spreads out in the focal plane.

Appendix H: Phase Retrieval

The phase retrieval problem is, in general terms, concerned with the question of how spectral information may be derived from a knowledge of only spectral magnitude (or intensity) information. The importance of phase in imaging is well attested. From a complete knowledge of the Fourier transform (including both magnitude and phase) it is possible to determine by inverse Fourier transformation the image of an object. This fundamental capability is guaranteed by the uniqueness of the relation that exists between a function $f(x)$ and its Fourier transform $F(\xi)$. However, if it is the case that only the magnitude of the Fourier transform is known, it is not possible, in general, to infer uniquely the characteristics of an object $f(x)$ as any number of objects can have the same Fourier magnitude. The distinguishing feature among these objects in the spectral domain lies in the phase of the Fourier transform.

In recent years some important advances have been made regarding the problem of reconstructing an image from only the knowledge of the Fourier magnitude. These methods employ phase retrieval algorithms when theoretical foundation is based on the fact that the real and imaginary parts of an analytic signal are Hilbert transform pairs (16). However, it is not the purpose of this research to explore the theory of phase retrieval as such. The interest here is to employ the scattering theory of Chapter II to analyze the efficacy of phase retrieval as it might be applied to the problem of image reconstruction in transillumination.

For the purposes of analysis, the phase retrieval problem to be considered is characterized as the problem of reconstructing an image

from a single intensity measurement in the Fourier transform (diffraction) plane and an estimate (based on theory) of the point spread function of an imaging system in the presence of a scattering medium. The particular phase retrieval algorithm that would be exercised on this is assumed to be of the error-reduction type such as the Gerchberg-Saxton algorithm. The error reduction method was chosen for analysis because it has the property that the error in the reconstruction can only decrease (or stay the same) at each iteration (14:197). In symbolic form, this property of the error-reduction algorithm may be written as

$$E_{F,k+1}^2 < E_{O,k}^2 < E_{F,k}^2 \quad (146)$$

where $E_{F,k}^2$ and $E_{O,k}^2$ are the errors in the Fourier modulus and object at the k^{th} iteration, respectively.

From the form of the equation (146), one can see that if the minimum error in the Fourier modulus can be calculated, and if at the k^{th} iteration $E_{F,k}^2$ is equal to the minimum error, then $E_{F,k+1}^2 = E_{F,k}^2$. Therefore, it would follow that $E_{O,k}^2 = E_{F,k}^2$ when $E_{F,k}^2$ is the minimum possible value of the Fourier modulus error. In this manner, then, one arrives at the least amount of error that can be expected in the reconstructed image.

Calculation of the Minimum Error in Image Reconstruction by Phase Retrieval as Applied to Transillumination.

The following calculation is based on the relationship that exists between the intensity and point spread function (as measured in the diffraction plane) to the Fourier modulus of the object. This relationship can be expressed as

(147)

where $|\hat{F}(f)|$, $|I(f)|$, and $|M(f)|$ represent the magnitude of the Fourier transforms of the object intensity, image intensity, and point spread function, respectively. The quantity $|M(f)|$ is called the modulation transfer function (MTF). The frequency f is measured in cycles per unit length.

The phase retrieval method consists of making an estimate of the Fourier modulus of the object by taking an intensity measurement in the diffraction (Fourier transform) plane and dividing this quantity by a measurement (or estimate based on a theoretical model) of the MTF. This estimate of the Fourier modulus of the object is then inserted into the error-reduction algorithm where object domain and Fourier domain constraints are applied to arrive at a new estimate of the object. The steps involved in the algorithms as described by Fienup are

"(1) Fourier transform an estimate the object; (2) replace the modulus of the resulting computed Fourier transform with the measured Fourier modulus to form an estimate of the Fourier transform; (3) inverse Fourier transform the estimate of the Fourier transform; and (4) replace the modulus of the resulting computed image with the measured modulus to form a new estimate of the object." (14:194)

For further discussion of the steps of the algorithm and a description of the function (object) and Fourier constraints on the problem the reader is referred to Fienup (14:217).

It can be seen that, in the case of transillumination, the measured value of the Fourier modulus of the object would be corrupted by noise generated by the scattering process. The noise in the Fourier modulus $|\hat{F}(f)|$ ultimately limits the efficacy of the phase retrieval method (14). Mathematically, this noise is expressed in the point spread function or its Fourier transform, the MTF. In practice, the MTF could be obtained by taking a measurement on a reference point source through

the scattering medium. Alternatively, the MTF could be derived from a calculated point spread function. (14:217).

Since the point spread function for a plane-parallel medium has already been obtained in Chapter II, the MTF can now be calculated and substituted into equation (147) to find the value of $|F(f)|$ which would be used in phase retrieval as the measured Fourier modulus.

Calculation of the MTF.

The reader will recall from Chapter II that the point spread function $P(\rho)$ may be written as

$$P(\rho) = P_c(\rho) + P_i(\rho) \quad (148)$$

where $P_c(\rho)$ is the coherent (average) intensity and $P_i(\rho)$ is the incoherent (fluctuating) intensity.

From equation (148) one obtains

$$\begin{aligned} \tilde{P}(f) &= \tilde{P}_c(f) + \tilde{P}_i(f) \\ &= M(f) \\ &= M_c(f) + M_i(f) \end{aligned} \quad (149)$$

Equation (149) is the Fourier transform of $P(\rho)$ and $M(f)$ is the optical transfer function. The quantity $M_c(f)$ represents what will be called the coherent portion of the transform and $M_i(f)$ the incoherent portion.

At the outset, the non-normalized incoherent $M_i'(f)$ and non-normalized coherent $M_c'(f)$ will be calculated. Following these calculations, the normalization factor will be obtained to arrive at the normalized MTF.

First, $M_i(f)$ is the Fourier transform of the incoherent portion of $P(\rho)$:

$$M_i(\vec{f}) = \int_0^\infty \tilde{P}_i(\vec{f}) \exp(i2\pi\vec{f} \cdot \vec{\rho}) d\vec{\rho} \quad (150)$$

where

$$P_i(\rho) = I_0 (a/\rho_i)^2 \exp[-\tau(1-W_0) - (\rho/\rho_i)^2] \quad (151)$$

and $2\pi f = (k/f_0) \rho_d$ (f_0 = focal length of lens in Figure 29).

$$\text{Let } \vec{\rho}_d = \rho_d (\cos\varphi' \hat{x} + \sin\varphi' \hat{y}),$$

$$\vec{\rho} = \rho (\cos\varphi \hat{x} - \sin\varphi \hat{y})$$

then,

$$\vec{\rho}_d \cdot \vec{\rho} = \rho \rho_d (\cos\varphi' \cos\varphi + \sin\varphi' \sin\varphi) = \rho \rho_d \cos(\varphi' - \varphi)$$

and

$$d\vec{\rho} = \rho d\rho d\varphi$$

Therefore, from equations (150) and (151):

$$M_i(\) = \int_0^\infty \int_0^{2\pi} P_i(\) \exp[i \frac{k}{f_0} \rho \rho_d \cos(\varphi' - \varphi)] \rho d\rho d\varphi \quad (152)$$

$$= \int_0^\infty \left\{ \int_0^{2\pi} \exp[i \frac{k}{f_0} \rho \rho_d \cos(\varphi' - \varphi)] P_i(\rho) \rho d\varphi \right\}$$

$$= \int_0^\infty 2\pi J_0(\frac{k}{f_0} \rho \rho_d) P_i(\rho) \rho d\rho$$

$$= 2\pi I_0 (a/\rho_i)^2 \exp[-\tau(1-W_0)] \quad (153)$$

$$\times \int J_0(\frac{k}{f_0} \rho \rho_d) \exp[-(\rho/\rho_i)^2] d\rho$$

Now using the formula

$$\int_0^\infty \exp[-a^2 t^2 (\nu + 1)] J_0(bt) dt = \frac{b^\nu}{(2a^2)^{\nu+1}} \exp(-b^2/4a^2)$$

$$(\operatorname{Re} \nu > -1, \operatorname{Re} a^2 > 0)$$

equation (153) becomes

$$M_i'(\rho_d) = \pi I_0 a^2 \exp[-\tau(1-W_0)] \exp\left[\frac{((k/f_0)\rho_d\rho_i)^2}{4}\right] \quad (154)$$

Now to calculate $M_c'(\rho_d)$ (the prime indicated denotes non-normalized). First, recall that

$$P_c(\rho) = I_0 \exp(-\tau) (a/\rho)^2 J_1^2(k\rho a/f_0) \quad (155)$$

and let $b \equiv ka/f_0$, then

$$M_c'(\vec{\rho}_d) = I_0 \exp(-\tau) a^2 \int \frac{1}{\rho^2} J_1^2(b\rho) \exp[i(k/f_0)\vec{\rho} \cdot \vec{\rho}_d] d\vec{\rho} \quad (156)$$

Following steps similar to those that led to equation (152) one obtains

$$M_c'(\rho_d) = I_0 e^{-\tau} a^2 \int_0^{2\pi} \int_0^\infty \frac{1}{\rho^2} J_1^2(b\rho) \exp[ik/f_0 \rho \rho_d \cos(\varphi' - \varphi)] \rho d\rho d\varphi$$

Interchanging orders of integration results in

$$M_c'(\rho_d) = I_0 \exp(-\tau) a^2 \int 2\pi I_0 (k/f_0) \rho_d (1/\rho) J_1^2(b\rho) d\rho$$

Now using the formula

$$\int_0^\infty \frac{J_\mu(at) J_\nu(bt) dt}{t^\lambda} = \frac{b^\nu (\frac{\mu+\nu-\lambda+1}{2})}{2^\lambda a^{\nu-\lambda+1} \Gamma(\nu+1) (\frac{\mu-\nu+\lambda+1}{2})} \\ \times {}_2F_1\left(\frac{\mu+\nu-\lambda+1}{2}, \frac{\nu-\mu-\lambda+1}{2}; \nu+1; \frac{b^2}{a^2}\right)$$

$$[\operatorname{Re}(\mu+\nu-\lambda+1) > 0, \operatorname{Re} \lambda > -1, 0 \leq b \leq a] \quad (157)$$

Setting $a = b$, $\mu = \nu = 1$, $M_c(\rho_d)$ can be written as

$$\begin{aligned}
 M'_c(\rho_d) &= 2\pi I_o \exp(-\tau) a^2 J_0\left(\frac{ka}{f_o} \rho_d\right) \\
 &\quad \times \frac{b\Gamma(1)}{2b\Gamma(2)\Gamma(1)} {}_2F_1(c; d; e; z) \\
 &= 2\pi I_o \exp(-\tau) a^2 J_0\left[\left(k/f_o\right) \rho_d\right] \\
 &\quad \times \frac{1}{2\Gamma(2)} \frac{\Gamma(e)\Gamma(e-c-d)}{\Gamma(e-c)\Gamma(e-d)} \\
 &= 2\pi I_o \exp(-\tau) a^2 J_0\left[\left(ka/f_o\right) \rho_d\right] \\
 &\quad \times \frac{1}{2\Gamma(2)} \frac{\Gamma(2)\Gamma(1)}{\Gamma(1)\Gamma(2)}
 \end{aligned}$$

and, therefore,

$$M'_c(\rho_d) = \pi I_o \exp(-\tau) a^2 J_0\left[\left(ka/f_o\right) \rho_d\right] \quad (158)$$

Finally, combining equations (154) and (158) and noting equation (149):

$$\begin{aligned}
 M'(\rho_d) &= I_o \exp(-\tau) a^2 J_0\left(\frac{ka}{f_o} \rho_d\right) \\
 &\quad + I_o a^2 \exp[-\tau(1-w_o)] \exp\left\{\frac{\left(\frac{k}{f_o} \rho_d \rho_i\right)^2}{4}\right\} \quad (159)
 \end{aligned}$$

Equation (159) is the desired result for the non-normalized MTF. The first term on the right side of equation (159) represents the coherent (average) part of the MTF and the second term represents the incoherent

(fluctuating) part.

To get the normalized MTF, it is necessary to calculate the Fourier transform of the point spread function at zero frequency:

$$\begin{aligned}\text{Normalizing Factor} &= \int_0^{\infty} P(\rho) d\rho \\ &= \int P_c(\rho) + P_i(\rho) d\rho\end{aligned}\quad (160)$$

$$\begin{aligned}\text{First,} \quad \int_0^{\infty} P_i(\rho) d\rho &= I_0 \left(\frac{a}{\rho_i}\right)^2 \exp[-\tau(1-W_0)] \int_0^{\infty} \exp(\rho/\rho_i)^2 d\rho \\ &= I_0 \left(\frac{a}{\rho_i}\right)^2 \exp[-\tau(1-W_0)] (1/2) \rho_i (\pi)^{1/2}\end{aligned}\quad (161)$$

Equation (161) is the incoherent portion of the normalization factor.

Now set

$$\int P_c(\rho) d\rho = I_0 \exp(-\tau) a^2 \cdot \int_0^{\infty} \frac{1}{\rho^2} J_1^2\left(\frac{k\rho a}{f_0}\right) d\rho\quad (162)$$

Using equation (157) and letting $c = ka/f_0$:

$$\begin{aligned}\int_0^{\infty} P_c(\rho) d\rho &= I_0 \exp(-\tau) a^2 \left[\frac{c \Gamma(1/2)}{4 \Gamma(2) \Gamma(3/2)} \right] \\ &\quad \times {}_2F_1(1/2; -1/2; 2; 1) \\ &= I_0 \exp(-\tau) a^2 c \frac{\Gamma(1/2)}{4 \Gamma(3/2)} \frac{\Gamma(2) \Gamma(2)}{\Gamma(3/2) \Gamma(5/2)} \\ &= I_0 \exp(-\tau) a^2 c (1/2) \frac{8}{3\pi} \\ &= I_0 \exp(-\tau) a^2 c \frac{4}{3\pi}\end{aligned}$$

Therefore,

$$\int_0^{\infty} P_c(\rho) d\rho = I_0 \exp(-\tau) a^2 \frac{k a}{f_0} \frac{4}{3\pi}$$

and

$$\int_0^{\infty} P(\rho) d\rho = I_0 \exp(-\tau) a^3 \frac{k}{f_0} \frac{4}{3\pi} + I_0 \frac{(\pi)^{1/2}}{2\rho_i} a^2 \exp[-\tau(1-W_0)] \quad (163)$$

Now dividing $M_c'(\rho_d) + M_i'(\rho_d)$ by the normalizing factor one gets for the optical transfer function

$$M(\rho_d) = \frac{\pi a^2 J_0\left(\frac{k}{f_0} \rho_d\right) + \pi a^2 \exp(\tau W_0) \exp\left[-\frac{\left(\frac{k}{f_0} \rho_d \rho_i\right)^2}{4}\right]}{a^3 \frac{k}{f_0} \frac{4}{3\pi} + \frac{(\pi)^{1/2}}{2\rho_i} a^2 \exp(\tau W_0)} \quad (164)$$

and the MTF = $\left| M(\rho_d) \right|$.

From equation (147):

$$\left| \hat{F}(\rho_d) \right| = \frac{\left| I(\rho_d) \right|}{\left| M(\rho_d) \right|} = \frac{\left| I(\rho_d) \right|}{\left| M_c(\rho_d) + M_i(\rho_d) \right|} \quad (165)$$

Equation (165) may be rewritten as

$$\left| \hat{F}(\rho_d) \right| = \frac{\frac{\left| I(\rho_d) \right|}{\left| M_c(\rho_d) \right|}}{1 + \frac{\left| M_i(\rho_d) \right|}{\left| M_c(\rho_d) \right|}} \quad (166)$$

It is clear that $\left| I(\rho_d) \right| / \left| M_c(\rho_d) \right|$ is the correct Fourier transform of the object. Denoting by $\left| F(\rho_d) \right|$ the exact modulus of Fourier transform

of the object, equation (166) becomes

$$\left| \hat{F}(\rho_d) \right| = \frac{\left| F(\rho_d) \right|}{1 + \frac{\left| M_i(\rho_d) \right|}{\left| M_c(\rho_d) \right|}} \quad (167)$$

Subtracting $\left| F(\rho_d) \right|$ from both sides of equation (167) and squaring and dividing the result by $\left| F(\rho_d) \right|^2$ yields

$$\frac{\left| \hat{F}(\rho_d) - F(\rho_d) \right|^2}{\left| F(\rho_d) \right|^2} = \left| \frac{1}{1 + \frac{\left| M_i(\rho_d) \right|}{\left| M_c(\rho_d) \right|}} - 1 \right|^2$$

where the left side of the equation is the definition which the error-reduction algorithm gives the error in the Fourier modulus estimate. Therefore,

$$E_F^2 = \left| \frac{1}{1 + \frac{\left| M_i(\rho_d) \right|}{\left| M_c(\rho_d) \right|}} - 1 \right|^2 \quad (168)$$

Now if one can find the minimum value of $M_i(\rho_d) / M_c(\rho_d)$, then substituting that minimum value into equation (168) will yield the minimum error that can be expected in the estimate of the Fourier modulus.

The ratio $\left| M_i(\rho_d) / M_c(\rho_d) \right|$ is

$$\frac{\left| M_i(\rho_d) \right|}{\left| M_c(\rho_d) \right|} = \frac{\exp(\tau W_0) \exp \left[-\frac{[(k/f_0)\rho_d \rho_i]^2}{4} \right]}{J_0 \left[\frac{k}{f_0} \rho_d \right]} \quad (169)$$

This equation has many relative minima. In fact, the absolute minimum of equation (169) occurs at $\rho_d = \infty$. At $\rho_d = \infty$, equation (169) implies that the error in the estimate of the Fourier modulus is zero (by equation (168)). However, there is a practical limit on the magnitude of ρ_d since ρ_d has a cutoff value of $2a$ (the diameter of the aperture). Without further argumentation, therefore, it is difficult to assess the implications of equation (169).

Consider, however, the following argument which will show that, for very large T , the only way to obtain a mathematically defined estimate of the Fourier modulus is to evaluate ρ_d at approximately its zero value.

First, evaluate $M_c(\rho_d) + M_i(\rho_d)$:

$$M_c(\rho_d) + M_i(\rho_d) = \frac{\pi a^2 J_0\left(\frac{k}{f_0} \rho_d\right) + \pi a^2 \exp(TW_0) \exp\left[\frac{-\left(\frac{k}{f_0} \rho_d \rho_i\right)^2}{4}\right]}{a^3 \frac{k}{f_0} \frac{4}{3\pi} + \frac{(\pi)^{1/2}}{2\rho_i} a^2 \exp(TW_0)}$$

For large T (and any value of ρ_d), this expression becomes

$$M_c(\rho_d) + M_i(\rho_d) \approx M_i(\rho_d) = \frac{\pi a^2 \exp(TW_0) \exp\left[\frac{-\left(\frac{k}{f_0} \rho_d \rho_i\right)^2}{4}\right]}{\frac{(\pi)^{1/2} a^2}{2\rho_i} \exp(TW_0)} \quad (170)$$

$$M_c(\rho_d) + M_i(\rho_d) = 2(\pi)^{1/2} \rho_i \exp \left\{ \frac{-(K \rho_d \rho_i)^2}{4} \right\}$$

(171)

Recalling that

$$\rho_i^2 = (K \tau \frac{f}{K})^2 (\frac{\tau W_o}{\alpha_p})$$

equation (170) becomes

$$M_i(\rho_d) = 2(\pi)^{1/2} \rho_i \exp \left\{ \frac{-\frac{K^2}{f^2} \rho_d^2 \frac{f^2}{K^2} \frac{\tau W_o K_r^2}{\alpha_p}}{4} \right\}$$

$$= 2(\pi)^{1/2} \rho_i \exp \left\{ \frac{\rho_d^2 \tau W_o K_r^2}{4 \alpha_p} \right\} \quad (172)$$

Now using the same values for τ , W_o , K_r and α_p that were used in Chapter II:

$$M_i(\rho_d) = 2(\pi)^{1/2} \rho_i \exp \left[- \frac{\rho_d^2 (3156 \pi^2 \times 10^{12})}{(4)(130.4)} \right] \quad (173)$$

It can be seen that for any value of ρ_d ($0 < \rho_d < 2a$) other than zero, equation (173) is virtually zero due to the exponential factor.

Consequently, by equations (170) and (171) the Fourier modulus estimate becomes undefined. Therefore, to get a meaningful Fourier modulus

estimate, ρ_d must be evaluated at virtually its zero value.

Substituting $\rho_d = 0$ into equation (164) one gets

$$|M_i(0)|/|M_c(0)| = \exp(\tau W_0) \quad (174)$$

Now substituting equation (168) the result is

$$E_F^2 = \left| 1/(1 + \exp(\tau W_0)) - 1 \right|^2 \quad (175)$$

For large τ and $W_0 \approx 1$, $E_F^2 = 1$, or in other words, the error in Fourier modulus estimate is virtually 100 percent.

Equation (175) expresses the minimum error one can expect in the estimate of the Fourier modulus. Therefore, by the inequality relation

$$E_{F,k+1}^2 \leq E_{0,k}^2 \leq E_{F,k}^2$$

characteristic of the error-reduction algorithm,

$$E_0^2 = E_F^2 = \left| 1/(1 + \exp(\tau W_0)) - 1 \right|^2 \quad (176)$$

for large τ . Consequently, it can be concluded that the error in the reconstructed image is, for all intents and purposes, 100 percent and that the phase of the object cannot be retrieved.

Appendix I: The Scattering Cross Section

The scattering cross section σ_s may be defined in terms of the differential scattering cross section σ_d where

$$\begin{aligned}\sigma_d(\hat{o}, \hat{i}) &= \lim_{R \rightarrow \infty} [(R^2 S_s) / S_i] \\ &= |f(\hat{o}, \hat{i})|^2 \\ &= (\sigma_t / 4\pi) p(\hat{o}, \hat{i})\end{aligned}\tag{177}$$

R is the distance from the scatterer to the point of observation, S_i and S_s are the magnitude of the incident and scattering power flux density vectors, σ_t is the total scattering cross section ($\sigma_s + \sigma_a$) and $p(\hat{o}, \hat{i})$ is the phase function.

The total observed scattered power at all angles is produced by a particle with scattering cross section σ_s :

$$\begin{aligned}\sigma_s &= \int_{4\pi} \sigma_d d\omega \\ &= \int_{4\pi} |f(\hat{o}, \hat{i})|^2 d\omega \\ &= (\sigma_t / 4\pi) \int_{4\pi} p(\hat{o}, \hat{i}) d\omega\end{aligned}\tag{178}$$

where $d\omega$ is the differential solid angle.

The albedo w_0 of a particle is

$$\begin{aligned}w_0 &= \frac{\sigma_s}{\sigma_t} \\ &= \frac{1}{\sigma_t} \int_{4\pi} |f(\hat{o}, \hat{i})|^2 d\omega \\ &= \frac{1}{4\pi} \int_{4\pi} p(\hat{o}, \hat{i}) d\omega\end{aligned}\tag{179}$$

Appendix J: Solution to the Transport Equation Using the Large Particle Approximation (19:236)

As shown in Chapter II, if the size of scatterers is much greater than a wavelength, it is possible to simplify the equation of transfer (transport equation) using the small angle approximation (see Chapter II, page). One then obtains

$$\begin{aligned} \frac{\partial}{\partial z} I(z, \vec{\rho}, \vec{s}) + \vec{s} \cdot \nabla_t I(z, \vec{\rho}, \vec{s}) \\ = -\rho_n \sigma_t I(z, \vec{\rho}, \vec{s}) + \frac{\rho_n \sigma_t}{4\pi} \int_{-\infty}^{\infty} p(\vec{s} - \vec{s}') I(z, \vec{\rho}, \vec{s}') d\vec{s}' \end{aligned} \quad (180)$$

where $\mathbf{r} = x\hat{x} + y\hat{y} + z\hat{z} = \vec{\rho} + z\hat{z}$, $\nabla_t = \frac{\partial}{\partial x}\hat{x} + \frac{\partial}{\partial y}\hat{y}$,
 $\vec{s} = l\hat{x} + m\hat{y}$ (19:236).

A general solution of equation (180) may be obtained by a Fourier transform method. Denote by I_1 the Fourier transform of I with respect to $\vec{\rho}$ (19:236):

$$I_1(z, \vec{k}, \vec{s}) = \int_{-\infty}^{\infty} I(z, \vec{\rho}, \vec{s}) \exp(i\vec{k} \cdot \vec{\rho}) d\vec{\rho} \quad (181)$$

$$I(z, \vec{\rho}, \vec{s}) = \frac{1}{(2\pi)^2} \int_{-\infty}^{\infty} I_1(z, \vec{k}, \vec{s}) \exp(-i\vec{k} \cdot \vec{\rho}) d\vec{k} \quad (182)$$

Now the Fourier transform of equation (180) may be obtained. First, note that

$$\begin{aligned} \mathcal{F}\left\{\frac{\partial}{\partial z} I(z, \vec{\rho}, \vec{s})\right\} &= \frac{\partial}{\partial z} \mathcal{F}\{I(z, \vec{\rho}, \vec{s})\} \\ &= \frac{\partial}{\partial z} I_1(z, \vec{k}, \vec{s}) \end{aligned} \quad (183)$$

which is the Fourier transform of the first term on the left side of equation (180) (19:236).

To get the Fourier transform of the second term note that

$$\begin{aligned}\vec{s} \cdot \nabla_t I(\vec{z}, \vec{s}) &= \vec{s} \cdot \left[\frac{\partial}{\partial x} I(\vec{z}, \vec{s}) \hat{x} + \frac{\partial}{\partial y} I(\vec{z}, \vec{s}) \hat{y} \right] \\ &= \vec{s} \cdot \frac{\partial}{\partial x} \left\{ \frac{1}{(2\pi)^2} \int_{-\infty}^{\infty} I_1 e^{-i\vec{k} \cdot \vec{\rho}} d\vec{k} \right\} \hat{x} \\ &\quad + \vec{s} \cdot \frac{\partial}{\partial y} \left\{ \frac{1}{(2\pi)^2} \int_{-\infty}^{\infty} I_1 e^{-i\vec{k} \cdot \vec{\rho}} d\vec{k} \right\} \hat{y}\end{aligned}\tag{184}$$

Now,

$$\begin{aligned}\vec{k} \cdot \vec{\rho} &= (\kappa_x \hat{x} + \kappa_y \hat{y}) \cdot (x \hat{x} + y \hat{y}) \\ &= \kappa_x x + \kappa_y y\end{aligned}$$

and

$$\frac{\partial}{\partial x} (\kappa_x \hat{x} + \kappa_y \hat{y}) = \kappa_x, \quad \frac{\partial}{\partial y} (\kappa_x \hat{x} + \kappa_y \hat{y}) = \kappa_y$$

and, therefore,

$$\begin{aligned}\vec{s} \cdot \nabla_t I(\vec{z}, \vec{\rho}, \vec{s}) &= -i\vec{s} \cdot \frac{1}{(2\pi)^2} \int_{-\infty}^{\infty} I_1 \kappa_x \hat{x} e^{-i\vec{k} \cdot \vec{\rho}} d\vec{k} \\ &\quad - i\vec{s} \cdot \frac{1}{(2\pi)^2} \int_{-\infty}^{\infty} I_1 \kappa_y \hat{y} e^{-i\vec{k} \cdot \vec{\rho}} d\vec{k} \\ &= -i\vec{s} \cdot (\kappa_x \hat{x} + \kappa_y \hat{y}) \frac{1}{(2\pi)^2} \int_{-\infty}^{\infty} I_1 e^{-i\vec{k} \cdot \vec{\rho}} d\vec{k} \\ &= -i\vec{s} \cdot \frac{1}{(2\pi)^2} \int_{-\infty}^{\infty} I_1 e^{-i\vec{k} \cdot \vec{\rho}} d\vec{k} \\ &= \frac{1}{(2\pi)^2} \int_{-\infty}^{\infty} -i\vec{s} \cdot \vec{k} I_1(\vec{z}, \vec{k}, \vec{s}) e^{-i\vec{k} \cdot \vec{\rho}} d\vec{k}\end{aligned}\tag{185}$$

But equation (184) expresses the Fourier transform relation:

$$\mathcal{F}\{\vec{s} \cdot \nabla_t I(\vec{z}, \vec{\rho}, \vec{s})\} = -i\vec{s} \cdot \vec{\kappa} I_1(\vec{z}, \vec{\kappa}, \vec{s}) \quad (186)$$

which yields, then, the Fourier transform of the second term on the left side of equation (180).

The Fourier transform of the first term on the right side of equation (B-1) is straightforward:

$$\mathcal{F}\{-\rho_n \sigma_t I(\vec{z}, \vec{\rho}, \vec{s})\} = -\rho_n \sigma_t I_1(\vec{z}, \vec{\kappa}, \vec{s}) \quad (187)$$

The Fourier transform of the second term on the right side of equation (180) is

$$\begin{aligned} \mathcal{F}\left\{\frac{\rho_n \sigma_t}{4\pi} \int \int_{-\infty}^{\infty} p(\vec{s} - \vec{s}') I(\vec{z}, \vec{s}) d\vec{s}'\right\} \\ = \frac{\rho_n \sigma_t}{4\pi} \int \int_{-\infty}^{\infty} p(\vec{s} - \vec{s}') \mathcal{F}\{I(\vec{z}, \vec{\rho}, \vec{s})\} d\vec{s}' \\ = \frac{\rho_n \sigma_t}{4\pi} \int \int_{-\infty}^{\infty} p(\vec{s} - \vec{s}') I_1(\vec{z}, \vec{\kappa}, \vec{s}) d\vec{s}' \end{aligned} \quad (188)$$

Collecting equations (183), (186), (187), and (188) one obtains

$$\left[\frac{\partial}{\partial \vec{z}} (-i\vec{s} \cdot \vec{\kappa}) + \rho_n \sigma_t \right] I_1(\vec{z}, \vec{\kappa}, \vec{s}) - \rho_n \sigma_t \int \int_{-\infty}^{\infty} p(\vec{s} - \vec{s}') I_1(\vec{z}, \vec{\kappa}, \vec{s}) d\vec{s}' = 0 \quad (189)$$

It is convenient to simplify the first term of equation (189) by letting (19:237)

$$I_1(\vec{z}, \vec{\kappa}, \vec{s}) = I_2(\vec{z}, \vec{\kappa}, \vec{s}) \exp\{(i\vec{s} \cdot \vec{\kappa} - \rho_n \sigma_t) \vec{z}\} \quad (190)$$

then equation (189) becomes

$$\frac{\partial}{\partial z} I_2(z, \vec{s}) - \frac{\rho n \sigma_t}{4\pi} \int_{-\infty}^{\infty} \int_{-\infty}^{\infty} p(\vec{s} - \vec{s}') \exp\{-i \cdot (\vec{s} - \vec{s}') z\} I_2(z, \vec{k}, \vec{s}) d\vec{s}' = 0 \quad (191)$$

Now using the relations

$$P(\vec{q}) = \int_{-\infty}^{\infty} \int_{-\infty}^{\infty} p(\vec{s}) \exp(i\vec{s} \cdot \vec{q}) d\vec{s} \quad (192)$$

$$F(z, \vec{k}, \vec{q}) = \int_{-\infty}^{\infty} \int_{-\infty}^{\infty} I_2(z, \vec{k}, \vec{s}) \exp(i\vec{s} \cdot \vec{q}) d\vec{s} \quad (193)$$

the Fourier transform of the convolution integral in equation (191) is taken. First, let $\vec{r} = \vec{s} - \vec{s}'$ and $d\vec{r} = d\vec{s}$ then,

$$\begin{aligned} \mathcal{F}\{p(\vec{s} - \vec{s}')\} &= -\frac{\rho n \sigma_t}{4\pi} \int_{-\infty}^{\infty} \int_{-\infty}^{\infty} p(\vec{r}) \exp(-i\vec{k} \cdot \vec{r}) \exp[i(\vec{r} + \vec{s}') \cdot \vec{q}] d\vec{r} \\ &= -\frac{\rho n \sigma_t}{4\pi} \int_{-\infty}^{\infty} \int_{-\infty}^{\infty} p(\vec{r}) e^{-i\vec{k} \cdot \vec{r} + i\vec{r} \cdot \vec{q} + i\vec{s}' \cdot \vec{q}} d\vec{r} \\ &= -\frac{\rho n \sigma_t}{4\pi} \int_{-\infty}^{\infty} \int_{-\infty}^{\infty} p(\vec{r}) e^{i\vec{r} \cdot (\vec{q} - \vec{k})} e^{i\vec{s}' \cdot \vec{q}} d\vec{r} \end{aligned} \quad (194)$$

Substituting equation (194) into equation (191) yields

$$\begin{aligned} \iiint \left\{ \iiint p(\vec{r}) e^{i\vec{r} \cdot (\vec{q} - \vec{k})} d\vec{r} \right\} I_2(z, \vec{k}, \vec{s}') e^{i\vec{s}' \cdot \vec{q}} d\vec{s}' \\ = \iint P(\vec{q} - \vec{k}) I_2(z, \vec{k}, \vec{s}') e^{i\vec{s}' \cdot \vec{q}} d\vec{s}' \\ = P(\vec{q} - \vec{k}) F(z, \vec{k}, \vec{q}) \end{aligned} \quad (195)$$

(by equations (192) and (193)).

The Fourier transform of the first term in equation (191) is straightforward:

$$\begin{aligned} \mathcal{F}\left\{\frac{\partial}{\partial z} I_2(z, \vec{s})\right\} &= \frac{\partial}{\partial z} \int_{-\infty}^{\infty} \int_{-\infty}^{\infty} I_2(z, \vec{k}, \vec{s}) e^{i\vec{s} \cdot \vec{q}} d\vec{s} \\ &= \frac{\partial}{\partial z} F(z, \vec{k}, \vec{q}) \end{aligned} \quad (196)$$

Then, one obtains from equations (195) and (196):

$$\frac{d}{dz} F(z, \kappa, \vec{q}) - \frac{\hbar \sigma_t}{4\pi} P(\vec{q} - \vec{\kappa} z) F(z, \vec{\kappa}, \vec{q}) = 0 \quad (197)$$

Equation (197) is exact and may be solved using the integration factor

$$\exp \left\{ \int_0^z \frac{\hbar \sigma_t}{4} P(\vec{q} - \vec{\kappa} z') dz' \right\} :$$

$$\exp \left\{ \int_0^z B P dz' \right\} \frac{dF}{dz} + B P \exp \left\{ \int_0^z B P dz' \right\} F = 0 \quad (198)$$

where $B = \frac{\hbar \sigma_t}{4\pi}$, $P = P(\vec{q} - \vec{\kappa} z)$, $F = F(z, \vec{\kappa}, \vec{q})$.

Therefore,

$$\frac{d}{dz} \left[\exp \left(\int_0^z B P dz' \right) F \right] = 0$$

or

$$\exp \left[\int_0^z B P dz' \right] F = C \quad (199)$$

where C is a constant of integration. Setting $z = 0$ the constant c may be evaluated:

$$\left\{ \exp \left[\int_0^z B P(\vec{q} - \vec{\kappa} z') dz' \right] F(z, \vec{\kappa}, \vec{q}) \right\} \Big|_{z=0} = C$$

then

$$C = F(0, \vec{\kappa}, \vec{q})$$

From equation (199) one then obtains

$$\exp \left[\int_0^z B P dz' \right] F(z, \vec{\kappa}, \vec{q}) = F(0, \vec{\kappa}, \vec{q})$$

or

$$F(z, \vec{\kappa}, \vec{q}) = F(0, \vec{\kappa}, \vec{q}) \exp \left\{ - \int_0^z \frac{\rho_n \sigma_t}{4} P(\vec{q} - \vec{\kappa} z') dz' \right\} \quad (200)$$

The final solution $I(z, \vec{\rho}, \vec{s})$ for the small angle approximation may now be derived. First,

$$\begin{aligned} I(z, \vec{\rho}, \vec{s}) &= \frac{1}{(2\pi)^2} \int_{-\infty}^{\infty} I_1(z, \vec{\kappa}, \vec{s}) \exp(-i\vec{\kappa} \cdot \vec{\rho}) d\vec{\kappa} \\ &= \frac{1}{(2\pi)^2} \int_{-\infty}^{\infty} I_2(z, \vec{\kappa}, \vec{s}) \exp \left\{ (i\vec{s} \cdot \vec{\kappa} - \rho_n \sigma_t) z \right\} \\ &\quad \times \exp(-i\vec{\kappa} \cdot \vec{\rho}) d\vec{\kappa} \end{aligned} \quad (201)$$

$$\text{Since } I_2(z, \vec{\kappa}, \vec{s}) = \frac{1}{(2\pi)^2} \int_{-\infty}^{\infty} F(z, \vec{\kappa}, \vec{q}) e^{-i\vec{s} \cdot \vec{q}} d\vec{q}$$

equation (201) becomes

$$\begin{aligned} I(z, \vec{\rho}, \vec{s}) &= \frac{1}{(2\pi)^4} \int_{-\infty}^{\infty} d\vec{\kappa} \exp \left\{ -i\vec{\kappa} \cdot \vec{\rho} + (i\vec{s} \cdot \vec{\kappa} - \rho_n \sigma_t) z \right\} \\ &\quad \times \int d\vec{q} \exp(-i\vec{s} \cdot \vec{q}) F(z, \vec{\kappa}, \vec{q}) \end{aligned} \quad (202)$$

Now using equation (200) and changing the variable $\vec{q}' = \vec{q} - \vec{\kappa} z$ and then removing the prime ($q \rightarrow q + \vec{\kappa} z$):

$$\begin{aligned} I(z, \vec{\rho}, \vec{s}) &= \frac{1}{(2\pi)^4} \int_{-\infty}^{\infty} d\vec{\kappa} \exp \left\{ i\vec{\kappa} \cdot \vec{\rho} + (i\vec{s} \cdot \vec{\kappa} - \rho_n \sigma_t) z \right\} \\ &\quad \times \int d\vec{q} \exp(-i\vec{s} \cdot \vec{q}) F_0(\vec{\kappa}, \vec{q}) \exp \left[- \int_0^z \frac{\rho_n \sigma_t}{4} P(\vec{q} - \vec{\kappa} z') dz' \right] \\ &= \frac{1}{(2\pi)^4} \int_{-\infty}^{\infty} d\vec{\kappa} \exp(i\vec{\kappa} \cdot \vec{\rho}) \exp(i\vec{s} \cdot \vec{\kappa} z) \exp(-\rho_n \sigma_t z) \\ &\quad \times \int_{-\infty}^{\infty} d\vec{q} \exp[-i\vec{s} \cdot (\vec{q} + \vec{\kappa} z)] F_0(\vec{\kappa}, \vec{q} + \vec{\kappa} z) \\ &\quad \times \exp \left[- \int_0^z \frac{\rho_n \sigma_t}{4} P(\vec{q} + \vec{\kappa} z - \vec{\kappa} z') dz' \right] \end{aligned}$$

Then, simplifying terms $I(z, \vec{\rho}, s)$ becomes

$$I(z, \vec{\rho}, \vec{s}) = \frac{1}{(2\pi)^4} \int_{-\infty}^{\infty} d\vec{k} \exp\{i\vec{k} \cdot \vec{\rho} - i\vec{s} \cdot \vec{q}\} \int_{-\infty}^{\infty} d\vec{q} F_0(\vec{k}, \vec{q} + \vec{k}z) \\ \times \exp\left[-\int_0^z R_n \sigma_t \left[1 - \frac{1}{4\pi} P(\vec{q} + \vec{k})(z - z') dz'\right]\right] \quad (203)$$

Equation (203) is Ishimaru's solution for $I(z, \vec{\rho}, s)$ (19:238).

Appendix K: Calculation of the Fourier Transform of the Gaussian Phase Function

The phase function describing the angular distribution of scattered radiation can be written as

$$p(\vec{s}) = 4\alpha_p W_0 \exp(-\alpha_p s^2) \quad (204)$$

To find the Fourier transform $P(\vec{q})$ of $p(\vec{s})$ the following formula is used:

$$\begin{aligned} P(\vec{q}) &= \int p(\vec{s}) \exp(i\vec{s} \cdot \vec{q}) d\vec{s} \\ &= \iiint_{-\infty}^{\infty} 4\alpha_p W_0 \exp(-\alpha_p s^2) \exp(i\vec{s} \cdot \vec{q}) d\vec{s} \end{aligned} \quad (205)$$

Letting

$$\begin{aligned} \vec{s} &= \sin\theta (\cos\varphi \hat{x} + \sin\varphi \hat{y}) \\ \vec{q} &= q (\cos\varphi' \hat{x} + \sin\varphi' \hat{y}) \end{aligned}$$

then,

$$\begin{aligned} \vec{s} \cdot \vec{q} &= q \sin\theta \cos\varphi \cos\varphi' + q \sin\theta \sin\varphi \sin\varphi' \\ &= q \sin\theta [\cos\varphi \cos\varphi' + \sin\varphi \sin\varphi'] \\ &= q \sin\theta [\cos(\varphi - \varphi')] \end{aligned} \quad (206)$$

Substituting into equation (205):

$$\begin{aligned} P(\vec{q}) &= \iiint_{-\infty}^{\infty} 4\alpha_p W_0 \exp(-\alpha_p s^2) \exp\{iq \sin\theta [\cos(\varphi - \varphi')]\} d\vec{s} \\ &= \int_0^{2\pi} \int_0^{\pi} 4\alpha_p W_0 \exp(-\alpha_p s^2) \exp(iq \sin\theta \cos(\varphi - \varphi')) \\ &\quad \times \cos\theta \sin\theta d\theta d\varphi \end{aligned} \quad (207)$$

Rearranging, and changing order of integration gives

$$\begin{aligned}
 P(\bar{q}) &= \int_0^\pi 4\alpha_p W_0 \exp(-\alpha_p \sin^2 \theta) \left\{ \int_0^{2\pi} \exp[iq \sin \theta \cos(\varphi - \varphi')] d\varphi \right\} \\
 &\quad \times \cos \theta \sin \theta d\theta \\
 &= \int_0^\pi 4\alpha_p W_0 2\pi J_0(q \sin \theta) \exp(-\alpha_p \sin^2 \theta) \\
 &\quad \times \cos \theta \sin \theta d\theta \\
 &= 4\pi W_0 \int_0^\pi J_0(q \sin \theta) \exp(-\alpha_p \sin^2 \theta) 2\alpha_p \\
 &\quad \times \cos \theta \sin \theta d\theta \quad (208)
 \end{aligned}$$

Since $|\vec{s}| = \sin \theta$,

$$\begin{aligned}
 P(q) &= 4\pi W_0 \int_0^\infty J_0(qs) \exp(-\alpha_p s^2) 2\alpha_p s ds \\
 &= 4\pi W_0 (2\alpha_p) \int_0^\infty J_0(qs) \exp(-\alpha_p s^2) s ds \\
 &= 4\pi W_0 (2\alpha_p) \int_0^\infty J_0(qs) \exp\left\{-[(\alpha_p)^{1/2}]^2 s^2\right\} s ds \quad (209)
 \end{aligned}$$

Now use the formula (1)

$$\begin{aligned}
 \int_0^\infty J_\nu(at) \exp(-p^2 t^2) t^{\nu+1} dt \\
 = \frac{a^\nu}{(2p^2)^{\nu+1}} \exp\left(-\frac{a^2}{4p}\right)
 \end{aligned}$$

to get

$$\begin{aligned}
 P(q) &= 4\pi W_0 (2\alpha_p) \cdot \frac{1}{2\alpha_p} \cdot \exp\left(-\frac{q^2}{4\alpha_p}\right) \\
 &= 4\pi W_0 \exp\left(-\frac{q^2}{4\alpha_p}\right) \quad (210)
 \end{aligned}$$

which is the desired result.

BIBLIOGRAPHY

1. Abramowitz, M., and I. Stegun. Handbook of Mathematical Functions with Formulas, Graphs, and Mathematical Tables, U.S. Department of Commerce, National Bureau of Standards Applied Mathematics Series 55, 1965.
2. Anderson, R.R., and J.A. Parish. "The Optics of Human Skin," Journal of Investigative Dermatology, 77: 13-19 (1981).
3. Anderson, R.R., and J.A. Parrish. "Optical Radiation Transfer in the Human Skin and Applications in vivo Remittance Spectroscopy," Bioengineering and the Skin, edited by R. Marks and P.A. Payne. Lancaster: MTP Press, 1979.
4. Barer, R., K.F.A. Ross, and S. Tkaczyk. "Refractrometry of Living Cells," Nature, 171:720-724 (1953).
5. Bartrum, R.J., and Harte C. Crow. "Transillumination Lightscanning to Diagnose Breast Cancer: A Feasibility Study," American Journal of Radiology, 142:409-414 (February 1984).
6. Beahrs, O.H., S. Shapiro and C. Smart. "Report of the Working Group to Review the National Cancer Institute--American Cancer Society Breast Cancer Detection Projects," Journal of the National Cancer Institute, 62:641-709.
7. Cartwright, C.H. "Infrared Transmission of the Skin," Journal of the Optical Society of America, 20:81-84 (1930).
8. Cole-Beuglet, C.M., B.B. Goldberg, A.S. Patchetsky, C.S. Rubin, C.D. Schneck, and R.Z. Soriano. Atlas of Breast Ultrasound, edited by Normal C. Telles. Philadelphia: Technicare, 1980.
9. Cutler, M. "Transillumination as an Aid in the Diagnosis of Breast Lesions," Surgery, Gynecology, and Obstetrics, 48:721-729 (1929).
10. DePalma, J.J., and J. Gasper. "Determining the Optical Properties of Photographic Emulsions by the Monte-Carlo Method," Photography, Science, and Engineering, 16:181-191 (1972).
11. Duguay, M.A. and A.T. Mattick. "Ultra High Speed Photography of Picosecond Light Pulses and Echoes," Applied Optics, 10:2162-2170 (1971).
12. Egan, Robert L. Mammography, Springfield: Charles C. Thomas, 1964.
13. Feynman, F.R. and A.R. Hibbs. Quantum Mechanics and Path Integrals, New York: McGraw-Hill, 1965.
14. Fienup, J.R. "Comparison of Phase Retrieval Algorithms," Advances in Computer Vision and Image Processing, Volume 1, edited by Thomas S. Huang. Greenwich: JAI Press, 1984.

15. Findlay, G.H. "Blue Skin," British Journal of Dermatology, 83:127-134 (1970).
16. Goodman, J.W. Introduction to Fourier Optics, San Francisco: McGraw-Hill, 1968.
17. Hardy, J.D., H.T. Hammell, and D. Murgatroyd. "Spectral Transmittance and Reflectance of Excised Human Skin," Journal of Applied Physiology, 9:257-264, 1956.
18. Holliday, H.W., and R.W. Blamey. "Breast Transillumination Using the Sinus Diaphanograph," British Medical Journal of Clinical Research, 283:411 (1981).
19. Ishimaru, Akira. Wave Propagation and Scattering in Random Media, Volume 1, New York: Academic Press, 1978.
20. Ishimaru, Akira. Wave Propagation and Scattering in Random Media, Volume 2, New York: Academic Press, 1978.
21. Johnson, Curtis C., and Arthur W. Guy. "Nonionizing Electromagnetic Wave Effects in Biological Materials and Systems," Proceedings of the IEEE, 60:692-718 (June 1972).
22. Kortum, Gustav. Reflectance Spectroscopy, Berlin: Springer-Verlag, 1969.
23. Lafreniere, R., F.S. Ashkar, and A.S. Ketcham. "Infrared Light Scanning of the Breast," The American Surgeon, 52:123-128 (March 1986).
24. Maarek, J.M., G. Jarry, J. Crowe, M.-H. Bui, and D. Laurent. "Simulation of Laser Tomoscopy in a Heterogeneous Biological Medium," Medical and Biological Engineering and Computing, 24:407-414 (July 1986).
25. Macovski, Albert. Medical Imaging Systems, Englewood Cliffs: Prentice-Hall, 1983.
26. Morton, R., and S.S. Miller. "Infrared Transillumination Using Photography and Television," Journal of Audiovisual Media in Medicine, 4:86-90 (1981).
27. Ricci, John L., Maj, USAF. Technical Radiologist, Human Engineering Division, Wright-Patterson AFB, OH. Personal Interview, June 1987.
28. Sandison, A.T. An Autopsy Study of the Adult Human Breast, National Cancer Institute Monograph No. 8, U.S. Department of Health, Education, and Welfare, 1962.
29. Sickles, E.A. "Breast Cancer Detection with Transillumination and Mammography," American Journal of Radiology, 142:841-844 (April 1984).

30. Steinke, J.M., and A.P. Shepherd. "Role of Light Scattering in Whole Blood Oximetry," IEEE Transactions on Biomedical Engineering, 33:294-301 (March 1986).
31. Stoller, Milton. Design Engineer. Telephone Interview. Spectrascan, New Haven, CT, 5 July 1987.
32. Twersky, Victor. "Multiple Scattering of Waves and Optical Phenomena," Journal of the Optical Society, 52:145-171 (February 1962).
33. Twersky, Victor. "Interface Effects in Multiple Scattering by Large, Low-Refracting, Absorbing Particles," Journal of the Optical Society of America, 60:908-914 (July 1970).
34. Twersky, Victor. "Absorption and Multiple Scattering by Biological Suspensions," Journal of the Optical Society of America, 60:1084-1093 (August 1970).
35. Twersky, Victor. "On Propagation in Random Media of Discrete Scatterers," Proceedings of Symposium in Applied Mathematics, Contracts AF-AFOSR-66-63 and DA-31-124-ARO(D)-81. American Mathematical Society, Providence, R.I., 1984.
36. U.S. Department of Commerce, National Bureau of Standards Handbook of Mathematical Functions with Formulas, Graphs and Mathematical Tables. Applied Mathematics Series 55. Edited by Milton Abramowitz and Irene A. Stegun, U.S. Government Printing Office, 1965.
37. Villee, Claude A. Biology, Philadelphia: W.B. Saunders Company, 1967.
38. Wallberg, Hakan. Diaphanography: A Clinical and Experimental Study of Benign and Malignant Mammary Diseases. Huddinge Sweden: Karolinska Institute, 1984.
39. Watmough, D.J. "Diaphanography: Mechanism Responsible for the Images," Acta Radiologica Oncology, 21:11-15 (1982).
40. Woodhead-Galloway, John. Collagen: the Anatomy of a Protein, London: Edward Arnold, 1980.
41. Zdrojowski, R.J., and N.R. Pisharoty. "Optical Transmission and Reflection by Blood," IEEE Transactions in Biomedical Engineering, 17:122-128 (1970).

VITA

Captain David W. Sanders was born on 29 September 1949 in Stockton, California. He graduated from High School in the same city in 1967. In 1970 he enlisted in the Air Force and served for 8 years. He attended the University of California, Irvine from which he received the degree of Bachelor of Science in Electrical Engineering in June, 1982. Upon graduation, he received a commission from the USAF through the Officer Training School at Medina AFB, San Antonio, Texas. He then served for 4 years as a Support Engineer at the Satellite Control Facility located in Sunnyvale, California. In June, 1986, he entered the School of Engineering, Air Force Institute of Technology.

Permanent Address: 2332 Funston Ave.

Stockton, California 95205

UNCLASSIFIED

SECURITY CLASSIFICATION OF THIS PAGE

REPORT DOCUMENTATION PAGE

Form Approved
OMB No. 0704-0188REPORT SECURITY CLASSIFICATION
UNCLASSIFIED

1b. RESTRICTIVE MARKINGS

2a. SECURITY CLASSIFICATION AUTHORITY

3. DISTRIBUTION / AVAILABILITY OF REPORT

2b. DECLASSIFICATION / DOWNGRADING SCHEDULE

Approved for public release;
distribution unlimited.

4. PERFORMING ORGANIZATION REPORT NUMBER(S)

5. MONITORING ORGANIZATION REPORT NUMBER(S)

AFIT/GEO/ENP/87D-4

6a. NAME OF PERFORMING ORGANIZATION

6b. OFFICE SYMBOL
(If applicable)
AFIT/ENG

7a. NAME OF MONITORING ORGANIZATION

6c. ADDRESS (City, State, and ZIP Code)

Air Force Institute of Technology
Wright-Patterson AFB, OH 45433-6583

7b. ADDRESS (City, State, and ZIP Code)

8a. NAME OF FUNDING / SPONSORING
ORGANIZATION8b. OFFICE SYMBOL
(If applicable)

9. PROCUREMENT INSTRUMENT IDENTIFICATION NUMBER

8c. ADDRESS (City, State, and ZIP Code)

10. SOURCE OF FUNDING NUMBERS

PROGRAM
ELEMENT NO.PROJECT
NO.TASK
NO.WORK UNIT
ACCESSION NO.

11. TITLE (Include Security Classification)

See box 19.

PERSONAL AUTHOR(S)

David W. Sanders, B.S., B.S.E.E., Capt, USAF

13a. TYPE OF REPORT

MS Thesis

13b. TIME COVERED

FROM _____ TO _____

14. DATE OF REPORT (Year, Month, Day)

1987 December

15. PAGE COUNT

156

16. SUPPLEMENTARY NOTATION

17. COSATI CODES

FIELD	GROUP	SUB-GROUP
17	05	01

18. SUBJECT TERMS (Continue on reverse if necessary and identify by block number)
Transillumination, Multiple Scattering

19. ABSTRACT (Continue on reverse if necessary and identify by block number)

Title: Theoretical Analysis of Cancer Detection in the Human Breast
By TransilluminationThesis Chairman: Theodore E. Luke
Associate Professor Of Engineering Physics

Approved for public release; distribution unlimited.
 David W. Sanders
 Captain, USAF
 Director for Research and Development
 Air Force Institute of Technology
 Wright-Patterson AFB, OH 45433-6583
 31 Mar 87

DISTRIBUTION / AVAILABILITY OF ABSTRACT

☒ UNCLASSIFIED/UNLIMITED ☐ SAME AS RPT ☐ DTIC USERS

21. ABSTRACT SECURITY CLASSIFICATION

UNCLASSIFIED

22a. NAME OF RESPONSIBLE INDIVIDUAL

Theodore E. Luke

22b. TELEPHONE (Include Area Code)

(513) 255-4498

22c. OFFICE SYMBOL

AFIT/ENP

DD Form 1473, JUN 86

Previous editions are obsolete.

SECURITY CLASSIFICATION OF THIS PAGE

UNCLASSIFIED

UNCLASSIFIED

— This investigation is a theoretical analysis of the propagation of near infrared light through human breast tissue with a view to improving imaging of breast cancers by transillumination. The analysis employed multiple scattering and radiation transport theory.

Calculation showed that breast tissue is optically thick and does not allow for imaging details of tumors which may be imbedded in the tissue. An example calculation carried out on the method of phase retrieval demonstrated that the error in the estimate of the Fourier modulus is, for normal breast tissue, nearly 100 percent and that, therefore, the phase of an object (tumor) cannot be retrieved by this method.

A Monte Carlo simulation employing time gating and spatial filtering (TGSF) was presented showing that, in some cases, an improvement in image contrast of 77 percent is theoretically possible when transilluminating a dilute blood medium containing a blood vessel. A calculation of total transmittance obtained by Monte Carlo simulation on one hand and by multiple scattering and radiation transport theory on the other, indicated an essential agreement of the results for tissue thicknesses less than 60mm.

A method of tying the results of Monte Carlo simulation to those of multiple scattering and radiation transport is presented. An effective optical thickness reduced by TGSF is defined and a method is described to determine if the reduced effective thickness allows for reasonable images to be obtained.

UNCLASSIFIED

END

DATE

FILM

4-88

DTIC